Universitat Autònoma de Barcelona

Image Analysis of Bacterial Colonies in Classic and Alternative Gel-Based Growth Media

Enric Maroto Fernández

ADVERTIMENT. L'accés als continguts d'aquesta tesi doctoral i la seva utilització ha de respectar els drets de la persona autora. Pot ser utilitzada per a consulta o estudi personal, així com en activitats o materials d'investigació i docència en els termes establerts a l'art. 32 del Text Refós de la Llei de Propietat Intel·lectual (RDL 1/1996). Per altres utilitzacions es requereix l'autorització prèvia i expressa de la persona autora. En qualsevol cas, en la utilització dels seus continguts caldrà indicar de forma clara el nom i cognoms de la persona autora i el títol de la tesi doctoral. No s'autoritza la seva reproducció o altres formes d'explotació efectuades amb finalitats de lucre ni la seva comunicació pública des d'un lloc aliè al servei TDX. Tampoc s'autoritza la presentació del seu contingut en una finestra o marc aliè a TDX (framing). Aquesta reserva de drets afecta tant als continguts de la tesi com als seus resums i índexs.

ADVERTENCIA. El acceso a los contenidos de esta tesis doctoral y su utilización debe respetar los derechos de la persona autora. Puede ser utilizada para consulta o estudio personal, así como en actividades o materiales de investigación y docencia en los términos establecidos en el art. 32 del Texto Refundido de la Ley de Propiedad Intelectual (RDL 1/1996). Para otros usos se requiere la autorización previa y expresa de la persona autora. En cualquier caso, en la utilización de sus contenidos se deberá indicar de forma clara el nombre y apellidos de la persona autora y el título de la tesis doctoral. No se autoriza su reproducción u otras formas de explotación efectuadas con fines lucrativos ni su comunicación pública desde un sitio ajeno al servicio TDR. Tampoco se autoriza la presentación de su contenido en una ventana o marco ajeno a TDR (framing). Esta reserva de derechos afecta tanto al contenido de la tesis como a sus resúmenes e índices.

WARNING. The access to the contents of this doctoral thesis and its use must respect the rights of the author. It can be used for reference or private study, as well as research and learning activities or materials in the terms established by the 32nd article of the Spanish Consolidated Copyright Act (RDL 1/1996). Express and previous authorization of the author is required for any other uses. In any case, when using its content, full name of the author and title of the thesis must be clearly indicated. Reproduction or other forms of for profit use or public communication from outside TDX service is not allowed. Presentation of its content in a window or frame external to TDX (framing) is not authorized either. These rights affect both the content of the thesis and its abstracts and indexes.

Image Analysis of Bacterial Colonies in Classic and Alternative Gel-Based Growth Media

Tesi doctoral presentada per

Enric Maroto Fernández

Direcció i tutela acadèmica per

Dr. Jordi Barbé García

Tesi sotmesa per optar al grau de Doctor per la Universitat Autònoma de Barcelona

Programa de Doctorat en Microbiologia

Departament de Genètica i Microbiologia
Universitat Autònoma de Barcelona

-

Pla de Doctorats Industrials

Departament d'Investigació i Desenvolupament
IUL, S.A.

Image Analysis of Bacterial Colonies in Classic and Alternative Gel-Based Growth Media

Tesi sotmesa per Enric Maroto Fernández per optar al grau de Doctor per la Universitat Autònoma de Barcelona

Vist-i-plau del director de la tesi doctoral

Dr. Jordi Barbé García

Programa de Doctorat en Microbiologia

Departament de Genètica i de Microbiologia
Universitat Autònoma de Barcelona

Image Analysis of Bacterial Colonies in Classic and Alternative Gel-Based Growth Media

Enric Maroto Fernández

Microbiology Doctorate Program
Department of Genetics and Microbiology
Universitat Autònoma de Barcelona
2018

Abstract

Microbiology laboratories are increasingly adopting automated imaging technologies as means to leverage their productivity and increase traceability and objectivity of test results. Specifically, colony enumeration and detection of color development in these stand as the two most common applications of machine vision in microbiology laboratories. In the advent of the age of computer vision, colony counting and analysis stands as yet another process that can be automated by means of image-driven artificial intelligence.

The present work assesses the capacity of flatbed scanners to capture images for the detection and measurement of color development in colonies. Effects of different concentrations of chromogens and the differences in color development over time are evaluated. Affordable approaches to interpret derived data are suggested and insights related to the analysis of color development are supplied. Metrological aspects of the measurement technique are duly addressed. Thus, particular care is devoted to characterize the measurement technique employed, to highlight its limitations, and to assess the cross-device reproducibility of obtained results.

First-in-class accounts of enumeration of colonies in alternative culture media, based on kinetic imaging of their growth, are also reported. Furthermore, time to the earliest detection of colonies is evaluated, along with colony recovery evaluation, as a means to assess stress induction related to the presence of potentially toxic matrices.

Acknowledgements

I would like to dearly thank the following individuals:

Jordi Barbé (UAB, Barcelona) and Vicenç Font (IUL, Barcelona) for their guidance throughout the project. José Pereira (creator of the Rough profiler), Wolf Faust (IT-8 card manufacturer), Phil Green (ICC, USA) for their assistance in the establishment of correct ICC profiles. Kai Uwe Barthel (HTW, Berlin) for the information he supplied regarding the FIJI 3-D color Inspector Plugin. Xavier Fernández (IUL, Barcelona) for his general guidance regarding image processing and analysis. Francesc Carmona (UB, Barcelona) and Charles Zaiontz, (Real-Statistics add-in developer) for their advice regarding statistical analysis of data. Francesc Codony (ENAC auditor) for his comments regarding colony enumeration. Judith García, Pablo Amieiro, and Raquel Freire (PCB, Barcelona), for their flexibility and assistance, when implementing several experimental set-ups in the PCB.

-

This thesis was co-funded by IUL S.A. and the Catalan Government`s plan for Industrial Doctorates (Grant No. 2015DI017).

Table of Contents

1. INTRODUCTION

1.1. Automated Colony Counting and Analysis

1.1.1. Image Acquisition for Colony Counting

Since the advent of the first automated colony counter in 1957, which required a specifically devised imaging device[1], automated colony counting has come a long way. Affordability and ubiquity of high-quality consumer electronics for imaging purposes, namely digital cameras and flatbed scanners, have elicited widespread development and use of automated colony counting and analysis technologies[2–15]. Additionally, the ever-increasing capacities of present-day personal computers (PC) and mobile device processors, allow for processing and analysis of high-resolution colony images in a time scale of seconds[16].

The present work will focus on use of flatbed scanners for colony imaging, use of CCD-camera-based digital colony counters is however more common than that of flatbed scanners[4,8,16–18].

1.1.1.1. Flatbed Scanner-Based Image Acquisition

Use of flatbed scanners has been widely implemented to image colonies[6,7,11,13,14,19,20] and to perform colorimetric readings[21–25]. Readers are referred to Göröcs and Ozcan's article on the topic of bioimaging with scanners for accounts of other significant applications[21]. Imaging properties of flatbed scanners have been noted to be stable, with optimal illumination and rather constant background. This enables spatial and color features of captured images to be reasonably accurate and stable when applied to bioassay imaging[26].

1.1.1.1.1. Types of Flatbed Scanners

Two main types of flatbed scanners are commercially available, these are classified according to their core sensing technologies. The latter can consist in Charge-Coupled-Device (CCD)-based sensors or, alternatively, in contact image sensors (CIS). In CCD scanners, input images are demagnified by a lens in order to fit CCD sensors, which are usually only a few cm long[21]. CCD scanner sensors are characterized by their trilinear structure, these sensors are constituted by three consecutive lines of CCD sensor elements which are selectively responsive to red, green and blue light, respectively (see Figure 1.1 A). CCD sensors are typically characterized by a very high color gamut. Use of linear sensors in combination with a good lens and mirror system enables to overcome many limitations of image quality in camera based images, namely intensity, color aberration and geometric inaccuracies[27].

CIS scanners usually make use of a gradient index lens array (GRIN) to focus incoming light into a (usually monochromatic) sensor array (see Figure 1.1 B). Use of GRIN lenses implies a limited field depth and can generate several shifted images when imaging an out-of-focus object. CCD-based scanners are recommendable when larger field depths are necessary. Thus, these are preferable for Petri plate scanning. While CCD sensors usually have a pixel size of ~ 3μm, pixel size of CIS-based sensors is ~10 μm, larger pixel size allows to reduce noise, enhancing image quality[21]. Quality CCD scanners, however, are known to have sizes of ~10 μm[27]. Since CIS scanners use multiple sensor arrays (see Figure 1.1 B), small gaps ~40 μm long can be found between each sensor, this compromises image quality by creating dead spots at certain image points[21].

Optical resolution of scanners also conditions scans, this parameter allows to measure the number of distinct points read during a scan, that is the amount of points that can be sampled in a given read distance. Resolutions might differ between scan movement orientations and the (perpendicular) sensor direction. Movement-orientation resolutions depend on step-size and motor precision. Sensor direction resolutions depend on pixel density of the sensors. Many commercial scanner manufacturers supply false resolution claims based on the theoretical resolution of their scanners and not in actual empirical data that contemplates spatial sampling and undersampling. Arguably, supplied resolutions can be taken as maximum theoretical value and not as a truly functional one[21]. Table 1.1 displays the technical specifications for the scanners used in the research reported in the present thesis. All scanner manufacturers claim equal resolutions in the scans with independence of the direction taken under consideration (be it movement direction or sensor direction).

Table 1.1. Scanner Specifications CS, OPS and V39 stand, respectively, for CanoScan 9000F MarkII, OpticSlim 2610 and Perfection V39 scanner models.

Model	CS	OPS	V39
Scanning Element	CCD	CIS	CIS
Illumination	White LED	RGB LED Array	RGB LED Array
Optical Resolution (DPI)	4800	1200	4800

1.1.1.1.2. Use of Flatbed Scanners for Colony Imaging

Several arrangements have been used to image colonies with a flatbed scanner. Due to the limited field depth of scanners (see section 1.1.1.1.1 for information regarding scanner types and field depth), it is preferable to image colonies at a short distance from the imaging area glass. Usually, Petri dish bottoms are placed against the imaging glass to ensure optimal field depth and, furthermore, to keep condensation from interfering with reads, this is by far the most common approach used in the reviewed bibliography. Only one account of an alternative approach is known to the author[7].

A second matter, critical to image capture, is the use of transmitted or reflected illumination. Transmitted illumination is the most common approach[6,11,13,14,20], it requires use of an illumination panel or a scanner equipped with an illuminating cover. Light captured by the scanner in a transmitted illumination scan travels through the gel media that contains the colonies and onto the CCD sensor (see figure Figure 1.1 C). Reflected light set-ups, whether imaging the top of colonies[7], or their bottom, through the agar[11], have also been used (see Figure 1.1 D). Note must be made that Figure 1.1 A and B depict reflective light set-ups.

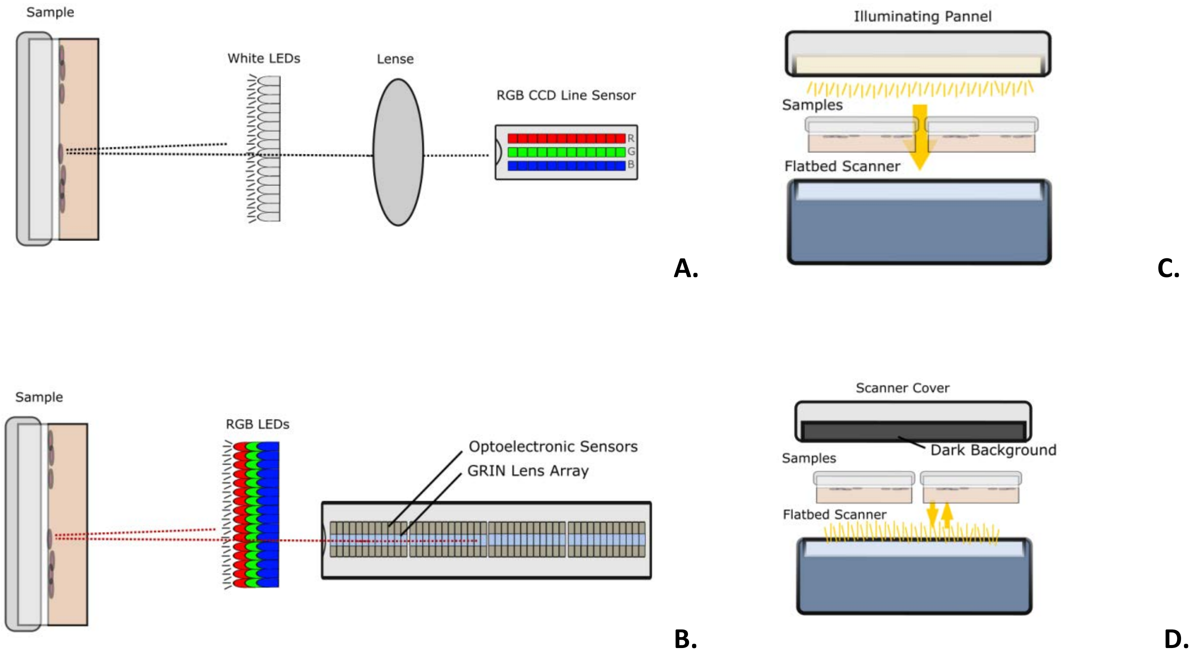

Figure 1.1. A. Schematic depiction of a CCD type scanner. B. Schematic depiction of a CIS scanner. C. Diagram of transmitted Petri dish illumination. D. Diagram of reflective Petri dish illumination.

1.1.2. Image Processing and Analysis of Colonies

Many algorithms have been devised for the enumeration and analysis of colonies in digital images. Algorithms can be based in use of a single endpoint reading or that of several time-series images.

1.1.2.1. End-point Colony Image Processing and Analysis

Currently developed end-point digital colony counting and analysis (EDCCA) software solutions namely rely on the use of an initial thresholding phase in combination with segmentation algorithms that spot overlapping colonies. Furthermore, denoising algorithms are used throughout the process[5]. EDCCA is challenged by several phenomena, colony confluence or overlapping of colonies, image resolution limits, Petri plate irregularity, and growth of colonies with irregular morphologies are some of the most common obstacles[12]. Additionally, matrix-related challenges like the presence of sample debris or pigmentation are frequent.

Marotz proposed grayscale image preprocessing low-pass average filtering, intensity rescaling, and a special cross-based low-pass filtering technique. Next, fuzzy logic-based algorithms were used for colony recognition. Interestingly, Marotz's fuzzy algorithms are meant to be "trainable", thus this constitutes the first example of image learning in the reviewed bibliography[12].

Clarke et al. developed the National Institute of Standards and Technology (NIST) Integrated Colony Enumerator, a Matlab-based colony counting software package (see Table 1.2). In this software, local minima are used to detect colony centers. This approach is suggested as a means to tackle artefactual local contrast changes. Furthermore, this algorithm allows enumeration of overlapping colonies with distinguishable centers. Last, automatic thresholding is applied to the image, all minima which lie below the threshold value are considered valid colonies. A rather unusual characteristic of this algorithm is the absence of a minimum colony size criterion for colony detection[6].

In his program, OpenCFU, Geissman proposes use of image denoising and detection of colonies by means of a score map that highlights regions displaying morphological attributes of a putative circular object, or a set of these. Further processing and analysis of the thresholded score map particles allows to isolate individual colonies or, otherwise, discard colony candidates.

Choudhry developed an ImageJ-based macro (IMJ Edge Macro) that featured initial image processing for image enhancement and denoising followed by Sobel edge detection. Next, thresholding and several denoising algorithms are applied. Binary hole filling and Watershed binary processing gives way to final particle analysis segmentation according to minimal size and circularity criteria (see Table 1.2)[5].

Table 1.2. Main steps in processing and analysis steps for EDCCA featured in several published works.

Publication	Main Processing and Analysis Steps
Clarke et al. (2010)[6]	Grayscale Luminance/Gaussian Smoothing /Minima Analysis/Minima Analysis vs. Threshold Comparison
Geissman (2013)[16]	Channel Median Filtering/Laplacian of Gaussian Subtraction/ Channel Normalization/ Grayscale Merge/ Score Map/ Thresholding
Choudhry (2016)[5]	Denoising/ Edge Detector/ Thresholding/ Denoising and Processing/ Watershed/ Particle Analysis

1.1.2.2. Multipoint Colony Image Processing and Analysis

Clinical laboratories are increasingly incorporating full microbiology lab automation solutions that encompass automated plating, incubation and kinetic imaging technologies [28]. Some reports make accounts of very successful performances of commercially available multipoint systems in the detection of color development in chromogenic growth media [29].

Use of kinetic imaging technologies, in particular, with scanners, has been applied by a number of authors to retrieve data regarding phenotypic growth characteristics of colonies. In these works, authors capitalize on the kinetic aspects of time-series imaging to recover descriptive data of colony growth that might allow isolation of colonies with several goals.

Use of flatbed scanner imaging for clinical colony imaging is restricted to colony growth detection, in the consulted works [9]. Most multipoint colony imaging research carried out with flatbed scanners has concentrated on retrieval of phenotypic characteristics for screening and characterization of genetic variants[11,13,14,20,30]. Large-scale colony tracking of environmental isolates has also been proposed as a means to portray the diversity of growth strategies in a given microbial community in the field of microbial ecology[7]. Meanwhile, other works focus on retrieving particular growth patterns from samples as a means of detecting phenotypic variants [11,30].

1.1.2.3. Processing and Analysis of Chromogenic Plates

Some commercial software programs allow to selectively count colonies based on their color, this is an interesting feature when working with chromogenic or differential media. Examples of such software programs are the QCount (Advanced Instruments, Norwood, MA), and WASPLab (Copan, Brescia, Italy). The Copan WASPLab colony color analysis has been reported to depend on the use of an HSV “bubble-shaped” tolerance level[31]. Thus, this approach allows for sophisticated color recognition.

1.1.2.4. Measures of Colony Color and Related Measurements

Performing absolute measurements of color is a remarkably demanding task. Colorimetry of colonies is a particularly challenging topic as no known regulations or standard practices exist. Despite this, use of color for identification and differentiation of colonies is a very common practice, in particular when using chromogenic media. When validating [32,33] or comparing chromogenic media[34,35] use of qualitative, markedly subjective, color measurement criteria is ubiquitous. Thus, despite the profuse use of chromogenic culture media, at present, no standard procedure has been adopted to measure color development in colonies.

1.1.2.4.1. Grayscale Measurements

Grayscale representations of RGB images allow for a simplified scheme to compare color-derived grayscale values developed by colonies. Grayscale conversion of RGB-based color images simplifies, initially complex, three-dimensional color space attributes into a single dimension. The loss of color information in this process is inevitable. However, this hasn't posed an obstacle to the use of grayscale values to extract color-related conclusions in bioassays[24,36,37].

A great number of grayscale conversion methods exist, often these are used without paying much attention to image capture or imaging device calibration. Grayscale conversion is a matter that commonly gives way to confusions and inconsistencies in the field of digital imaging.

Readers are made weary that a common practice is use of ITU's BT 601-7 luma (L_{601}) formula values to directly convert non-linear sRGB values to luma. The latter is theoretically incorrect as BT 601-7 and its formulas were developed for use with the NTSC RGB space and not sRGB[38,39]. Use of this approach, however, is so widespread that it has become somewhat of a standard, it is therefore considered valid and implemented in the present thesis. ITU's BT 601 is perhaps one of the most common RGB to grayscale conversions, it is referred to commonly as "luminance" [39], it is noteworthy, however, that other sources refer to this same value as "luma"[40,41].

ITU's BT 709 luma (L_{709}) constitutes, in fact, the equivalent conversion of RGB primaries to "luma" values supplied for the RGB standardized primaries for high definition television[42]. These primaries, in fact, coincide with those used in the sRGB color space, perhaps the most widely implemented color space in present-day consumer electronic devices and the standard color space for the internet[43].

A third very common grayscale conversion comes from the use of the Y dimension in the 1931 CIEXYZ color space (see Equation 3.6), also known as "luminance", from here on it will be referred to as "luminance". Thus, readers are cautioned against confusing the latter with luma values for ITU's BT 601-7 (L_{601}) and with ITU's BT 709-6 (L_{709}). Although XYZ luminance is considered a physically accurate measurement it is noteworthy that this measurement isn't representative of the human perception of a color's brightness[40]. Furthermore, XYZ luminance is a linearized value, in order for its comparative use and grayscale representation it is delinearized. Section 3.1.2.3.4 covers all the mathematical procedures involved in the delinearization of XYZ luminance, delinearized luminance is referred to as L'.

Typically, grayscale values are coded in 8-bit grayscales, which assign values that range between 0 and 255 for any given data point, a pixel in the case of conventional digital images. RGB channels in the sRGB color space are also typically assigned 8-bit resolution for each channel. Thus, any given pixel in an sRGB image with these characteristics is assigned 3 coordinates with values ranging between 0 and 255.

A common grayscale conversion of any RGB based image consists in simply using the values for one of its 3 color channels, alternatively, an average of all three channels can be used. The latter will be referred to as channel average grayscale (C_{Avg}). While other grayscales intend to (loosely) represent the human perception of a color's brightness average channel grayscale simply supplies a conversion that assigns equal weights to each channel and is occasionally used[44].

1.1.2.4.2. Colorimetry

Grayscale values can only convey a very limited amount of color-related information. Use of complex color spaces allows more accurate modeling of color. A number of red/green/blue additive color-based systems (RGB) exist. One such color space is sRGB, a widely adopted standard additive RGB-based color space. sRGB is used as a reference color space and it is characterized by a limited color gamut[38].

HSB is a projection of RGB primary color space that is commonly used in the field of digital imaging to retrieve color information. Particularly, HSB is used to retrieve information related to color hue, saturation, and brightness, hence its name (HSB). Each of these corresponds, in fact, to one of the three dimensions that configure the HSB color space. A simple 3-D projection of colors in HSB reveals color data in a remarkably intuitive way[45].

Colorimetric measurements ideally should be performed using absolute colorimetric values in widely adopted color spaces and, at present, this requires the use of color spaces other than sRGB. The International Commission on Illumination (CIE) developed XYZ (CIEXYZ), an absolute colorimetric space, in 1931. It was later followed by CIE's L*a*b* (CIELAB), regulated in 1976 [46].

CIEXYZ and CIELAB device independent color spaces have become somewhat of a standard, especially in the field of digital imaging[47], nevertheless, many alternatives to these two color spaces exist. While CIEXYZ is a device invariant colorimetric color space, CIELAB pursues matching human color perception. The CIELAB color space is derived from CIEXYZ (see Equation 3.11). Essentially, CIELAB comprises a perceptually uniform, nonlinear representation of CIEXYZ. It is important to highlight that the CIELAB color space has no reference white[47]. CIELAB under Illuminant D50, which is the default illuminant recommended in the ICC profile specifications[47], is taken as the preferred CIELAB representation in this thesis.

A widely adopted distance metric to calculate color differences, formally known as ΔE_{ab}, is based in use of CIELAB (see Equation 3.13). Some authors suggest use of a threshold of 3 as a hardly perceptible ΔE_{ab} difference, this is technically referred to as a just noticeable difference[22]. Indeed, the just-noticeable difference intends to account for the minimum perceptible difference between two given colors.

1.1.2.5. Metrological Considerations

Many colony-related metrics have been studied in the past[48]. Most of these are specific to the work of certain authors and lie far from widespread use. Beyond CFUs and concentrations of these per unit mass or volume[49,50], no standardized measurement metrics exist in relation to colonies in the reviewed bibliography.

According to the Bureau Internationale des Poids et Mesures (BIPM), measurement accuracy is defined as the “closeness of agreement between a measured quantity value and a true quantity value of a measurand”[51] (see Figure 1.2). Measurands are defined by the BIPM as the quantity that intends to be assessed during a given measurement. Unlike measurement accuracy, measurement precision doesn’t require the establishment of a true value as it measures “closeness of agreement between indications or measured values obtained by replicate measurements on the same or similar objects under specified conditions”, as stated in the BIPM metrological vocabulary compendium[51] (see Figure 1.2). In scenarios with a lack of standards for comparison, the accuracy of the metrics being studied can’t be measured, as no true quantity values are available for comparison with measured values.

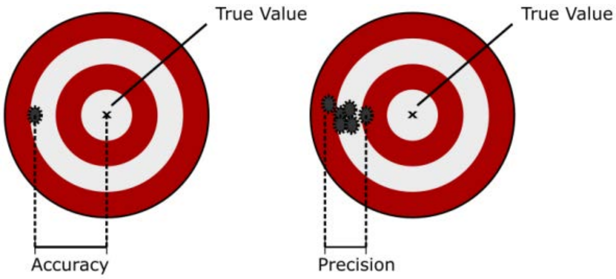

Figure 1.2. Bull's eye diagrams exemplifying accuracy and precision.

Typically, precision is expressed numerically through standard deviation and it encompasses reproducibility and repeatability [51,52]. Both of these are usually measured in terms of the standard deviation of a series of measurements. The NIST suggests use of the term uncertainty in place of standard deviation when referring to the measurement of precision, and proposes a number of approaches to measuring it[53]. Experimentally determined uncertainty is known as type A uncertainty, it is commonly used to assess uncertainties of measurements under given conditions in a lab.

In the present work, repeatability constitutes a measure of the closeness of agreement between successive measures of a given sample under identical conditions. Meanwhile, reproducibility assesses closeness of agreement between measurements of the same sample under different conditions. Repeatability and Reproducibility make reference to values obtained from a single sample or samples that are esteemed to have identical values of a measurand and identical properties in any matter that might affect the measurement of the measurand[51]. It is important to remark that, given the non-destructive nature of employed techniques, the definition of repeatability undertaken in the present work doesn't include repeated sampling, thus, it ignores sampling uncertainty[54].

1.2. Gel-Based Microbial Growth Media

The current work uses the term gel-based media to refer to culture media that contain gelling agents. Gel-based media encompass widely used and universally available agar media, which have been present in the field of microbiology for many years[55,56], and a more recent generation of media which is simply referred to as “alternative media”. Both alternative and agar-based media are meant to foster growth of colonies [57,58].

Advantages of the use of alternative media encompass long expiry dates and readiness to be used as shipped. This greatly differs from agar media which are usually served in the shape of dry powders that must be duly processed. Prepoured agar-media Petri plates are also available; these have short expiry dates and are remarkably more bulky for storage than alternative media. Additionally, most alternative media don’t require the use of means to spread inocula over the plate surface.

A number of alternative media are commercially available, the present work, however, will focus exclusively on Sanita-kun AC Plus media (JNC Corporation, Tokyo) and the Filmplate Bacteria Colony Count plate (Guangdong Dayuan Oasis Food Safety Technology, Guangzhou, China), onward these will simply be referred to as Sanita-kun and Filmplate, respectively. Variants of these media allow enumeration of different microorganism groups[59–61]. The versions of the plates covered in this work, as mentioned, will be limited to general purpose heterotrophic count Sanita-kun and Filmplate plates.

Very little information is available regarding the composition of Filmplate media. Filmplate is known to contain a gelling agent and 2,3,5-Triphenyltetrazolium Chloride (TTC) chromogen (section 1.2.1.1 introduces this chromogen). Use of chromogens in alternative media is particularly important. Alternative media usually contain a growth pad that is opaque and whitish, thus, in absence of chromogens, colonies grown in such pads would not be readily distinguishable. Sanita-kun plate formulations include three tetrazolium dyes (section 1.2.1.1 introduces these), according to the consulted bibliography, one of these dyes is TTC the nature of the other two remains undisclosed[58]. However, they are known to be tetrazolium dyes, and general characteristics of these are fairly well characterized (see section 1.2.1.1). Filmplate media also contain basic nutrients presumed to be similar to those of any generalistic growth media, such as trypticase soy agar, for instance.

The general structure of studied alternative media is featured in Figure 1.3. Note is made that whereas the structure of Sanita-kun plates is depicted according to accounts present in a commercial presentation[62], that of Filmplate remains unknown. Briefly, Sanita-kun plates feature two bottom impermeable plastic layers that isolate the growth pad from its surroundings, these layers are topped by a layer that contains the chromogens, nutrients, and the gelling agent. A very similar structure is presumed to exist in Filmplate consumables. While Filmplate growth pads are made out of paper, those of Sanita-kun are made out of non-woven fabric.

Once inoculated, growth pads diffuse water throughout their whole extension, Chisso corporation claims that, next, a viscous phase, apparently generated in the layer that contains the gelling agent, is released, effectively pushing bacteria upwards onto the growth pad’s surface, rendering colonies formed readily visible when they reduce the chromogenic dyes[62].

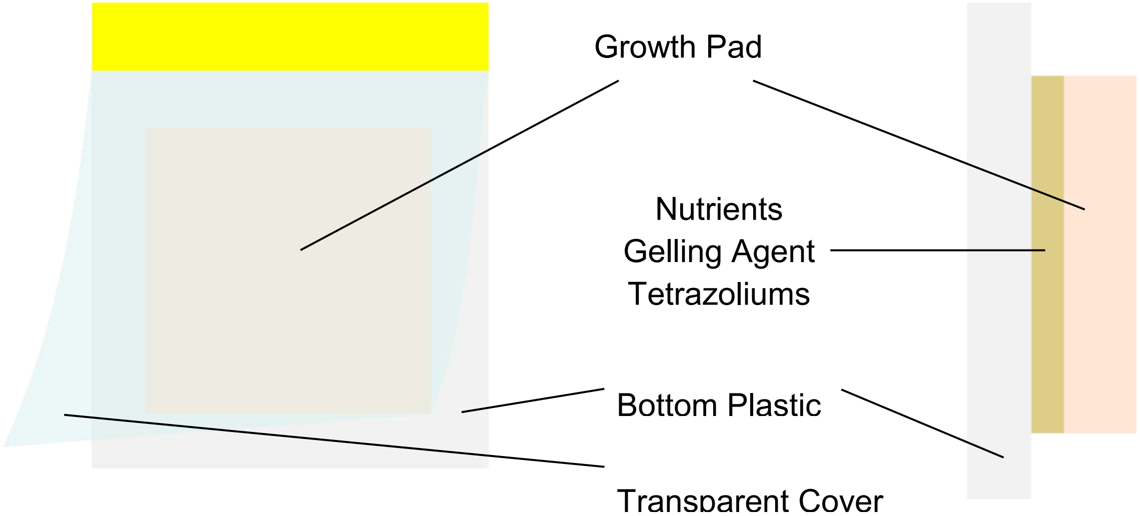

Figure 1.3. Diagram depicting the main structure of Filmplate and Sanita-kun components. Note is made that, in the case of Filmplate consumables, the nutrients and chromogen might be present in the growth pad, instead of the bottom layer.

1.2.1. Chromogens in Gel-Based Microbial Growth Media

The use and study of chromogens in microbiological agar-based media are profuse. Colonies of microorganisms that cleave the chromogenic moieties of substrate molecules, or modify these otherwise, develop distinct colors. This characteristic has been used in many microbiological media, in order to differentiate or identify colonies of certain microorganisms[57].

While some researchers have focused their efforts on the development or validation of a given chromogenic media formulation [32,33], others have delivered parallel comparisons of several media and substrates[34,35].

1.2.1.1. Tetrazolium Chromogens

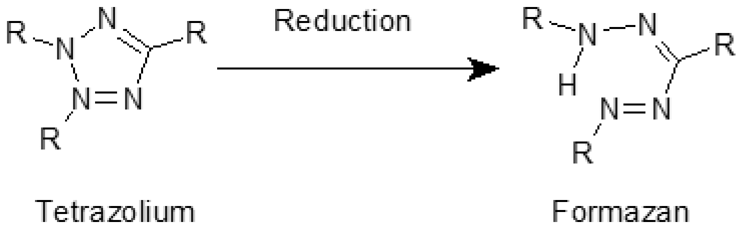

Figure 1.4. General tetrazolium reduction reaction.

Tetrazolium salts are widely used as biological reagents. Their unique properties depend on a positively charged quaternary tetrazole ring core; this central structure is surrounded by three aromatic groups. Disruption of the tetrazolium ring during reduction of tetrazolium molecules induces the formation of formazan molecules (see Figure 1.4), this is accompanied by marked color development. Many tetrazolium compounds have been successfully implemented in bioassays, displaying varying degrees of toxicity and color development[63]. It is believed that respiring bacteria reduce tetrazolium dyes in their electron transport chain, however, the exact point within the electron transport chain where this occurs is still a rather disputed topic[64].

An interesting characteristic of tetrazolium dyes is that they successfully develop color in colonies of bacteria of many different taxa, this has led to their use in many culture media.

Some authors have reported TTC-color development deficiency in colonies of certain microorganisms, frequency of the color development deficiency was reported to be remarkably higher amongst Gram-positive bacteria[65]. Tetrazolium salts are known to inhibit Gram-positive bacteria growth, in fact, this property is used in the formulation of Lactose-TTC agar [66]. Toxicity of tetrazolium salts on Gram-negative bacteria has also been reported[67]. Accounts of tetrazolium-induced toxicity reduction by means of culture media additives have been made in *Salmonella spp.*[67] and *Listeria monocytogenes*[68].

Despite the existence of exceptions in color development, tetrazolium dyes are generally considered very flexible chromogenic dyes and their use ranges from microbial identification systems[69] to general media for microbiology. Despite its toxicity for Gram-positive microorganisms, TTC is present in commercial formulations intended for detection and differentiation of Gram-positive microorganisms such as KF *Streptococcus* agar [55], proving the eligibility of this reagent for use with Gram-positive microorganisms. The possibility of using tetrazolium salts to mark colonies of microorganisms that belong to a wide array of taxa has also been exploited in alternative microbiological media[58,70–73].

Accounts of the use of TTC to enhance the contrast between bacterial growth regions and surrounding media in digital images have been made by several authors both for opsonophagocytic killing assays[74] and for regular colony enumeration[6,75].

1.3. Full Body Lotion Cream as an Inhibitory Matrix Model

The present work covers the effects of a full-body lotion cream on the performance of tested media. Its formulation is rather Standard, with two boosting agents, ethylhexyl glycerin, and tetrasodium glutamate diacetate, these enhance the performance of a single main preservative, phenoxyethanol.

Phenoxyethanol, a common solvent present in many cosmetic formulations, can be used as a preservative. Its presumed mechanism of action is the solvation of hydrophobic molecules in the cell membrane, this compromises membrane integrity, and derives in cell lysis[76]. Some authors, however, suggest the existence of diverse effects that depend on the compound's concentrations[77].

Tetrasodium glutamate diacetate is a chelant, thus it captures Ca^{+2} and Mg^{+2}, resulting in the destabilization of microbial cell walls. The latter is thought to facilitate entry of preservatives inside microorganisms, thereby increasing the preservative activity of these[78].

The mechanism of action of the potentiation induced by ethylhexylglycerin has been well documented in *Escherichia coli*. Ethylhexylglycerin displays a strong interaction effect with phenoxyethanol that potentiates its effect through damage of the cell membrane integrity[77].

Common practices in the cosmetic microbiology laboratory, as reproduced in the present work, encompass cosmetic preservative neutralization before sample testing[76,79]. Neutralization is usually tested as its performance may vary depending on employed preservation approaches. Recommended neutralization practices for cosmetics preserved with phenoxyethanol encompass dilution in Letheen broth. Dilution of the matrix as a means of neutralization is also a widely employed approach[80], this, however, limits the lower enumeration limits of a sample's contamination.

1.4. ImageJ, FIJI and the ImageJ Macro Language

ImageJ is an image processing and analysis software designed by the U.S.A.'s National Institute of Health for use in bioimaging. ImageJ supplies a very simple graphical user interface (GUI) and basic functions to display and save images in a wide number of formats. Furthermore, basic image-processing functionality is coupled with powerful extension mechanisms[44]. Its most remarkable trait is, indeed, its great scalability; numerous extensions can be added or removed to the core software, these consist of plug-ins and macros. A very active user community supplies constant contributions that build on all previously available functionalities[81,82].

FIJI is simply a distribution of ImageJ. Despite retaining ImageJ's simple GUI (see Figure 1.5), FIJI uses powerful plug-in libraries that enable rapid prototyping of fairly advanced image-processing algorithms[45]. A very remarkable trait of FIJI is its seamless automated updating system, this allows to dynamically enhance the plug-ins that have originated from numerous sources and eases schemes of productive collaboration, improving upon ImageJ growth capacities and fostering the constant growth of available plug-ins and macros [82].

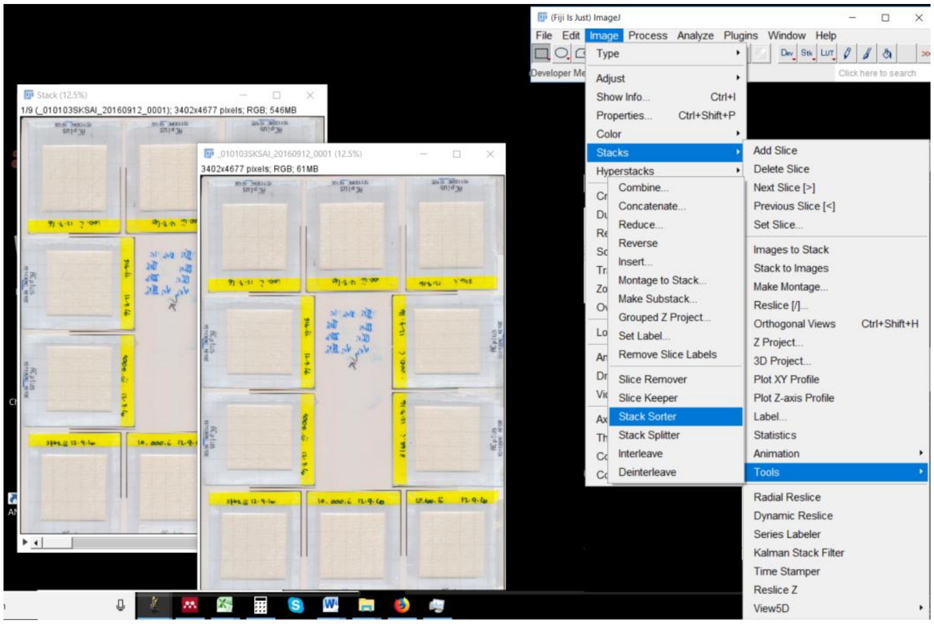

Figure 1.5. Screenshot featuring FIJI's GUI.

ImageJ's macro language (IJM) is rather powerful and well developed. Many advanced functionalities of ImageJ can be readily accessed through IJM, moreover, many plug-ins can be controlled employing this macro language. Thus, IJM allows piecing together powerful scripts that can be implemented in algorithmic prototyping without requiring deep knowledge of any programming environment[83,84].

1.5. Fourier Transformation of Images

Fourier transformation (FT) of images allows conversion of image signals from the spatial domain (i.e. a regular image) into a frequency domain. Use of this function in signal analysis is very common[40]. Although the complexity of the mathematics underpinning this transformation lies beyond the scope of the present work, several insights of its use and implementation that are applicable to image processing are hereby addressed.

FT converts available data through a complex function that is constructed with a number of sine and cosine waves. Although rather unintuitive at first glance, analysis of the intensity fluctuations in many images readily evidences the validity of a sinusoid-based representation of images. Figure 1.6 shows the grayscale intensity plot of an image transect, it is readily apparent in the intensity plot that the image can be considered as an overlap of a number of waves of varying amplitudes and wavelengths.

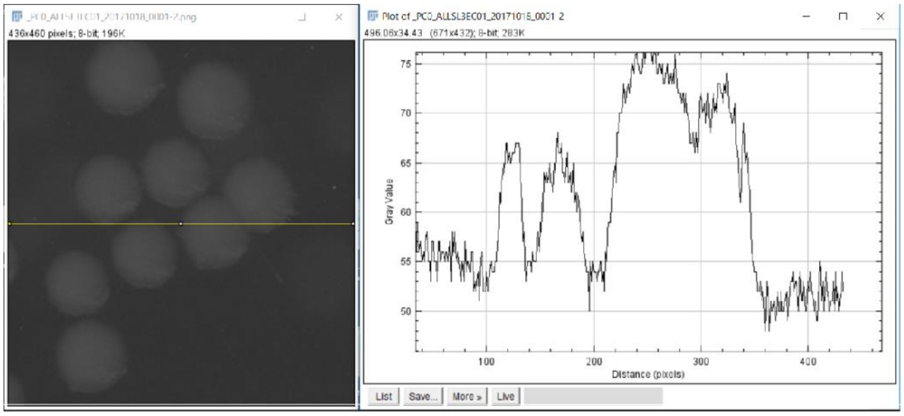

Figure 1.6. Partial screenshot of an 8-bit image of a group of colonies and the grayscale value intensity plot of a transect of the image. The plotted transect is featured in yellow.

The so-called power spectrum of FT is commonly used to process images (see Figure 1.7 for an example of a power spectrum). Power spectrums represent images in a frequency domain, allowing to filter image frequency-related aspects. Pixels of a power spectrum represent several aspects of the FT. The location of a given pixel in a power spectrum relates to the frequency of the sines and cosines that it represents. Low-frequency sines and cosines, that is ample wave sines and cosines, are represented by pixels that lie close to the image's central point. Conversely, high-frequency features, corresponding to spatial domain features with high variations, such as edges, appear in the periphery of the power spectrum. The value of a given pixel in a power function indicates the wave amplitude of the sinusoid functions associated with it. Furthermore, the particular angle at which a given pixel is located in a power spectrum indicates the spatial domain image angle at which the image intensity fluctuations take place.

Figure 1.7 displays a spatial domain image and its corresponding FT-derived power spectrum image. At first glance, the information supplied by a power spectrum image might seem unintuitive. It is however evident that a number of light spots can be distinguished from the general image. These spots very likely correspond to features in the image with a rather periodic appearance and a particular angle of orientation[40].

An FT of a spatial domain image can be easily calculated through a Fourier transform (also known as Fourier Forward Transform). Every single element of a Fourier transform and its spatial domain counterpart can be easily calculated without any loss of information through the Fourier Reverse Transform. The combination of these two properties of FTs, that is the availability of forward and reverse transforms, together with the lack of information loss during these, indeed confers FT great power and flexibility in many applications. Many image processing techniques capitalize on the use of FT forward and reverse transforms to process aspects of images related to the frequency domain. FT is particularly useful in contrast enhancement and clipping and stretching operations[85].

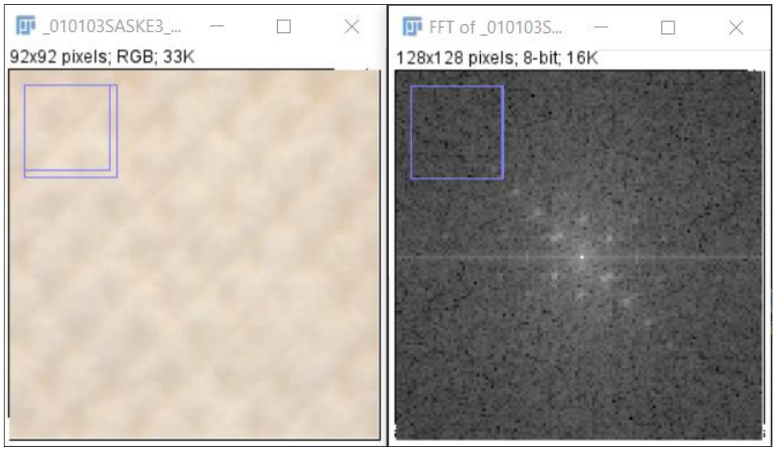

Figure 1.7. Partial screenshot of a Sanita-kun media that confronts a brightness domain image with its Fourier transform power spectrum in FIJI.

2. OBJECTIVES

This thesis pursues an assessment of microbiological media performance by means of image analysis. It addresses the study of colonies in both traditional agar-based media and alternative microbiological growth media. Means to assess growth media performance in terms of the color development of colonies, rapidity of colony detection, and colony enumeration will be developed and confronted with a microbial stress model based on cosmetic matrix addition to samples.

3. MATERIALS AND METHODS

3.1. Colony Colorimetry and Grayscale Measurements

3.1.1. Calibration Target Analysis

3.1.1.1. IT8 Patch Color Homogeneity

Visual inspection of IT-8 calibration target images following their ICC profile attachment and sRGB conversion (see section 3.1.2.2), allowed to establish possible non-homogenous color patterns in the calibration target color patches. Basic image processing techniques such as the use of contrast enhancement, sharpening, and median filtering were applied to highlight existing patterns. Further characterization of color homogeneity in the patches was achieved using 3-D surface plots of CIELAB Luminance (L*) channel images, this proved to be a simple and effective mean to characterize noise in images, such noise could be clearly viewed as crests and troughs in the Luminance plot. All image processing and visualization were performed using FIJI[82], an ImageJ[81] 1.51 distribution.

3.1.1.2. IT8 Patch Color Inspection

Visual inspection of IT-8 calibration target images following their ICC profile attachment and sRGB conversion (see section 3.1.2.2). This analysis concentrated on the IT-8 target color patches that appeared to be somewhat similar in color to the colonies that were being imaged during the agar-based media experiments, thus, these were mostly dark patches of brown, red, blue, and purple colors (i.e. patches in columns 1-4 of rows A-C and J-L of the IT-8 target). Patches that would be analyzed were simply selected and analyzed using the Color Inspector 3-D plug-in [86] for FIJI[82], images were viewed under the HSB projection of the sRGB values of the images, this proved to be convenient to qualitatively assess the performance of the calibrated scanners.

3.1.2. Colony Color and Grayscale Values in Agar Media

3.1.2.1. Media, Reagents, and Plating

Respectively, solutions of 1.5% triphenyl tetrazolium chloride (TTC; Alfa-Aesar, Ward Hill (MA), USA) and 2.5 % tetrazolium violet (TV; Sigma-Aldrich, Saint Louis, MO) were prepared and filter sterilized in a PBS solution prepared from PBS tablets (AMRESCO, Solon, Ohio, USA).

Modified Letheen agar (LA) and modified Letheen broth dehydrated media (both from Merck, Darmstadt, Germany) were prepared according to manufacturer specifications with polysorbate 80 (Reactivos Para Diagnóstico, Sentmenat, Spain). During the preparation of additional agar media, following autoclaving, bottles were kept in a water bath at 60ºC. Next, aliquots of the tetrazolium solutions were added in order to obtain concentrations of 2.24 µM TTC, 1.12 µM TTC, and 0.56 µM TTC and 1.12 µM TV, 0.56 µM TV, and 0.28 µM TV, respectively. All agar media were plated into 90 mm Petri plates. The note is made that when mentioned throughout the present work, unless specified otherwise, “TTC media” and “TV media” will always refer to the high concentration media formulations (2.24 µM TTC and 1.12 µM TV, respectively).

Unless specified otherwise, strains were kept in 20 % glycerol (Labbox Labware, Vilassar de Dalt, Spain), in PBS solution, prepared from PBS tablets (AMRESCO, Solon, Ohio, USA), vials were stored at -20ºC. A *Pseudomonas aeruginosa* CECT 110 1R (CECT, Paterna, Spain) primary culture vial was stored according to supplier specifications. *Escherichia coli* NCTC 9001, *Staphylococcus aureus* CECT 240, and *P. aeruginosa* CECT 110 were streaked directly from their cryovials onto LA plates and incubated overnight at a temperature of 37 ºC. A single overnight colony was picked and inoculated onto a falcon tube containing 5 ml of modified Letheen broth and vortexed. Once inoculated, vials were incubated for 2.5 h, 4 h in the case of *P. aeruginosa* vials. Three such replicate samples were created for each microorganism. Incubation always took place at 37 ºC, while tubes were agitated at 220 RPM. 550nm absorbances of the cultures were measured using a UV mini 1240 spectrophotometer (Shimadzu, Kyoto, Japan), broth CFU concentrations were calculated according to linear regression (data not shown). Samples were then diluted to achieve a concentration of $5\cdot10^4$CFU/ml. Aliquots of each diluted sample were then spiral plated twice in LA, and high concentration TV and TTC media, respectively, using an Eddy Jet 2 spiral plater (IUL, Barcelona, Spain). In order to characterize the technique and to establish chromogen concentration-grayscale development relationships, a second experimental set-up featured three *E. coli* replicates and duplicate spiral plating in all seven media (LA and low, medium and high concentration TV and TTC media, respectively).

Spiral plates were incubated at 37ºC. Plates were imaged after 16 h and 48 h of incubation, respectively. During reads, plates were removed from their incubation ovens for a period of time that never exceeded 1 hour.

3.1.2.2. Scanner Calibration, ICC Profiling, and Imaging

R1 IT 8.7/2 Reflective Scanner Targets (Wolf Faust, Frankfurt, Germany) were used to create Scanner ICC profiles using CoCa, Color Camera Calibrator, software version 1.9.7.6 (Andrew Stawowczyk Long, 2011).

All plates were scanned at a resolution of 1200 DPI using a CanoScan 9000F Mark II scanner (Canon, Ota, Japan), from now on this scanner will be referred to as CanoScan, images were saved, unprocessed, in PNG files.

Interior covers of scanners were coated with Iris 38 black smooth paper cardboard (Canson, Annonay, France). During all scans, lids remained closed, and six plates were imaged simultaneously, with their bottoms oriented towards the scanning area, using a plate layout of three rows with two plates each. Obtained images were first submitted to an image processing phase, followed by an image analysis phase.

Interscanner reproducibility tests featured an Epson Perfection V39 scanner (Epson, Tokyo, Japan), an OpticSlim2610 scanner (Plustek, Taipei, Taiwan), and three additional CanoScan 9000F Mark II scanners, including scanner 1. Interior covers of scanners were covered with Iris 38 Black smooth paper cardboard (Canson, Annonay, France). During all scans, six plates were imaged simultaneously, allowing for a layout of three rows with two plates each

Photoshop CC 2018 (Adobe, San José, California, United States) was used to transform images into sRGB (sRGB IEC 61996-2.1 profile in Adobe Photoshop), using the ICC profiles created for every scanner during calibration. The rest of image processing and analysis was carried out in FIJI [82], an ImageJ 1.51n [81] distribution.

3.1.2.3. Colony Segmentation and Analysis of Colony Color

3.1.2.3.1. Segmentation of Colonies

Each of the plates in the images was closely cropped and separated into an individual image for analysis. Areas with irregular lighting due to Petri plate edge gleaming were manually removed from images. Red channel manual thresholding was used to select areas where growth took place. In places where thresholding didn’t successfully separate growth areas, these were added manually.

48 h low inoculum plates from *P. aeruginosa* cultures featured heavily spread colonies, selection of these in TC and TV plates was achieved by means of green channel thresholding. Respectively, 48 h low inoculum plates from *P. aeruginosa.* culture LA plates were red-channel thresholded and particle filtered according to size (450-150000

px^2) and circularity (0.4 -1.0). Only central regions of colonies were segmented due to their spreading.

Following segmentation, binary masks were created. These masks were tweaked with case-specific erosion and dilation operations in order to accurately match growth areas. Finally, standardized smoothing was applied to all images, briefly, two consecutive erosion iterations, 3 dilation iterations, Gaussian blurring ($\sigma = 2$), and Otsu autothresholding were applied, giving way to analysis masks. Analysis masks were used to generate analysis images, these solely featured a foreground with selected colonies or continuous (lawn) growth regions, elsewhere, the color was set to black.

3.1.2.3.2. Color Data Retrieval and Processing

Plate images were analyzed individually. 48 regions of interest (ROI) were analyzed, each accounted for a particular spiral wedge (there are 8 symmetrical wedges in total) and ring (there are 6 rings in total) of the spiral plating grid[87]. An additional combined analysis selected the 8 ROIs of each of the 6 rings, allowing for retrieval of global data for each ring. Thus, in total, 48 ROIs were analyzed for each plate. Each ROI was individually selected and submitted to RGB channel data retrieval. RGB channel (R', G', and B') average values were taken for each of the 48 ROIs. Since available images had already been assigned an ICC profile and converted to the sRGB color space, sRGB channel data for each sampled area could be employed to carry out pertinent colorimetric color space transformations. Color data processing throughout all experiments required the use of average values, wherever the present work makes reference to “average values” the procedure that was carried out always encompassed transformation of every data point that was analyzed to a given grayscale or color space. Next, further processing and analysis of the data were carried out. This approach allowed to extract statistical data based on the grayscales and color spaces that were studied and not on ultimate conversions of general average RGB values for a data set.

3.1.2.3.3. Color Space Conversions and Color Distance Calculations

All calculations were performed in Microsoft Excel 2010 (Microsoft, Seattle, Washington, USA), using user-defined functions. Functions were coded according to the equations that are supplied in the present section of this work. Appendix I of the present work features the exact VBA functions that were implemented and adds notes regarding the origin of the values in the formulas and critical factors that must be kept in mind when implementing the functions. Input values consisted of three channel 24-bit sRGB images thus each channel could have a range of integer values that ranged from 0 to 255.

3.1.2.3.4. Grayscale Conversions

sRGB values were used to calculate C_{Avg}, L_{601}, L_{709}, and L'. C_{Avg} was simply calculated by averaging the three sRGB channels (R', G', and B'; see Equation 3.1).

$$\boldsymbol{C_{Avg} = \frac{R'}{3} + \frac{G'}{3} + \frac{B'}{3}}$$

Equation 3.1.

L_{601} was calculated according to NTSC Recommendation 601 (see Equation 3.2)[39]. It is important to highlight that the conversion featured in Equation 3.2 was originally implemented to calculate image luma in the NTSC RGB space, since then, this very formula, with the same weights for each channel, has been widely used with sRGB inputs. It is, in fact, the default RGB to grayscale conversion in the ImageJ software. Although rather unorthodox, its use with sRGB inputs has become profuse enough to consider it a standard practice.

$$L_{601} = 0.299 \cdot R' + 0.587 \cdot G' + 0.114 \cdot B'$$

Equation 3.2.

L_{709} of each average sRGB set was calculated according to specification NTSC Recommendation 709 (see Equation 3.3)[42].

$$L_{709} = 0.309 \cdot R' + 0.609 \cdot G' + 0.082 \cdot B'$$

Equation 3.3.

Any of the grayscale conversions reviewed so far simply establishes respective weights for all channels which are then summed. Calculating delinearized luminance, *L'*, required linearization of all three sRGB channels, this was achieved through function f_2, featured in Equation 3.5. Note must be taken that *v*, in Equation 3.4, represents linear values, on a scale from 0 to 1. Meanwhile, in Equation 3.5 delinearized channel values, in a 0 to 255 8-bit scale, are represented by *V*. Equation 3.4 delinearizes the weighted sum of values featured in Equation 3.6. Thus, Equation 3.6 features the entire calculation of luminance, including individual channel linearization with f_2 (Equation 3.5.), the weighted sum of individual linearized channels, and delinearization of the sum with function f_1 (Equation 3.4.)[40].

$$f_1\,(v) = \begin{cases} 12.92 \cdot v & \text{if } v \leq 0.0031308 \\ 1.055 \cdot (v)^{1/2.4} - 0.055 & \text{otherwise} \end{cases}$$

Equation 3.4.

$$\boldsymbol{f_2\,(V) = \begin{cases} \dfrac{V}{3295} & \textbf{if } V \leq 0.04045 \\ \left(\dfrac{V}{269} + 0.05213\right)^{2.4} & \textbf{otherwise} \end{cases}}$$

Equation 3.5.

$$\boldsymbol{L' = 255 \cdot f_1\,(0.2125 \cdot f_2(R') + \ 0.7154 \cdot f_2(G') + \ 0.072 \cdot f_2(B'))}$$

Equation 3.6.

3.1.2.3.5. Color Space Conversions

sRGB values were converted onto CIE's 1931 XYZ color space under a reference D50 illuminant. This required conducting several conversions in order to achieve a full-color conversion and chromatic adaptation to the new illuminant. The conversion to the destiny color space was performed according to IEC 61966-2-1:1999, as detailed by Burger[40], conversion matrix (M_C) values, however, were sourced elsewhere. A full-color space and illuminant conversion matrix (M_C) was obtained from a reputed digital imaging webpage[88] (see Equation 3.7). sRGB R', G' and B' channel 8-bit values were linearized through equation f_2 (see Equation 3.5) *and* translated to a single-column matrix (M_{rgb}), as explicated in Equation 3.8. Last, the chromatic conversion formula featured in Equation 3.9 is implemented to obtain the final $\mathrm{XYZ_{D50}}$ value. Thus, calculated CIEXYZ values utilized in this thesis al refer to $\mathrm{XYZ_{D50}}$, that is CIE's 1931 XYZ values under illuminant D50, onward these will be simply referred to as $\mathrm{CIEXYZ_{D50}}$. This notation intends to avoid confusion with standard CIEXYZ values which should use a reference E illuminant.

$$\boldsymbol{M_C} = \begin{pmatrix} \mathbf{0.438495} & \mathbf{0.357580} & \mathbf{0.180423} \\ \mathbf{0.212671} & \mathbf{0.71516} & \mathbf{0.072169} \\ \mathbf{0.019334} & \mathbf{0.119193} & \mathbf{0.950227} \end{pmatrix}$$

Equation 3.7.

$$\boldsymbol{M_{rgb}} = \begin{pmatrix} \boldsymbol{f_2\,(R')} \\ \boldsymbol{f_2\,(G')} \\ \boldsymbol{f_2\,(B')} \end{pmatrix} = \begin{pmatrix} \boldsymbol{r} \\ \boldsymbol{g} \\ \boldsymbol{b} \end{pmatrix}$$

Equation 3.8.

$$\begin{pmatrix} \boldsymbol{X_{50}} \\ \boldsymbol{Y_{50}} \\ \boldsymbol{Z_{50}} \end{pmatrix} = \boldsymbol{M_C} \cdot \boldsymbol{M_{rgb}}$$

Equation 3.9.

Calculations of the CIELAB color space converted coordinates were conducted according to Burger [40]. Values for the X, Y and Z channels, were obtained as featured in Equation 3.7 through Equation 3.9. X, Y, and Z input values were first delinearized with Equation 3.10. Next, the delinearized counterpart values were used to calculate, respectively, the L*, a*, and b* values employing Equation 3.11. Delinearized values were indicated with a prima superscript (X', Y', and Z'). Note is made that, regularly, Equation 3.10 input values are obtained as a ratio between the origin-space illuminant and the destination space referent illuminant XYZ values. Nevertheless, since XYZ$_{\mathrm{D}}$~~$_{50}$~~ values are used as input, and CIELAB under illuminant D50 is taken as the pursued destination space no such ratio needs to be implemented.

$$\mathbf{C}' = \begin{cases} \mathbf{c}^{1/3} & \textbf{if } \boldsymbol{c} > \mathbf{0.008856} \\ \mathbf{7.787} \cdot \mathbf{c} + \dfrac{\mathbf{16}}{\mathbf{116}} & \textbf{otherwise} \end{cases}$$

Equation 3.10.

$$\begin{pmatrix} \boldsymbol{L}^* \\ \boldsymbol{a}^* \\ \boldsymbol{b}^* \end{pmatrix} = \begin{pmatrix} \mathbf{116} \cdot \boldsymbol{Y}' - \mathbf{16} \\ \mathbf{500} \cdot (\boldsymbol{X}' - \boldsymbol{Y}') \\ \mathbf{200} \cdot (\boldsymbol{Y}' - \boldsymbol{Z}') \end{pmatrix}$$

Equation 3.11.

3.1.2.3.6. Grayscale Delta Metric

A simple measure of the difference in grayscale values (Δ_{Gray}) was used, it simply consisted in the subtraction of two given grayscale values (g_1 and g_2, see Equation 3.12).

$$\boldsymbol{\Delta_{Gray}} = \boldsymbol{g_2} - \boldsymbol{g_1}$$

Equation 3.12.

3.1.2.3.7. CIEXYZD50 and CIELAB Color Distance

CIELAB distance was calculated according to the standard CIE 1976 color distance (ΔE^*_{ab}) formula, this is simply a Euclidean distance calculation in the CIELAB color space (see Equation 3.13). During colony color distance calculations, given that comparisons were made with the color of LA control media colonies, an average value for each of the three CIELAB dimensions was calculated for colonies in the areas that were being analyzed. This allowed calculating color differences of every individual tested area with the reference control media colony average, including control areas.

$$\Delta E_{ab} = \sqrt{(\mathbf{L}_2^* - \mathbf{L}_1^*)^2 + (\mathbf{a}_2^* - \mathbf{a}_1^*)^2 + (\mathbf{b}_2^* - \mathbf{b}_1^*)^2}$$

Equation 3.13.

Similarly, a Euclidean distance calculation of color coordinates was used to calculate color differences in the CIEXYZ$_{D50}$ color space (see Equation 3.14).

$$\Delta_{XYZ} = \sqrt{(\mathbf{X}_2 - \mathbf{X}_1)^2 + (\mathbf{Y}_2 - \mathbf{Y}_1)^2 + (\mathbf{Z}_2 - \mathbf{Z}_1)^2}$$

Equation 3.14.

3.1.2.4. Dye-Microorganism Assays

A comparative assessment of the effects of two chromogenic dye media formulations, TTC media, and TV media was carried out on *E. coli*, *P. aeruginosa*, and *S. aureus* colonies. Media preparation, microorganism culture, sample plating, and image capture were all carried out as documented in section 3.1.2.1. LA media results were used as control values. Data analyzed in this assay featured retrieval of the average sRGB channel values for each of the six spiral ROI crowns. Each experiment was repeated three times, each replicate featured plating of two plates per media type.

Retrieved data was respectively converted to C_{avg}, L_{601}, L_{709}, L', CIEXYZ$_{D50}$ and CIELAB as specified in section 3.1.2.3.3. Grayscale values of chromogenic plates were compared to LA control plates through the Δ_{Gray} metric when using grayscale values. Color Euclidean distances with control media were computed using Δ_{XYZ} (see Equation 3.14) and ΔE_{ab} (see Equation 3.13) when using CIEXYZ$_{D50}$ and CIELAB values, respectively. Plates were imaged twice, at 16 h and 48 h. Grayscale values were reviewed through box and whisker plots of absolute grayscale values and bar graphs of Δ_{Gray} metrics at different time points.

In between reads color development in TTC media was assessed in each model microorganism. To this end, a paired one-tail t-test for assessment of color development was used. Sample average grayscale values for each of the six spiral plate crowns were hereby compared. All tests were conducted using a significance level of 0.05 in Microsoft Excel 2010 (Microsoft, Seattle, Washington, USA), using the Real-Statistics add-in (Charles Zaiontz, 2016).

While results obtained using grayscale conversions were reviewed using a simple box and whisker charts and bar graphs, tridimensional data generated by the colorimetric conversions was analyzed employing the Color Inspector 3-D plug-in[86] for FIJI[82]. Two sRGB colony color pallets were created by retrieving average CIELAB and CIEXYZ$_{D50}$ values, respectively, and converting them back to the sRGB space, these conversions were performed using Bruce Lindbloom's web-based CIE Color Calculator (available online at http://www.brucelindbloom.com/index.html?ColorCalculator.html). The color pallets were generated using Microsoft Paint v.1709 (Microsoft, Seattle, Washington, USA). CIELAB sRGB-converted color palette values were then opened in FIJI and plotted using the Color Inspector plug-in to plot an HSB plot, for qualitative analysis. CIELAB plots were next used to obtain truly colorimetric 3-D plots. Similarly, the CIEXYZ$_{D50}$ sRGB palette was analyzed using CIEXYZ plots.

Average CIEXYZ$_{D50}$ and CIELAB values were used to calculate, respectively, ΔE_{XYZ} and ΔE_{ab} color difference values between every combination of microorganism, time of image capture and media type. A relevant difference threshold level was established to analyze values obtained with ΔE_{ab} metric, it was chosen arbitrarily and set to 5. Readers are referred to section 5.2 for a brief discussion regarding the use of this value and its implications. Obtained results were placed in a table and a heat map was created using the Microsoft Excel (Microsoft, Seattle, Washington, USA) default color scale function.

3.1.2.5. Media Performance Assays

To assess the performance of different concentrations of chromogen on *E. coli* colonies a media performance assessment was conducted. Color development induced by two chromogens TTC and TV was tested using three chromogen concentrations. Media preparation, microorganism culture, sample plating, and image capture were all carried out as documented in section 3.1.2.1. A single image capture of the plates was performed at 16 h. Three replicate tests were carried out and each sample was plated twice in every tested media formulation, including control LA media. Data from each 8th sector of the third crown of the spiral plates were then retrieved and converted, respectively, to each of the studied grayscale and color spaces.

3.1.2.5.1. Scanner Characterization, Gage R&R

Precision was used to characterize colony color measurements. A brief discussion of the particularities of measurement characterization, in absence of known value standards, is supplied in section 1.1.2.5. An ANOVA-based gage repeatability and reproducibility analysis (GRR, commonly referred to as Gage R&R) was carried out to assess method precision. In spite of being usually performed with several operators, to assess interoperator reproducibility, this assay's general testing scheme can be easily adapted to test for the reproducibility of automated measurements, as exposed by Immel[90]. The latter approach is taken as to assess color distance measurement performance of several instruments.

Two GRR set-ups were assessed, an intrascanner and an interscanner GRR, that is a same-model GRR analysis carried out in three different scanner units of the same model

(CanoScan) or on three different model units (CanoScan, Perfection V39, and OpticSlim), respectively. An alternative interscanner GRR was conducted without the OpticSlim scanner.

As established by the Automotive Industry Action Group GRR guidelines, ratios of repeatability, reproducibility and total combined repeatability and reproducibility were considered good when below 10%, marginally acceptable when above 10% and below 30%, and unacceptable when equal or greater than 30%. GRR, that yielded 5 or more distinct categories were considered good[91].

Only colonies present in the third crown of *E. coli* spiral plates were tested during the GRR assay, sufficient variability of scanned colony colors was achieved by testing reads of high, medium, and low TTC and TV concentration media, respectively, along with LA control media (see section 3.1.2.1 for details on media composition), two replicates plates of each media were read.

Δ_{Gray} calculations were performed according to Equation 3.12, employing grayscale values that were obtained from sRGB input values, respectively, as exposed by Equation 3.1 through Equation 3.6. Average grayscale values for LA media were calculated in order to obtain the Δ_{Gray} calculations.

Euclidean distance metrics for CIEXYZ$_{D50}$ and CIELAB color space metrics were calculated as detailed in section 3.1.2.3.7. Thus, global averages of each coordinate LA media value were first obtained and taken as references in either CIEXYZ$_{D50}$ or CIELAB coordinates and then inserted in Equation 3.13 and Equation 3.14 , respectively.

In order to further analyze data obtained in the interscanner GRR ANOVA for Δ_{XYZ} and ΔE_{ab}, respectively, follow-up *post-hoc* Tukey Honest Significant Distance tests (HSD) were conducted. These tests were carried out whenever interscanner GRR ANOVAs revealed the existence of significant differences in the means of the measured parts (i.e. media). This practice allowed comparing values obtained in each scanner to determine whether if, for a given chromogen, media with different concentrations of chromogen yielded different color distance values with respect to the control media. The absence of significant differences in the means of values retrieved for different media would imply scanners were working improperly as chosen media formulations produced colonies with marked differences in color. These differences in color were thought to be well above the discrimination capacity of any suitable colorimetric method.

Images taken for the GRR analysis were taken as specified in Section 3.1.2.2. Calculations were conducted using a significance level of 0.05 in Microsoft Excel 2010 (Microsoft, Seattle, Washington, USA), with the Real-Statistics add-in (Charles Zaiontz, 2016).

3.2. Measures of Colonies in Alternative Media

3.2.1. Growth Inhibition Assessment

A heavily inhibitory full-body lotion (Crema Para Todo Deliplus, RNB, La Pobla de Vallbona, Spain) was used as a inhibitory sample matrix model. The latter will be referred to simply as “matrix”. To assess the effects of matrix concentration on the enumeration capabilities of the alternative media that were being studied, the effects of several concentrations of the matrix were tested. An exploratory run of direct plating of 1:10 and 1:100 neutralized dilution of the sample matrix in all media indicated the product had a microbial load below the detection limit of the employed plating techniques.

3.2.1.1. Reagent Preparation and Plating

Modified Letheen agar (LA) and modified Letheen broth dehydrated media (both from Merck, Darmstadt, Germany) were prepared according to manufacturer specifications with polysorbate 80 (Reactivos Para Diagnóstico, Sentmenat, Spain). Strains were kept in 20 % glycerol (Labbox Labware, Vilassar de Dalt, Spain), in PBS solution, prepared from PBS tablets (AMRESCO, Solon, Ohio, USA), vials were stored at -20ºC.

Escherichia coli NCTC 9001 and *Staphylococcus aureus* ATCC 6538 were streaked directly from their cryovials onto LA plates and incubated overnight at a temperature of 37 ºC. A single overnight colony was picked and inoculated onto a falcon tube containing 5 ml of modified Letheen broth and vortexed. Once inoculated, vials were incubated for 2.5 h.

Five such replicate samples were created for each microorganism-media combination that was tested. Incubation always took place at 37 ºC, while tubes were agitated at 220 RPM. Sample matrix was diluted according to dilution factors of 10, 10^3, and 10^5, respectively, in a Letheen Broth solution and neutralized for 30 minutes. Following neutralization, broth cultures were diluted in PBS solution and spiked into neutralized sample dilutions to achieve a concentration of roughly 10^2 CFU/ml. Spiking inocula aliquots never surpassed volumes of 0.5% of the total volume of the neutralized matrix dilutions, minimally impacting matrix concentration. Spiking of broth cultures and follow-up platings were carried out independently for each matrix dilution replicate.

1 ml aliquots of each matrix dilution were then plated in Sanita-kun AC plus (JNC Corporation, Tokyo) and in Filmplate Bacterial Aerobic Count (Guangdong Dayuan Oasis Food Safety Technology, Guangzhou, China) plates, respectively, according to manufacturer specifications. 1 ml aliquots were surface plated in Letheen agar and carefully dried inside laminar flow cabinets. Incubation of all plates took place at 37ºC, plates were then incubated, as specified in section 3.2.3. All samples were plated twice in each media. Plates were counted manually after 48 h incubation, according to manufacturer specifications and standard practices for surface plates.

3.2.1.2. Statistical Analysis of Data

Differences between tested alternative media and reference LA media counts were calculated. A two factor ANOVA test was carried out to assess the presence of differences in colony recovery between Filmplate and Sanita-kun consumables, with different matrix concentration levels. Respectively, two two-factor ANOVAs were carried out, one for *E. coli* data and one for *S. aureus* data. All testing was carried out with a significance level of $\alpha < 0.05$. Following the ANOVA, post-hoc Tukey HSD tests were conducted, if necessary, to provide further insight in regards to the source of significant mean differences. All tests were conducted using a significance level of 0.05 in Microsoft Excel 2010 (Microsoft, Seattle, Washington, USA), using the Real-Statistics add-in (Charles Zaiontz, 2016).

3.2.2. Enumeration Limit Analysis

In order to evaluate the enumeration performance of media, sample microorganisms were plated at a wide range of concentrations and automated counts of these were carried out. Counting of colonies was automated as manual counting of colonies in plates with high concentrations of colonies would have been too time-consuming.

3.2.2.1. Reagent Preparation and Plating

Modified Letheen agar (LA) and modified Letheen broth dehydrated media (both from Merck, Darmstadt, Germany) were prepared according to manufacturer specifications with polysorbate 80 (Reactivos Para Diagnóstico, Sentmenat, Spain). Strains were kept in 20 % glycerol (Labbox Labware, Vilassar de Dalt, Spain), in PBS, prepared from PBS tablets (AMRESCO, Solon, Ohio, USA), vials were stored at -20ºC.

Escherichia coli NCTC 9001, *Staphylococcus aureus* ATCC 6538, and *P. aeruginosa* CECT 110 were streaked directly from their cryovials onto LA plates and incubated overnight at a temperature of 37 ºC. A single overnight colony was picked and inoculated onto a falcon tube containing 5 ml of modified Letheen broth and vortexed. Once inoculated, vials were incubated for 2.5 h, 4 h in the case of *P. aeruginosa* vials.

Three such replicate samples were created for each microorganism-media combination that was tested. Incubation always took place at 37 ºC, while tubes were agitated at 220 RPM. Samples were then diluted to achieve a concentration of roughly 10^4 CFU/ml and were diluted by a factor of $\sqrt{10}$, to achieve five resulting dilutions. Respective target concentrations of each dilution roughly corresponded to 10^4 CFU/ml, $3.16 \cdot 10^3$ CFU/ml, 10^3 CFU/ml, 316 CFU/ml, and 100 CFU/ml.

1 ml aliquots of each dilution were then plated in Sanita-kun (JNC Corporation, Tokyo) and in Filmplate (Guangdong Dayuan Oasis Food Safety Technology, Guangzhou, China) plates, respectively according to manufacturer specifications. 100 µl aliquots were surface plated into LA plates. All samples were plated twice in each media. LA plates were counted according to standard practices[50], thus, plates with counts beyond 250 CFUs were discarded, alternative media plates were counted through kinetic count (see section 3.2.2.3).

3.2.2.2. Image Capture and Analysis

Following plating, alternative media plates were inserted in CanoScan scanners, these scanners were placed in a 37ºC incubation chamber. LA plates were incubated regularly. During incubation, images of the plates were captured every 30 minutes at a resolution of 400 DPI, using a customized script which was run from AutoHotkey (AutoHotkey Foundation, Charlestown, Indiana, USA), a macro and automation software that allows automating processes that would regularly require human operation of a PC[92]. Images were saved in PNG file format.

3.2.2.3. Image Processing and Plate Enumeration

Image processing and follow-up enumeration were carried out in FIJI using specifically developed software package which is described in section 3.2.4.

3.2.2.4. Statistical Analysis of Data

Data for all enumerations was log-transformed and compared with counts obtained through regular enumeration in LA media (at low concentrations, according to standard practices). A linear regression analysis was performed in order to establish the adequacy of the enumeration performance employing the criteria defined by Ferrati and others[93], accordingly, the criteria featured in Table 3.1 are taken to classify enumeration quality for linearly regressed enumerations. Note is made that the term “poor” has been adopted to replace the term “fair” employed in the article where this classification was proposed[93]. In cases where different performance levels were met by the indexes, the regression was categorized as established by the most disfavorable index. For instance, given a regression that featured a good slope, an excellent intercept, and a poor determination coefficient, overall regression performance was classified as poor.

Table 3.1. Linear regression classification criteria.

Linear Regression Criteria

Index	Excellent	Good	Poor
Slope (m)	$1 \geq m \geq 0.9$	$0.9 > m \geq 0.8$	$m < 0.8$
Intercept (b)	$0.1 \geq b$	$0.2 \geq b > 0.1$	$b > 0.2$
Det. Coef. (r^2)	$1 \geq m \geq 0.81$	$0.81 > m \geq 0.64$	$m < 0.64$

3.2.3. Time to Detection Assessment

An undisclosed growth detection algorithm (UDA) was run in order to randomly select colonies imaged during the enumeration limit (see section 3.2.2) and growth inhibition tests (see section 3.2.1). The UDA next analyzed individual times of appearance of the colonies by undisclosed means.

3.2.3.1. Image Retrieval

Colonies in the growth inhibition tests were in fact imaged in a scheme that was completely homologous to that featured in section 3.2.2.2. The UDA's output was a list of detection times for all analyzed colonies. Detection times were duly processed in Microsoft Excel to generate time to detection (TTD) histograms for colonies located in plates with total colony concentrations between 30-300 CFUs. This procedure allowed the comparison of time to detection for *E. coli* and *S. aureus* in control plates and in plates with decreasing concentrations of hand lotion cream concentrations. TTD analysis was performed exclusively on Sanita-kun plates.

3.2.4. ImageJ Scripts

In order to properly develop and maintain the complex macro scripts that were executed under full automation, a rather unorthodox approach was followed. Multiple macros were run by so-called upper hierarchy macros (see Figure 3.1). Thus, macro scripts were interrelated hierarchically in such a way that upper hierarchy macros (UHM) ran lower hierarchy macros (submacros). This approach substituted the regular schemes of classes and objects that can be found in most programming languages.

Note must be made of the notation that will be employed in the present work to refer to submacro scripts. Submacro types will indicate their numerical hierarchy level by a number following the sign “^”, thus, following a general structure sub ^*n* macro. This can be omitted for macros of the first submacro layer, which can be referred to simply as “submacro”. Scripts directly run from the UHM will be simply referred to as submacros, subsequently, macros run by submacros will be referred to as sub^2macros. Macros run form sub^2macros will be referred to as sub^3macros, and so on (see Figure 3.1).

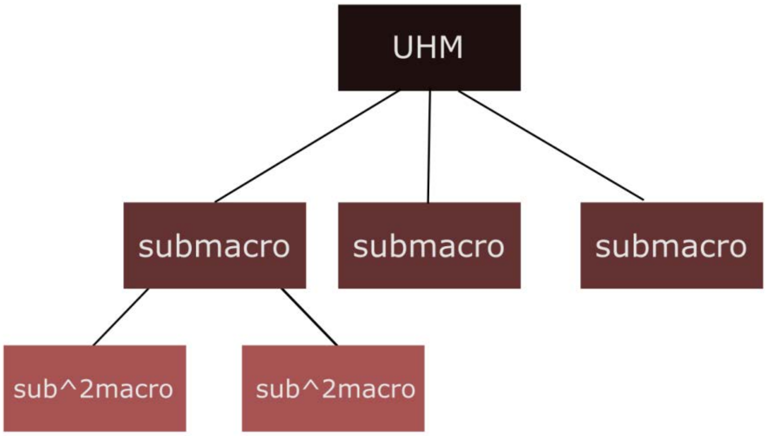

Figure 3.1. Diagram depicting the hierarchical macro system used to enable management of composite scripts. UHM stands for upper hierarchy macro while Sub^2Macro stands for second layer submacro.

3.2.4.1. Kinetic Count and Analysis Macro

Data retrieved for the analysis of alternative media, unless specified otherwise, was processed with KinCAn (name standing for Kinetic Count and Analysis Macro), a UHM, which runs several layers of submacros (for an explanation regarding submacros see 3.2.4). KinCAn performed counting and analysis of colonies in alternative growth media. Essentially, KinCAn consists of a brief script that runs several submacros. Run submacros are limited to Sequencer, a script that opens and processes time series scanned images of a given set of alternative media plates while running several sub^2macros. Scripts comprising KinCAn are featured, along with pertinent explanations and notes, in Appendix III.

3.2.4.2. Sequencer Submacro

Sequencer is a submacro run by the KinCAn UHM, its main roles are to open time series images in a user-selected folder and to process these in order to enhance follow-up analysis of imaged colonies. Processing of images for enhanced detection of colonies was elicited by running the Denz (named to resemble the word denoise) sub^2macro. Once images were duly processed, stacks were generated. Following image processing and stack generation, Sequencer is also in charge of opening the region of interest (ROI) file that contains locations of the growth regions of consumables. Thus ROI files must be added manually to the containing folders before starting the image processing phase.

3.2.4.3. Denz Sub^2macro

Denz sub^2macro was specifically developed to address denoising of alternative media with textured growth pads. Two denoising algorithms are applied to consumables in this sub^2 macro. One such algorithm is for Sanita-kun while the other is reserved to FilmPlate media.

Sanita-kun and FilmPlate both have grids in their transparent sheet covers and textured growth pads. Luckily, interferences caused by these can also be addressed using a frequency domain-based filter employed by the denoising algorithm. Thus, the denoising algorithm capitalizes on a very particular use of Fourier spectrum image filtering. Given the periodical and rather homogenous nature of the background noise of imaged alternative media, which is mainly due to the texture of their growth pads, it is feasible to treat images with FT-based filtration for noise removal (see Figure 3.2).

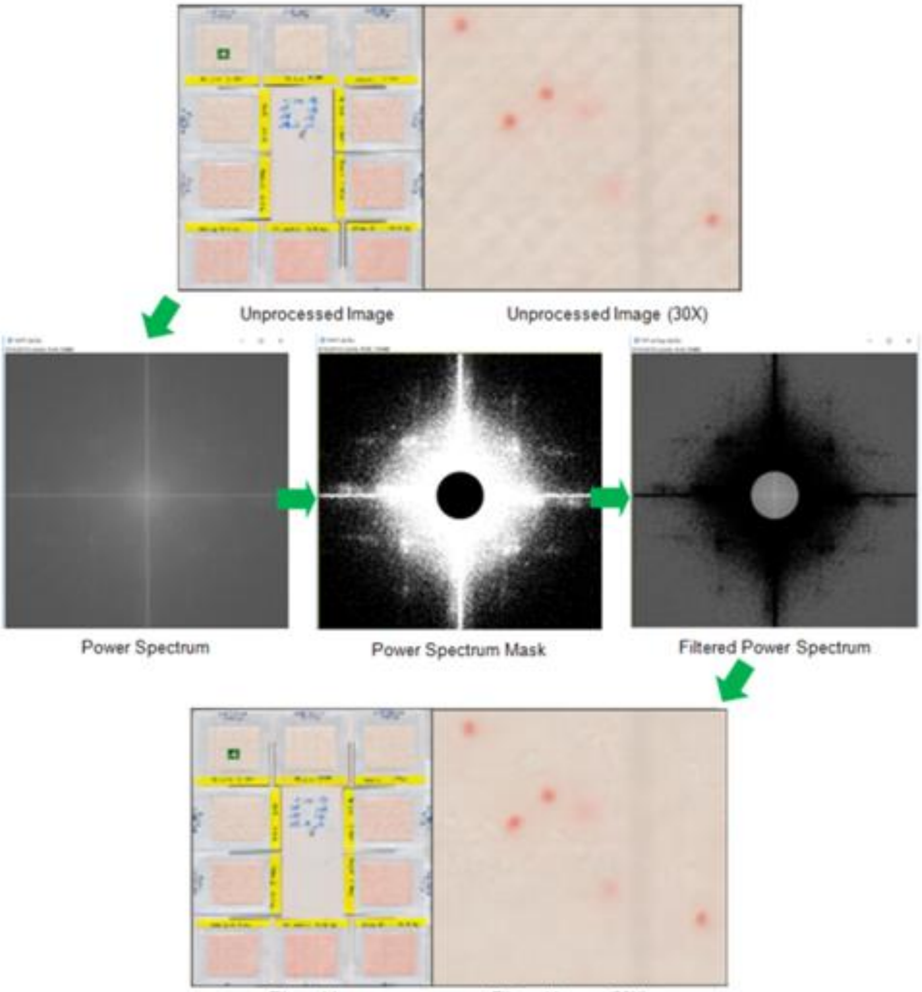

Unprocessed Image

Unprocessed Image (30X)

Power Spectrum

Power Spectrum Mask

Filtered Power Spectrum

Filtered Image

Filtered Image (30X)

Figure 3.2. Schematic representation of images as processed by the denoising Denz Sub^2macro. Augmented image details (30X) were obtained.

The denoising algorithm, in brief, consists in carrying out a FT and processing its derived power spectrum to create a mask that selectively contains regions in the power spectrum corresponding to interferences. Next, the power spectrum mask is applied on the original unprocessed power spectrum. A reverse FT concludes the process.

Images that are processed with this algorithm can be viewed in Figure 3.2. As featured in the power spectrum mask of Figure 3.2, clusters of lighter pixels are thresholded and masked in the power spectrum images, mostly in the intermediate frequency sections of the power spectrum. This filtering procedure targets the production of filtered images with lower periodic noise. The noise reduction achieved when applying this filtration algorithm is readily apparent when comparing 30x details of filtered and non-filtered images (see Figure 3.2).

3.2.4.4. fPCount and sKCount Sub^2macros

Both fPCount and sKCount macros summarize full stack image series into a single image suited for counting with a maxima selection algorithm. fpCount features a rather simple array of operations, essentially comprising slice by slice intermodes autothresholding of stacked images, removal of remaining noise through first image-based subtraction, and average z-projection of the stack into a single image followed by median filtering.

Operation of the sKCount macro is far more complex, it features a first iteration, which denoises images through subtraction with the first image in the time series, followed by thresholding of the images in the stack and average z-projection of these. Next, median filtering is applied and an initial preliminary count is performed. If the count is smaller than 500 the stack summary image proceeds to be duly counted. Otherwise, the stack is reprocessed differently, in order to adapt image processing to the characteristics of high count plates, mainly colony crowding and lower signal to noise ratios. A z-projection of the standard deviation of the stack is first obtained, next, the stack is denoised using the Denz macro, this is followed by Red channel denoising, and redenoising with Denz, followed by Otsu autothresholding. After several additional steps, the darker areas of the plate, presumed to be colonies, are preserved with low processing while surroundings are heavily smoothed and used as a background for darker pixels.

Resulting stack summary images are next analyzed by sequencer which, in turn, counts minima and generates and saves final results.

4. RESULTS

4.1. Results for Measures of Colony Color and Related Measurements in Agar-Based Media

4.1.1. Calibration Target Analysis

Qualitative analysis of the targets yielded several interesting results. Namely gamut limitations of the scanner models that were used during testing became particularly evident as well as their general performance characteristics.

4.1.2. IT8 Patch Color Homogeneity

Brightness fluctuations in Perfection V39 images could be spotted, in most color patches. On the other hand, CanoScan and OpticSlim target images didn't feature such apparent brightness fluctuations. A CIELAB luminance plot of the patches can be checked to confirm larger luminance fluctuations in images scanned with the Perfection V39 scanner (see Figure 4.1 A). Note must be taken that the red depiction of the Luminance surface plotted strip corresponds entirely to L* value intensities and not to the original color of the respective images.

In terms of color consistency in the pixels of any given IT8 color patch, while CanoScan and OpticSlim appeared to have similar luminance values throughout the patch, Perfection V39 scanners featured larger fluctuations. While typical CanoScan color fluctuations followed rather random pattern (see Figure 4.1 B), OpticSlim fluctuations displayed hardly discernible stripe-like alignments (see Figure 4.1 C), meanwhile, Perfection V39 fluctuations followed ring-like patterns (see Figure 4.1 D). It is noteworthy that, due to heavy modification of images, pursuing to highlight interference patterns, images in Figure 4.1 B - D aren't representative of the original colors in them.

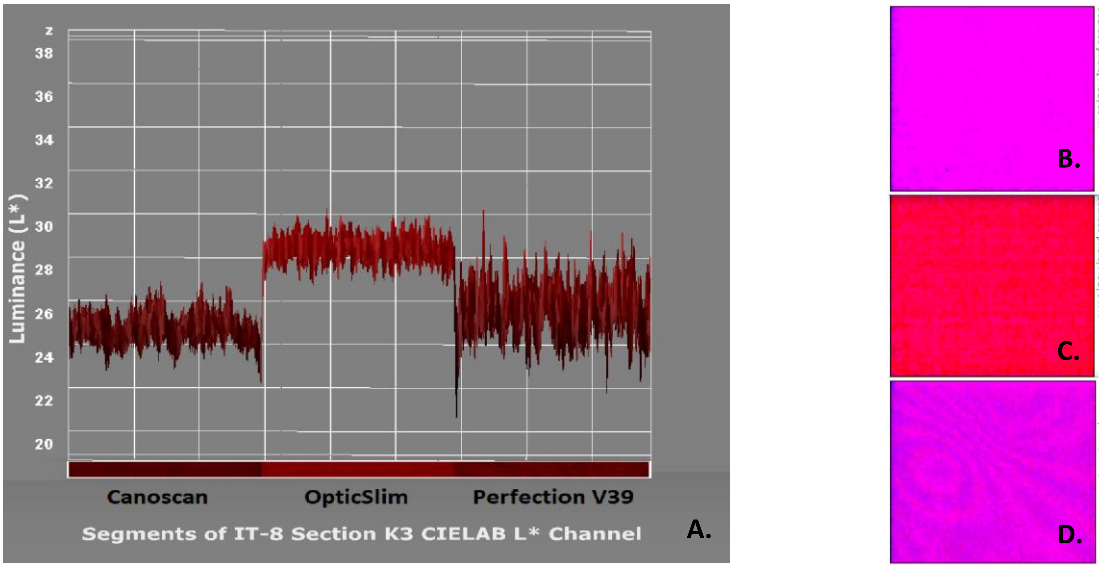

Figure 4.1. A. CIELAB luminance (L*) value plot of patch K3 IT8 image segments, as respectively scanned by CanoScan, OpticSlim and Perfection V39 scanners. B-D. Interference patterns detected in IT8 images, of patch K3, respectively scanned by CanoScan, OpticSlim and Perfection V39 scanners.

4.1.2.1. IT8 Patch Color Inspection

Analysis of IT-8 images with the Color Inspector plug-in supplied a clear view of the quality of the calibration and the available color data. Section 3.1.1.2 must be consulted for further background on the reasons for the selection of the analyzed color patches. A quick review of the target image details in Figure 4.2 reveals remarkably well the limitations of the scanners, while CanoScan performs quite well throughout, supplying images with a good contrast and very reasonable color fluctuations in pixels of any patch, OpticPlus scans appear to have a remarkably low contrast, Perfection V39 features more noisy images (as confirmed by Luminance fluctuations featured in Figure 4.1 A).

When reviewing HSB representations of the scanned colors it became apparent that dark red and brown sections of the IT8 target (i.e. patches in columns 1-4 of rows A-C) were best scanned by CanoScan (see Figure 4.2 A) which properly covered all the gamut of these patches featuring medium saturation values. Meanwhile, OpticSlim scans featured a remarkably limited amount of colors which were represented as individual points and didn’t form clusters, most points were located very close to the 0 saturation axis, thus OpticSlim appeared to generate low saturation images (see Figure 4.2 B). Perfection V39 scans, instead featured strong color saturation, this is clearly exemplified by the color clusters that stick to the HSB plot’s walls. Thus, pixels corresponding to patch “IT8 A4” appear on their own cluster at the bottom right of the HSB plot while “IT8 B4” and “IT8 C4” colors are responsible for the top left color cluster that also reaches absolute saturation values (see Figure 4.2 C).

Scanner performance appeared to be similar in the patches of columns 1-4 of rows J-L of the IT-8 target, while OpticSlim scans appeared to supply a few very low saturation colors (see Figure 4.2 E), Perfection V39 rendered many colors, with higher saturation values, featuring three small saturation clusters corresponding to the high brightness pixels of the fourth column patches (see Figure 4.2 F). In the case of the blue saturation cluster in Figure 4.2 F, it embodies fully the colors of patch “IT8 J4”.

Most patches in CanoScan images appear in the intermediate saturation zone. Never-the-less, as seen in Perfection V39, CanoScan scans of patch “IT8 J4” generate a cluster of saturated pixels (see Figure 4.2 F). The reason for this saturation is the loss of gamut occasioned by the conversion of images from proprietary device RGB spaces to sRGB. “IT8 J4” equates to out-of-gamut sRGB space coordinates (-12, 11, 144), the “-12” value indicates an out of gamut value in the R’ (red) sRGB dimension. The fact that

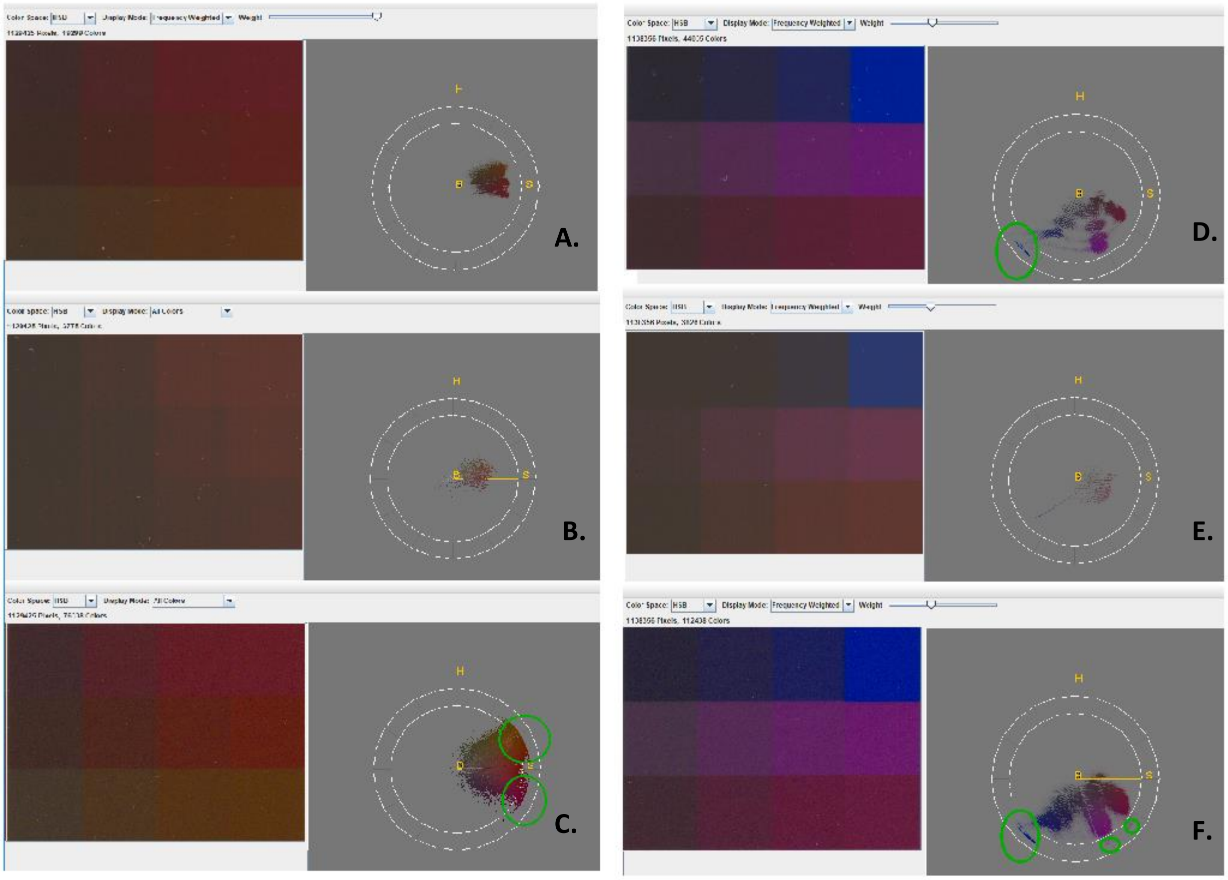

Figure 4.2.. Details of IT8 card images along with weighed frequency HSB (top view) representations of the colors present in them. Green circles in the image surround saturated colors. A - C. display images for IT8 patches “IT8 A1 - A4”, “IT8 B1 - B4”, and “IT8 C1 - C4”; image A was taken with CanoScan, image B corresponds to OpticSlim, and image C was imaged by Perfection V39. D – F. display results for IT8 patches “IT8 J1 - J4”, “IT8 K1 - K4”, and “IT8 L1 - L4”; image D was taken with CanoScan, image E corresponds to OpticSlim, and image F was imaged by Perfection V39.

OpticSlim doesn't generate fully saturated values for "IT8 J4", further stresses its low saturation values throughout and a clearly deficient sRGB conversion. All color chips that were used for the qualitative calibration target image analysis, other than IT8 J4, should be plotted inside sRGB coordinates.

4.1.3. Results of Colony Color and Grayscale Values in Agar Media

4.1.3.1. Grayscale Measurements in Dye-Microorganism Assays

Interesting patterns could be spotted when average grayscale values of chromogenic plates were compared with those of control plates using a Δ_{Gray} metric. Over time, Δ_{Gray} values became more negative, implying an increase in difference with control LA plates, this held true for all microorganisms, dye types and grayscale conversions (see Figure 4.3).

The increase in Δ_{Gray} values over time was particularly marked in *P. aeruginosa* and *S. aureus* plates. The Δ_{Gray} bar graph features remarkable differences between *E. coli* and *S. aureus* chromogenic plates, in 16 h reads, when compared with their *P. aeruginosa* counterparts.

It must be duly remarked that use of different grayscales didn't always contribute similar results. 48 h Δ_{Gray} TV average channel values, for instance, were markedly smaller in *S. aureus* plates than in *E. coli* plates, the opposite held true for Δ_{Gray} L_{709} values (see

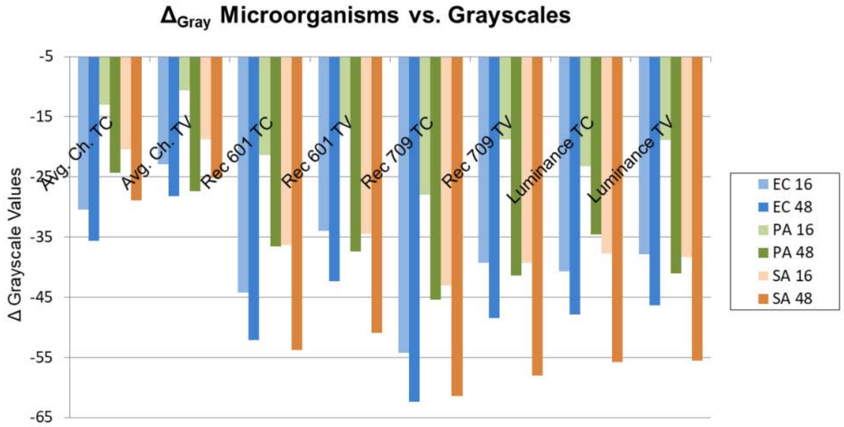

Figure 4.3. Full plate average ΔGray values for TTC (TC) and TV versus the control LA gray value given for each of the grayscales studied. EC 16, EC 48, PA 16, PA 48, SA 16, and SA 48 refer to *E. coli*, and *P. aeruginosa*, and *S. aureus* plates at 16 h and 48 h, respectively.

Figure 4.3). This is, of course, an account of the effects of applying different grayscale conversions. Thus, as expected, grayscale conversions are critical in determining the outcome values and conclusions extracted from a given experimental scheme.

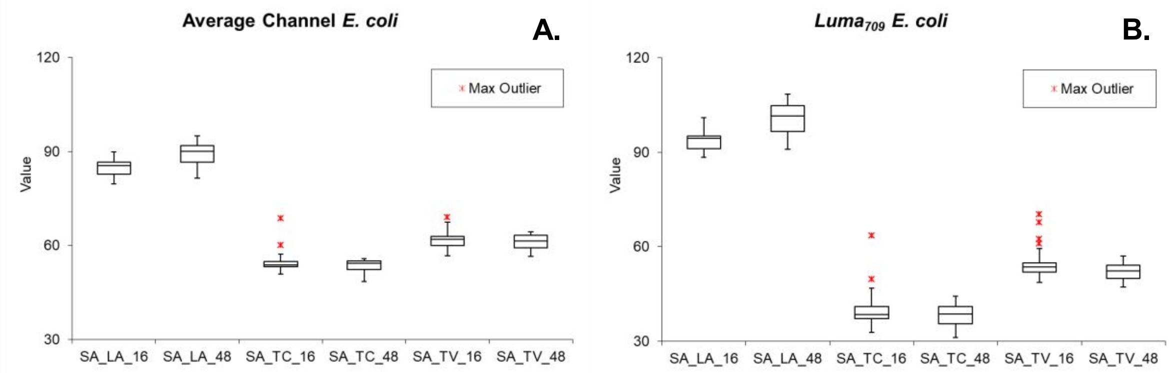

Figure 4.4. Box and whisker plot for whole-plate values of LA, TTC (TC), and TV *E. coli* plates at 16 h and 48 h, respectively. A. Plot for Average Channel grayscale values. B. Plot for average $Luma_{709}$ values.

In both TTC and TV media plates, *E. coli* box and whisker plots of general plate grayscale values at 16 h and 48 h display virtually no change in value for C_{Avg} and L_{709} (see Figure 4.4). Thus no evidence of changes in colony color between both reads beyond a slight increase in the interquartile range, this in fact could point out that colony color development didn't progress beyond the 16 h time frame in *E. coli* plates (section 4.1.3.1.1 addresses this matter from a statistical standpoint).

E. coli LA plate colonies display a slight increase in their grayscale values, in combination with the apparent stabilization of TTC and TV colony grayscale values (see Figure 4.4), this slight change in LA colonies is responsible for the change in Δ_{Gray} that takes place between the 16 h and 48 h reads, it can be remarked in the Δ_{Gray} bar graph of both C_{Avg} and L_{709} grayscales (see Figure 4.3).

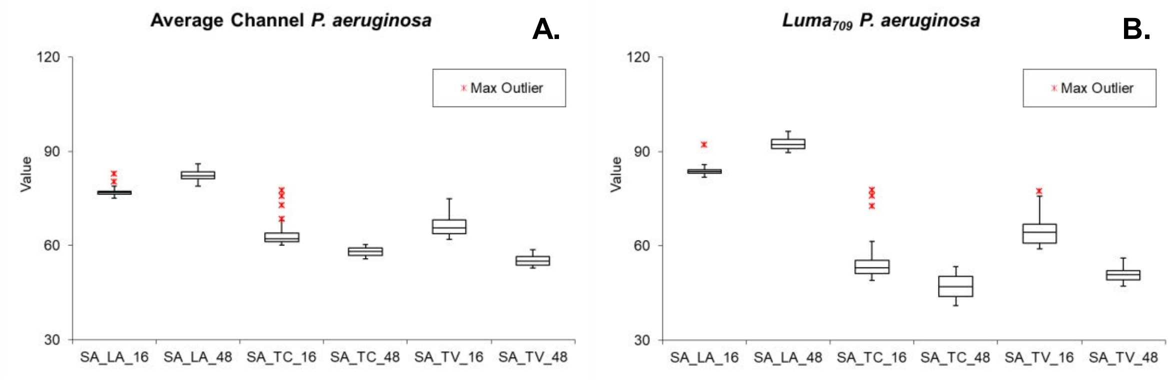

Figure 4.5. Box and whisker plot for whole-plate values of LA, TTC (TC), and TV *P. aeruginosa* plates at 16 h and 48 h, respectively. A. Plot for Average Channel grayscale values. B. Plot for average Luma709 values.

C_{Avg} values for *P. aeruginosa* colonies displayed in the box and whiskers plot evidence slight increases in values of LA colonies between reads and decreases for colonies in TTC and TV media, respectively (see Figure 4.5 A). Meanwhile, L_{709} reads featured trends that were similar to those observed in the C_{Avg} values, with slightly more apparent changes in value (see Figure 4.5 B).

Interestingly, review of the box plots (see Figure 4.5), indicates that a combined effect of the increase in LA colony values and a decrease in TTC and TV grayscale values results in the net swelling of Δ_{Gray} values.

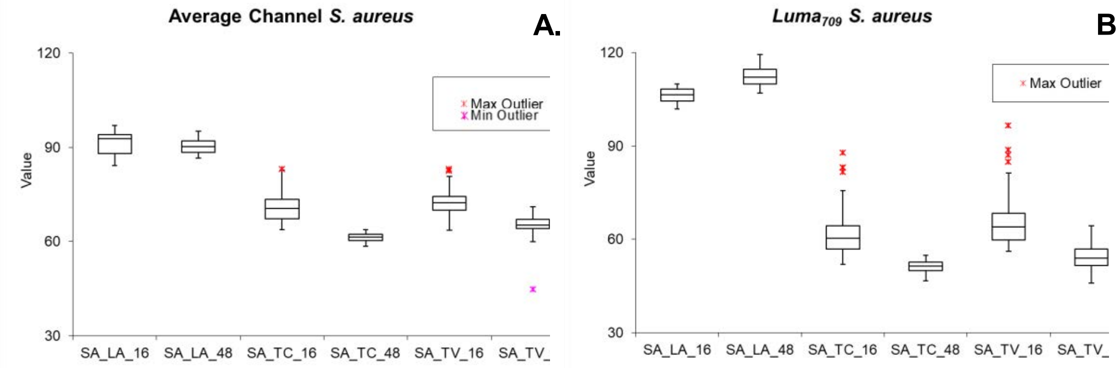

Figure 4.6 Box and whisker plot for whole-plate values of LA, TTC (TC), and TV *S. aureus* plates at 16 h and 48 h, respectively. A. Plot for Average Channel grayscale values. B. Plot for average Luma709 values.

C_{Avg} values for *S. aureus* colonies displayed no change in value in 16 h and 48 h reads of LA plates. Meanwhile, TTC and TV plates displayed a decrease between each read (see Figure 4.6 A). The box and whiskers plot points out that L_{709} values of both chromogenic and LA media are responsible for the change in the Δ_{Gray} of L_{709} of *S. aureus* (see Figure 4.6 B). While LA colonies increase their L_{709} values, TTC and TV colonies decrease their values, thus, chromogen and LA plate grayscale shifts yield a more negative Δ_{Gray} value. Furthermore, outlier values disappear in 48 h reads for *S. aureus* (see Figure 4.6 B). Differences in tendency of *S. aureus* colony grayscale values could be seen in LA plates, while their values remained stable in C_{Avg} grayscale reads they seemed to increase in the L_{709} scale (see Figure 4.6). Data dispersion seemed to decrease as interquartile ranges became smaller in all media for both C_{Avg} and L_{709} reads.

In the case of CA reads, Δ_{Gray} shifts between reads appear to be caused exclusively by changes in values of the chromogenic media. Unlike C_{Avg}, L_{709}, Δ_{Gray} values seem to be a product of a combined increase in LA colony values and decrease in chromogen plate colony values (see Figure 4.6 and Figure 4.3)).

4.1.3.1.1. Grayscale Statistics of Color Development

A paired one-tail Student t-test allows detection pursued color shifts beyond a given time point. Indeed, this can supply critical data regarding optimal minimum duration of chromogenic cultures. Use of a one-tailed t-test assumed chromogen- induced color development created a negative shift in grayscale values. As featured in 4.1.3.2, no significant changes in L709 average values take place beyond 16 h in *E. coli* TTC plates, meanwhile, *P. aeruginosa* and *S. aureus* plates continue to develop changes in L709

Table 4.1. Results of the Gauge R&R analysis. P-values below significance level are featured in bold letters. Gauge variance, repeatability, and reproducibility of variance ratios, as well as the number of distinct categories are surrounded by a square when good performance criteria are met. B. Paired Student t-test results for a comparison of $Luma_{709}$ values for 16 h and 48 h reads in the three model microorganisms that were studied.

Color Development			
Paired One-Tail Student T-test			
	E. coli	***P. aer.***	***S. aur.***
Mean Difference	1.22	9.09	12.2
Degrees of Freedom	35	35	35
t-stat	1.19	4.73	6.93
p-value	0.12	**1.79E-05**	**2.32E-08**

after the 16 h read (with p-values of 1.79 E-5 and 2.32 E-8, respectively). Data used in this test was recovered from all spiral plate crowns to account for full plate values.

4.1.3.1.2. Grayscale Measurements for Media Performance Comparison

An example of the use of grayscale values for media performance analysis would be using Δ_{Gray} as a media performance indicator. An instance of the use of this metric might encompass establishing a given value as the target grayscale change elicited by a given media formulation. Figure 4.7 confronts grayscale values against TTC concentration in a plot. This plot offers a simple way to relate increases in Δ_{Gray} to different media formulations that contain the same chromogen.

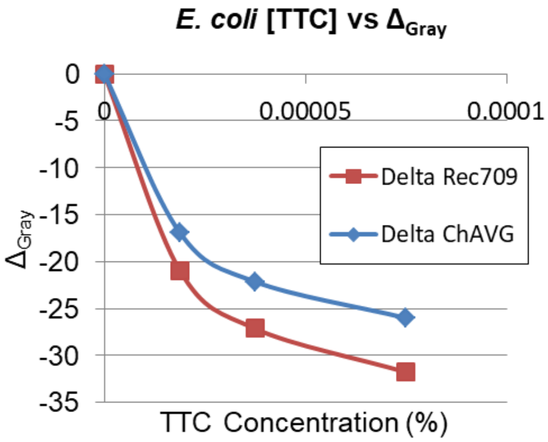

Figure 4.7. *Luma*$_{709}$ (Rec709) and average channel (ChAVG) Δ_{Gray} values are charted against TTC concentrations for colonies of the third crown of *E. coli* spiral plates in media with high, medium, and low TTC concentrations, Letheen agar grayscale values were taken as references to calculate Δ_{Gray}. A (0,0) intercept was plotted, representing the theoretical Δ_{Gray} value of 0 for colonies in LA plates.

Use of different grayscales produced different Δ_{Gray} plots. C_{Avg} values appeared to yield the smallest Δ_{Gray} values throughout, generating a plot that was rather separated from the rest. Meanwhile, other of grayscale Δ_{Gray} plots were very similar and virtually overlapped (see Figure 4.8 A). General tendencies of C_{Avg} curves, however, appeared to be remarkably similar to those of the rest of grayscales. Normalized curves of Δ_{Gray} values yielded a quasi-perfect overlap of curves corresponding to Δ_{Gray} values of all the studied grayscales (see Figure 4.8 B).

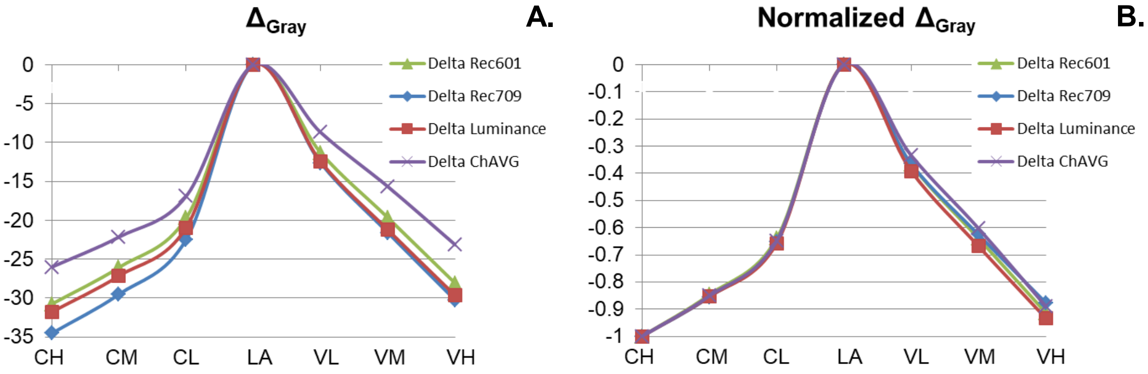

Figure 4.8. A. Plot of the average Δ_{Gray} values in the third crown of *E.coli* spiral plates for all studied grayscales. B; Normalized plot of the average Δ_{Gray} values in the third crown of *E.coli* spiral plates for all studied grayscales.

Further insight into the origin of the coincidence in the shape of plots following normalization led to the plotting of normalized single sRGB channel Δ_{Gray} plots. Clearly, when comparing values of the normalized sRGB channels against a plot of Δ_{Gray}, L_{709} values, the plot of the green channel Δ_{Gray} resembles Δ_{Gray}, L_{709} closely while the rest of channel Δ_{Gray} curves have very different shapes (see Figure 4.9).

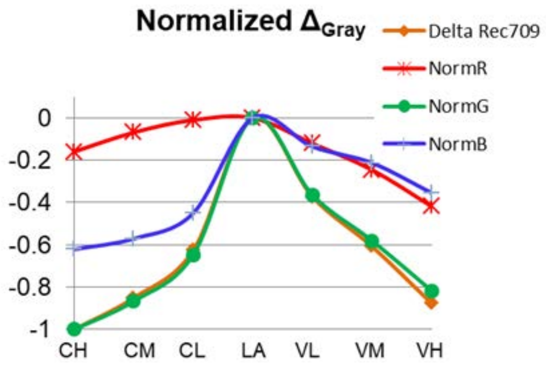

Figure 4.10. Plot of normalized Δ_{Gray} individual sRGB channel values (normalization was done accounting for values of all three channels) versus Δ_{Gray} $Luma_{709}$ values.

4.1.3.2. Color Measurements in Dye-Microorganism Assays

Development of color in colonies revealed divergent patterns in the different media and microorganisms that were tested. Use of tridimensional plots of colony colors in the HSB, CIELAB and XYZ projections enabled detection of apparent differences in color between colonies and assessment of colony color change through time.

A qualitative examination of HSB plots of reverse converted CIELAB D50 and $CIEXYZ_{D50}$ colony color average value palette points out the existence of rather diverse hues and saturation levels in captured images (see Figure 4.11 and Figure 4.12). The general arrangement of color coordinates in the HSB plots for $CIEXYZ_{D50}$ and CIELAB D50 average HSB plots was very similar. The only remarkable divergence between these was a slight change in hue that affected colonies in both chromogenic media, furthermore, chromogenic media colonies appeared to have closer hues in the $CIEXYZ_{D50}$ plot than in the CIELAB plot (see Figure 4.11 A and Figure 4.12 A).

Four color point clusters can be noted in the HSB plot (see Figure 4.11 A and Figure 4.12 A), while the top two clusters corresponded to colonies in LA, those in the bottom belonged to colonies in chromogenic media. Among LA colony colors, *E. coli* and *P. aeruginosa* colonies displayed similar dark green colors, meanwhile *S. aureus* colony colors appeared isolated and formed their own cluster, displaying higher color saturation, with a distinctive yellow color (see Figure 4.12 A and B). While TTC media yielded rather dark red colored colonies, colonies in TV media displayed a dark violet color, HSB plots of the colors featured intermediate and high saturation in TTC colonies and medium to low saturation in TV colonies (see Figure 4.11 and Figure 4.12). An outlier colony color was detected in 48 h *S. aureus* TV colonies, this color point belonged to the otherwise all TTC color cluster, its remarkable proximity to TC colony color can be seen by comparing it with its neighboring 48 h TTC 48 h counterpart in the color palette (see Figure 4.11 and Figure 4.12).

Without exception, colors of colonies appeared to shift towards more saturated values through time, shifts towards saturated colors between 16 h and 48 h reads were more apparent for chromogenic media *S. aureus* and *P. aeruginosa* colonies. Meanwhile, *S. aureus* control media colony saturation increased greatly between 16 h and 48 h reads (see Figure 4.11 and Figure 4.12).

Color differences were also readily apparent during the examination of colony average colors in CIEXYZ$_{D50}$ and CIELAB. Color coordinate points weren’t as readily distinguishable using the 3-D color profiler software, this called for an individual analysis of the colors for each model microorganism.

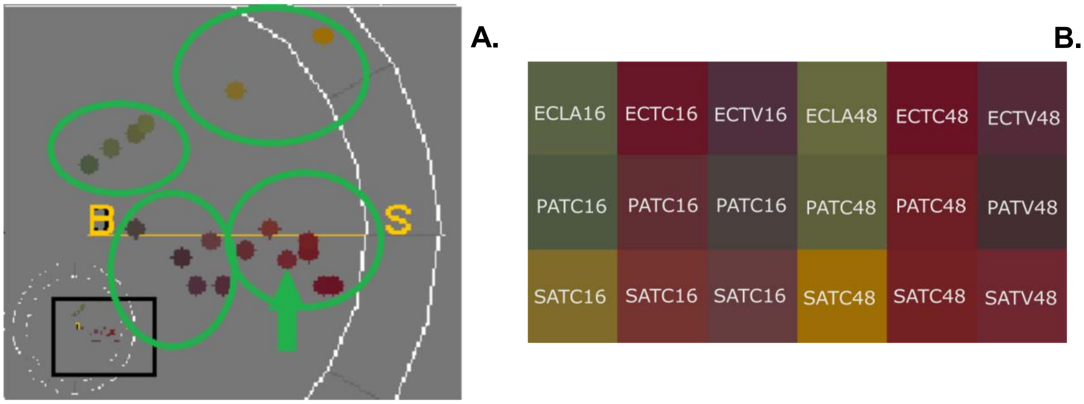

ECLA16	ECTC16	ECTV16	ECLA48	ECTC48	ECTV48
PATC16	PATC16	PATC16	PATC48	PATC48	PATV48
SATC16	SATC16	SATC16	SATC48	SATC48	SATV48

Figure 4.11. A. Detail of a top view of a tridimensional HSB plot of full-plate average CIEXYZ D50 colony color (converted to sRGB). Green circles surround clusters of colony color points which correspond to *S. aureus* colonies in LA (top right position) and, from here, clockwise to TTC media plate colonies (bottom right), TV media colonies (bottom left) and *E.coli* and *P.aeruginosa* colonies (top left). The green arrow indicates an outlier *S. aureus* TV colony color. B. Average plate CIEXYZ D50 colony color palette according to microorganism and time point. Each color in the palette is labeled according to its origin, initial letters stand for the colony microorganism (EC, PA, and SA; standing for *E. coli*, *S. aureus*, and *P. aeruginosa*) the media where the colonies grew on (LA, TC, TV) and read time points (16 and 48, standing for 16 h and 48 h) are all mentioned.

CIEXYZ$_{D50}$ color point plots of *E. coli* colonies displayed a shift in color of control media LA colonies between 16h and 48 h reads. Meanwhile, color coordinates of successive runs for colonies in TTC and TV media appeared to be indistinguishable, with overlapping 16h and 48 h point plots. Although TTC and TV plate colonies had rather close coordinates they could be distinguished between each other (see Figure 4.13 A).

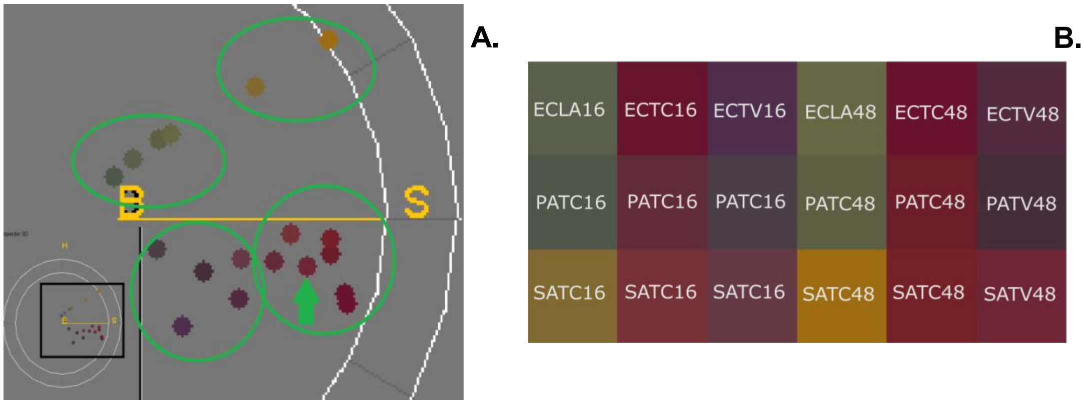

ECLA16	ECTC16	ECTV16	ECLA48	ECTC48	ECTV48
PATC16	PATC16	PATC16	PATC48	PATC48	PATV48
SATC16	SATC16	SATC16	SATC48	SATC48	SATV48

Figure 4.12. A. Detail of a top view of a tridimensional HSB plot of full-plate average CIELAB D50 colony color (converted to sRGB). Green circles surround clusters of colony color points which correspond to *S. aureus* colonies in LA (top right position) and, from here, clockwise to TTC media plate colonies (bottom right), TV media colonies (bottom left) and *E .coli* and *P. aeruginosa* colonies (top left).The green arrow indicates an outlier *S. aureus* TV colony color. B. Average plate CIELAB D50 (See notation) colony color palette according to microorganism and time point. The notation followed was initial two letters standing for the colony microorganism (EC, PA, and SA; standing for *E. coli*, *S. aureus*, and *P. aerugionsa*) the media where the colonies grew on (LA, TC, TV) and read time points (16 and 48, standing for 16 h and 48 h).

CIELAB D50 plots of obtained colors also pointed to a color change in control LA colonies between successive reads. A slight change in TV media colonies was also featured. The position change of points corresponding to TC colonies still appeared to be indistinguishable between reads in the CIELAB D50 plot (see Figure 4.13 B). In general, colonies appeared to have solid, homogenous color development in chromogenic media segmented colony images. Slightly different color regions could be spotted in outer (first) and inner (sixth) crown colonies of spiral plates. Outer crown 48 h colonies of TV plates

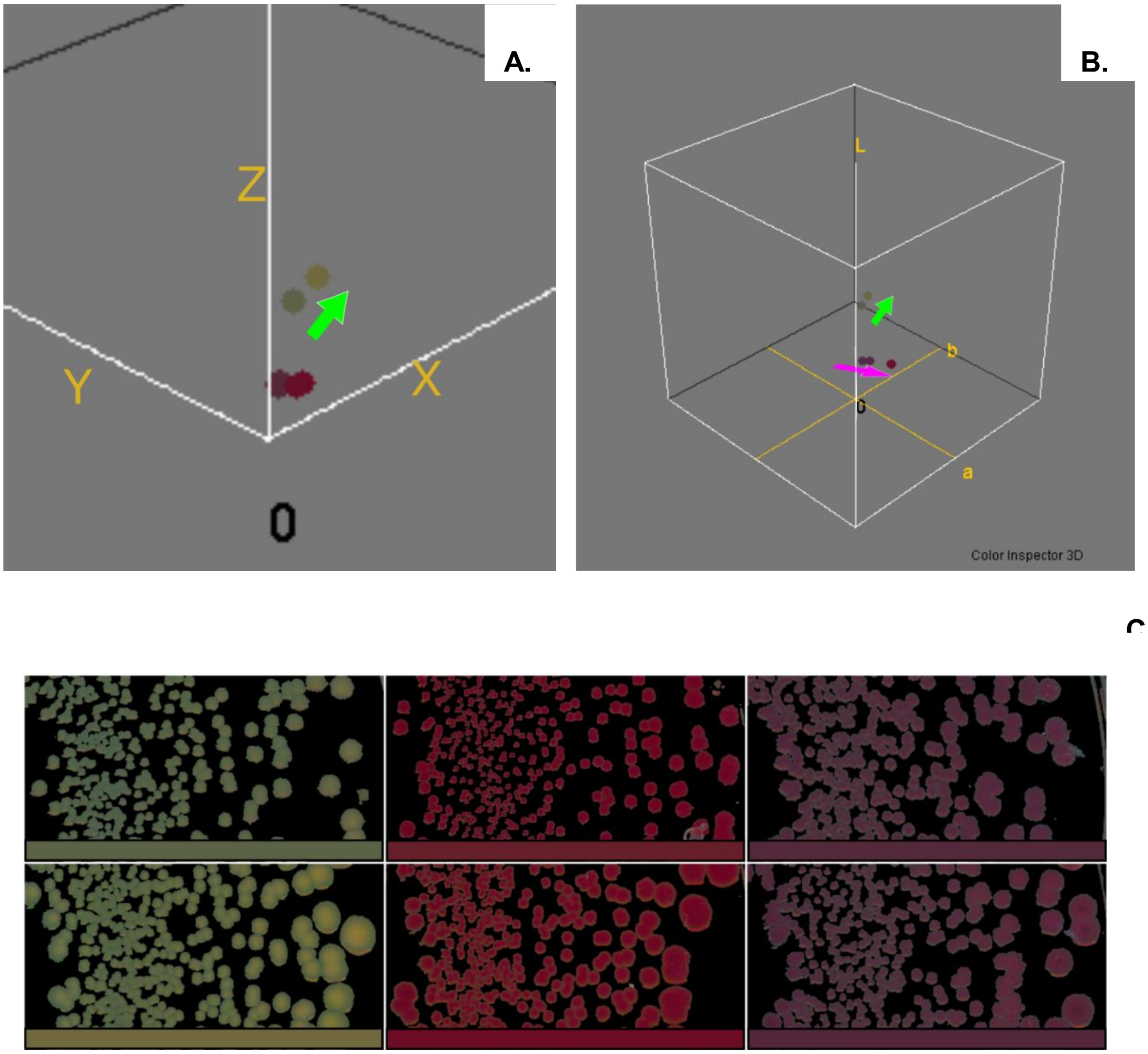

Figure 4.13. A. CIEXYZ$_{D50}$ average color palette plot for *E. coli* colonies at 16 h and 48 h reads for LA TTC and TV media, the green arrow indicates a color shift between reads in LA media, the absence of an arrow indicates virtual overlap of color coordinates in successive reads. B. CIELAB D50 average color palette plot for *E. coli* colonies at 16 h and 48 h reads for LA TTC and TV media, the green and violet arrows indicate a color shift between reads in LA and TV media, respectively. C. Details of *E. coli* colony images, on top of their respective average CIELAB color pallet color. Colonies correspond, from right to left, to LA colonies, TC colonies, and TV colonies, 16 h images appear on top while 48 h counterparts appear right below these.

featured slight differences in colony color. In both cases, outer colony regions featured less saturated colony colors, when compared to colony centers (see Figure 4.13 C).

The *P. aeruginosa* $CIEXYZ_{D50}$ D50 plot displayed slight changes in color between 16h and 48h reads in all media, TV being the media where largest colony color coordinate shifts took place (see Figure 4.14 A). CIELAB D50 counterpart plots featured clear changes in position for color coordinates with similar separations between reads for 16 h and 48 h coordinate sets of any given media (see Figure 4.14 B).

Examination of the segmented *P. aeruginosa* colony images reveals a clear increase in colony size between reads of colonies in chromogenic media. Colony segments in LA media appear to decrease in size and or grow very little. It must be highlighted that colony segmentation in control LA plates was particularly challenging in 48 h reads given the strong spreading of colonies. As mentioned in section 3.1.2.3.1, segmentation of *P. aeruginosa* 48 h plates required a specific approach. This particular segmentation successfully segmented colony centers, it was otherwise impossible to establish any clear borders. Thus, readers are cautioned against misinterpreting the size of 48 h segmented colony centers featured in segmented images as being representative of the full size of the colonies (see Figure 4.14 C). Colonies in TV displayed patches of differently colored regions in colony images of 48 h reads.

Amongst all tested model microorganisms, *S. aureus* LA colonies appeared to be the most separated from chromogen media colony coordinates in $CIEXYZ_{D50}$plots. Strong shifts in color occurred in $CIEXYZ_{D50}$ LA color coordinates between 16h and 48 h reads. Meanwhile, 16 h CIEXYZ D50 coordinates of TTC and TV media appeared to be separated, however, these converged in 48 h reads (see Figure 4.15 A).

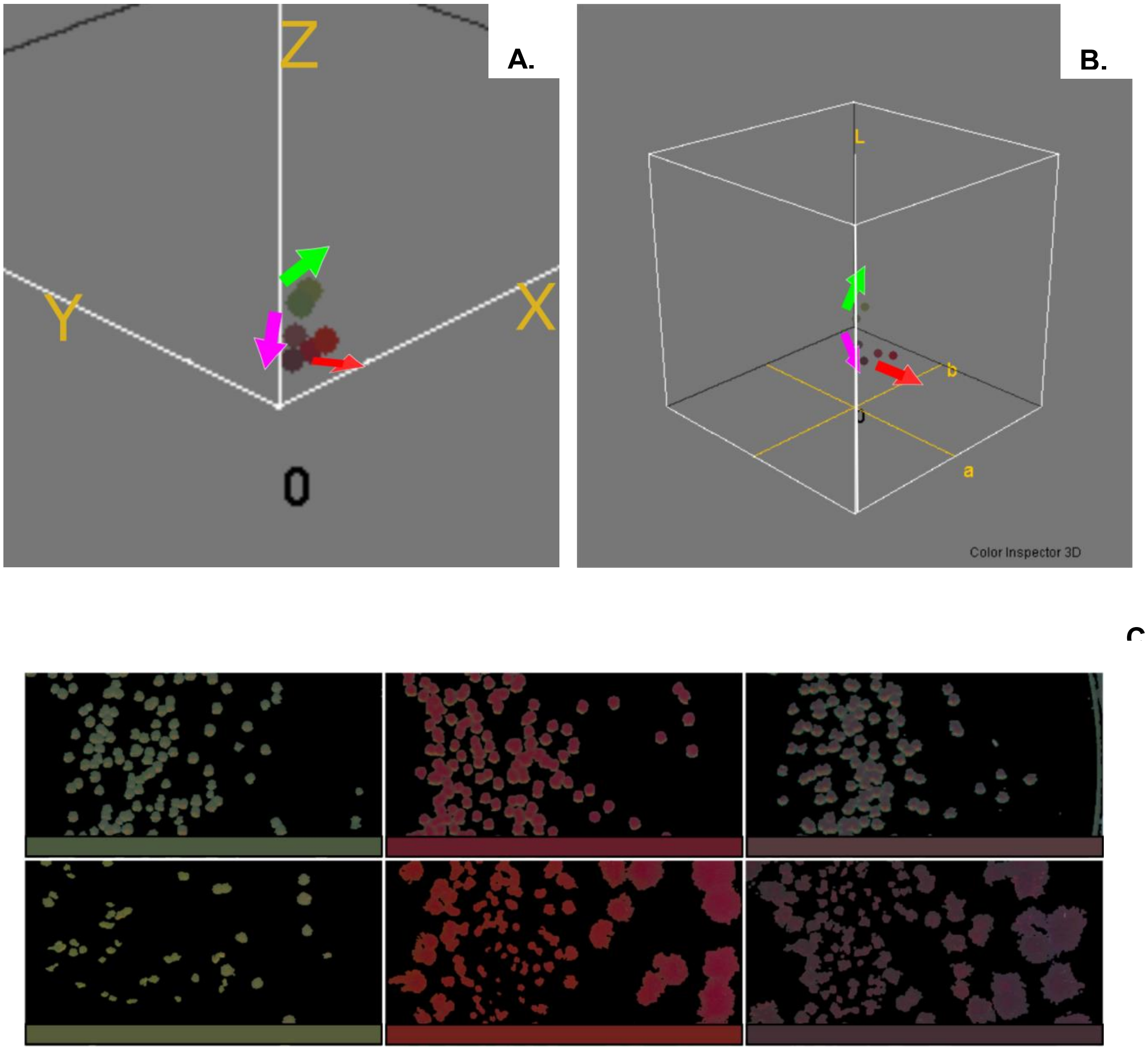

Figure 4.14. A. CIEXYZ_{D50} average color palette plot for *P. aeruginosa* colonies at 16 h and 48 h reads for LA TTC and TV media, the green, red, and violet arrows indicate a color shift between reads in LA, TTC and TV media, respectively. B. CIELAB D50 average color palette plot for *P. aeruginosa* colonies at 16 h and 48 h reads for LA TTC and TV media, the green, red, and violet arrows indicate a color shift between reads in LA, TTC and TV media, respectively. C. Details of *P. aeruginosa* colony images, on top of their respective average CIELAB color pallet color. Colonies correspond, from right to left, to LA colonies, TC colonies, and TV colonies, 16 h images appear on top while 48 h counterparts appear right below these.

CIELAB coordinate plots of *S. aureus* colony colors feature a strong shift in LA color between reads and depict separated 16 h colony coordinates for TTC and TV media colonies. The colors of these, however, converged in 48 h reads, with very close coordinates (see Figure 4.15 B).

Pictures of segmented *S. aureus* colonies featured homogenously colored control in all LA colonies as well as in 16h and 448 h TC and TV colonies. Meanwhile color of 48 h TC and TV colonies appeared to feature distinctive markedly different color regions, with strongly colored centers. Colors used in the color pallet seem to be reasonably representative of both colony regions, however, when reviewed (see Figure 4.15 C)

Δ_{XYZ} and ΔE_{ab} metrics that computed color differences between colonies in chromogenic plates and those of control LA plates were compared by using normalized bar graphs of both metrics. Divergent tendencies were spotted for TTC media in their respective bar graphs. Meanwhile, fairly similar values could be seen in TV media in a side by side comparison of both metrics (see Figure 4.16). *P. aeruginosa* values were the lowest at all times in both metrics, while *E. coli* always displayed the most moderate color shifts between reads (see Figure 4.16).

Δ_{XYZ} *E. coli* 16 hour values were the highest. The largest Δ_{XYZ} color development, however, was spotted in both chromogenic media, of 48 h *S. aureus* plates which suffered a dramatic increase in Δ_{XYZ} between 16 h and 48 h reads (see Figure 4.16). Values for both 48 h TTC and TV plates were remarkably higher than those of *E. coli* colonies (see Figure 4.16). Marked increases between reads in Δ_{XYZ} could be appreciated in TV plates of *S. aureus and P. aeruginosa* colonies (see Figure 4.16).

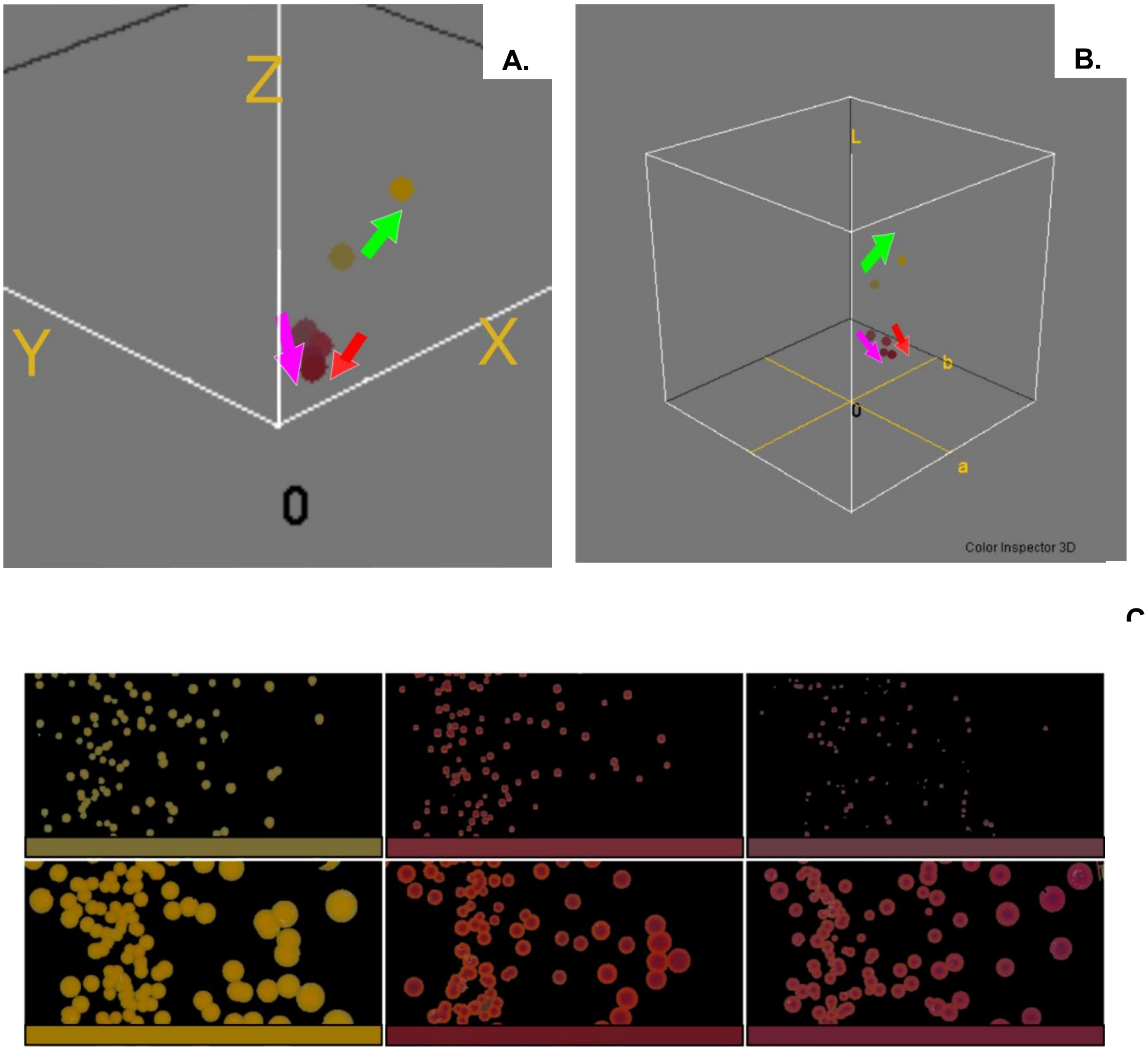

Figure 4.15. A. CIEXYZD50 average color palette plot for *S. aureus* colonies at 16 h and 48 h reads for LA TTC and TV media, the green, red, and violet arrows indicate a color shift between reads in LA, TTC and TV media, respectively. B. CIELAB D50 average color palette plot for *S. aureus* colonies at 16 h and 48 h reads for LA TTC and TV media, the green, red, and violet arrows indicate a color shift between reads in LA, TTC and TV media, respectively. C. Details of *S. aureus* colony images, on top of their respective average CIELAB color pallet color. Colonies correspond, from right to left, to LA colonies, TC colonies, and TV colonies, 16 h images appear on top while 48 h counterparts appear right below these.

TV media featured apparent increases in ΔE_{ab} for *S. aureus* and *P. aeruginosa* colonies between reads (see Figure 4.16). While ΔE_{ab} values for 48 h TC media *E. coli* and *S. aureus* colonies had close values, their TV counterparts featured much larger values for *S. aureus* colonies (see Figure 4.16).

As evidenced by the tridimensional color coordinate plots, *E. coli* colony ΔE_{ab} were mainly caused by changes in the reference LA colony colors, the same held true for ΔE_{XYZ} changes in TC colonies (see Figure 4.13). Conversely, the rest of color changes that were observed between separate reads could be attributed to changes in both control LA colonies and colonies in the chromogenic plates (see Figure 4.13, Figure 4.14, and Figure 4.15).

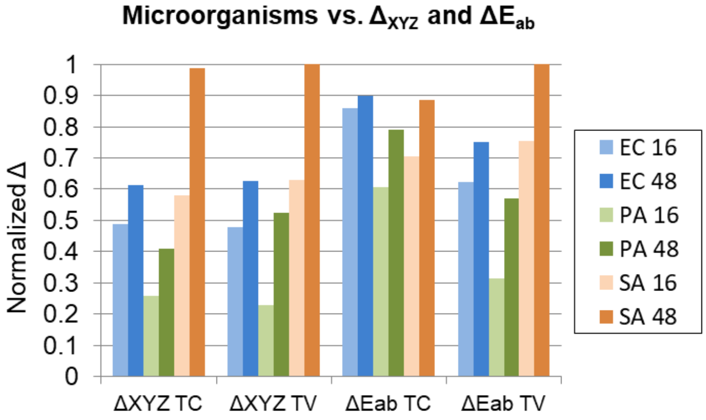

Figure 4.16. Full plate average Δ_{XYZ} and ΔE_{ab} normalized values for TTC (TC) and TV versus the control LA gray value given EC 16, EC 48, PA 16, PA 48, SA 16, and SA 48 refer to *E. coli*, and *P. aeruginosa*, and *S. aureus* plates at 16 h and 48 h, respectively.

Finally, ΔE_{ab} and Δ_{XYZ} heat maps supplied information regarding every possible colony color combination. Both ΔE_{ab} and Δ_{XYZ} heat maps featured a number of readily apparent patterns. Perhaps the most remarkable pattern was the high distance that *S. aureus* 48 h colony color reads held with all other colonies, meanwhile, *S. aureus* 16 h reads also displayed high distances with all other colonies (see Table 4.2 and Table 4.3). *E. coli* and *P. aeruginosa* LA colonies appeared to have close colony colors (see Table 4.2 and Table 4.3). *E. coli* 16 h TC color coordinates appeared to be very close to *E. coli* and *P. aeruginosa* 48 h TC colors (see Table 4.2 and Table 4.3). Rather low distances between TC and TV 48 h media colonies in *S. aureus* cultures could be detected in both heat maps (see Table 4.2 and Table 4.3).

Closeness of color coordinates between successive reads of colonies in the same media indicated low color development between reads. When comparing both heat maps, agreeably, fairly low color differences could be spotted for successive reads of colonies of a given chromogenic media, *S. aureus* and *P. aeruginosa* colonies, however, displayed larger color differences (see Table 4.2 and Table 4.3).

Table 4.2. Heat-map table of Δ_{XYZ} distances of average CIEXYZ$_{D50}$ values that confronts all microorganisms, media types and image capture times. Red cells correspond to low distances between colony colors, orange cells indicate intermediate low values, yellow cells indicate intermediate high values, and green ones indicate high distance values.

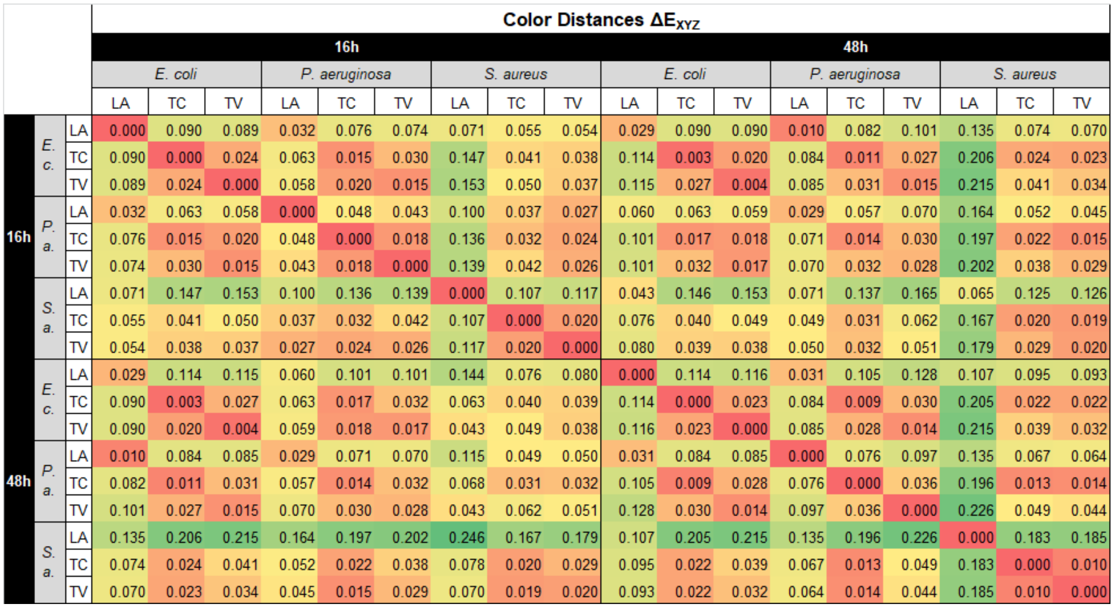

Color Distances ΔE_{XYZ}

			16h									**48h**								
			E. coli			*P. aeruginosa*			*S. aureus*			*E. coli*			*P. aeruginosa*			*S. aureus*		
			LA	TC	TV	LA	TC	TV	LA	TC	TV	LA	TC	TV	LA	TC	TV	LA	TC	TV
16h	*E. c.*	LA	0.000	0.090	0.089	0.032	0.076	0.074	0.071	0.055	0.054	0.029	0.090	0.090	0.010	0.082	0.101	0.135	0.074	0.070
		TC	0.090	0.000	0.024	0.063	0.015	0.030	0.147	0.041	0.038	0.114	0.003	0.020	0.084	0.011	0.027	0.206	0.024	0.023
		TV	0.089	0.024	0.000	0.058	0.020	0.015	0.153	0.050	0.037	0.115	0.027	0.004	0.085	0.031	0.015	0.215	0.041	0.034
	P. a.	LA	0.032	0.063	0.058	0.000	0.048	0.043	0.100	0.037	0.027	0.060	0.063	0.059	0.029	0.057	0.070	0.164	0.052	0.045
		TC	0.076	0.015	0.020	0.048	0.000	0.018	0.136	0.032	0.024	0.101	0.017	0.018	0.071	0.014	0.030	0.197	0.022	0.015
		TV	0.074	0.030	0.015	0.043	0.018	0.000	0.139	0.042	0.026	0.101	0.032	0.017	0.070	0.032	0.028	0.202	0.038	0.029
	S. a.	LA	0.071	0.147	0.153	0.100	0.136	0.139	0.000	0.107	0.117	0.043	0.146	0.153	0.071	0.137	0.165	0.065	0.125	0.126
		TC	0.055	0.041	0.050	0.037	0.032	0.042	0.107	0.000	0.020	0.076	0.040	0.049	0.049	0.031	0.062	0.167	0.020	0.019
		TV	0.054	0.038	0.037	0.027	0.024	0.026	0.117	0.020	0.000	0.080	0.039	0.038	0.050	0.032	0.051	0.179	0.029	0.020
48h	*E. c.*	LA	0.029	0.114	0.115	0.060	0.101	0.101	0.144	0.076	0.080	0.000	0.114	0.116	0.031	0.105	0.128	0.107	0.095	0.093
		TC	0.090	0.003	0.027	0.063	0.017	0.032	0.063	0.040	0.039	0.114	0.000	0.023	0.084	0.009	0.030	0.205	0.022	0.022
		TV	0.090	0.020	0.004	0.059	0.018	0.017	0.043	0.049	0.038	0.116	0.023	0.000	0.085	0.028	0.014	0.215	0.039	0.032
	P. a.	LA	0.010	0.084	0.085	0.029	0.071	0.070	0.115	0.049	0.050	0.031	0.084	0.085	0.000	0.076	0.097	0.135	0.067	0.064
		TC	0.082	0.011	0.031	0.057	0.014	0.032	0.068	0.031	0.032	0.105	0.009	0.028	0.076	0.000	0.036	0.196	0.013	0.014
		TV	0.101	0.027	0.015	0.070	0.030	0.028	0.043	0.062	0.051	0.128	0.030	0.014	0.097	0.036	0.000	0.226	0.049	0.044
	S. a.	LA	0.135	0.206	0.215	0.164	0.197	0.202	0.246	0.167	0.179	0.107	0.205	0.215	0.135	0.196	0.226	0.000	0.183	0.185
		TC	0.074	0.024	0.041	0.052	0.022	0.038	0.078	0.020	0.029	0.095	0.022	0.039	0.067	0.013	0.049	0.183	0.000	0.010
		TV	0.070	0.023	0.034	0.045	0.015	0.029	0.070	0.019	0.020	0.093	0.022	0.032	0.064	0.014	0.044	0.185	0.010	0.000

Far from giving way to similar conclusions, many discrepancies could be spotted between both heat maps. Perhaps the most remarkable of these arose when comparing difference values for *E. coli* 16 h LA vs. *E. coli* 16h and 48 h TC colonies. Other examples could be *P. aeruginosa* 16 h LA versus 48 h TTC or TV colors. Many other inconsistencies existed (see Table 4.2 and Table 4.3).

Table 4.3. Heat-map table of ΔE_{ab} distances of average CIELAB D50 values that confronts all microorganisms, media types and image capture times. Different-colony distances below a value of 5 are featured in bold letters and surrounded by a rectangle. Red cells correspond to low distances between colony colors, orange cells indicate intermediate low values, yellow cells indicate intermediate high values, and green ones indicate high distance values.

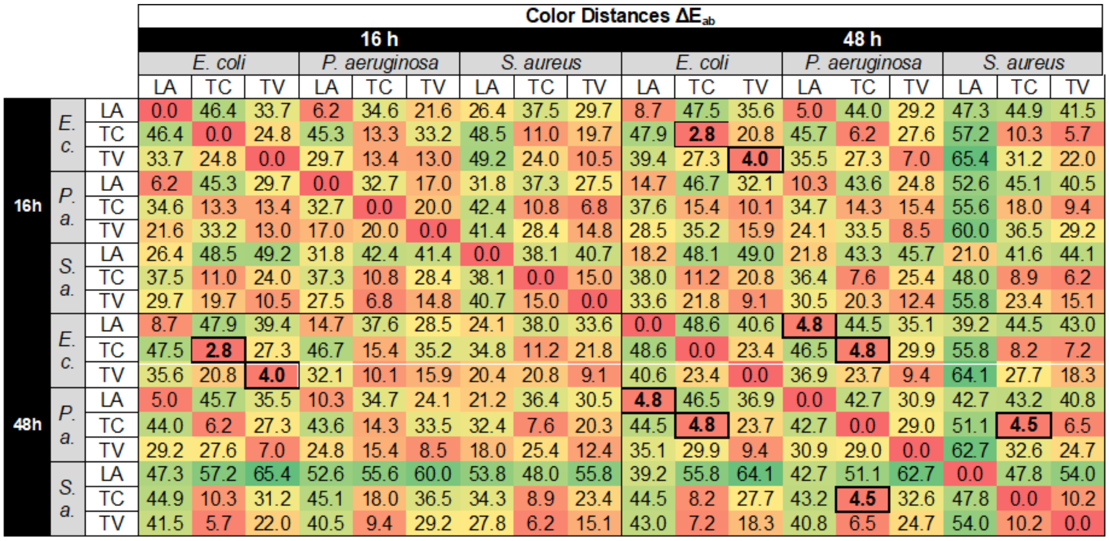

			Color Distances ΔE_{ab}																	
			16 h									48 h								
			E. coli			*P. aeruginosa*			*S. aureus*			*E. coli*			*P. aeruginosa*			*S. aureus*		
			LA	TC	TV	LA	TC	TV	LA	TC	TV	LA	TC	TV	LA	TC	TV	LA	TC	TV
16h	*E. c.*	LA	0.0	46.4	33.7	6.2	34.6	21.6	26.4	37.5	29.7	8.7	47.5	35.6	5.0	44.0	29.2	47.3	44.9	41.5
		TC	46.4	0.0	24.8	45.3	13.3	33.2	48.5	11.0	19.7	47.9	**2.8**	20.8	45.7	6.2	27.6	57.2	10.3	5.7
		TV	33.7	24.8	0.0	29.7	13.4	13.0	49.2	24.0	10.5	39.4	27.3	**4.0**	35.5	27.3	7.0	65.4	31.2	22.0
	P. a.	LA	6.2	45.3	29.7	0.0	32.7	17.0	31.8	37.3	27.5	14.7	46.7	32.1	10.3	43.6	24.8	52.6	45.1	40.5
		TC	34.6	13.3	13.4	32.7	0.0	20.0	42.4	10.8	6.8	37.6	15.4	10.1	34.7	14.3	15.4	55.6	18.0	9.4
		TV	21.6	33.2	13.0	17.0	20.0	0.0	41.4	28.4	14.8	28.5	35.2	15.9	24.1	33.5	8.5	60.0	36.5	29.2
	S. a.	LA	26.4	48.5	49.2	31.8	42.4	41.4	0.0	38.1	40.7	18.2	48.1	49.0	21.8	43.3	45.7	21.0	41.6	44.1
		TC	37.5	11.0	24.0	37.3	10.8	28.4	38.1	0.0	15.0	38.0	11.2	20.8	36.4	7.6	25.4	48.0	8.9	6.2
		TV	29.7	19.7	10.5	27.5	6.8	14.8	40.7	15.0	0.0	33.6	21.8	9.1	30.5	20.3	12.4	55.8	23.4	15.1
48h	*E. c.*	LA	8.7	47.9	39.4	14.7	37.6	28.5	24.1	38.0	33.6	0.0	48.6	40.6	**4.8**	44.5	35.1	39.2	44.5	43.0
		TC	47.5	**2.8**	27.3	46.7	15.4	35.2	34.8	11.2	21.8	48.6	0.0	23.4	46.5	**4.8**	29.9	55.8	8.2	7.2
		TV	35.6	20.8	**4.0**	32.1	10.1	15.9	20.4	20.8	9.1	40.6	23.4	0.0	36.9	23.7	9.4	64.1	27.7	18.3
	P. a.	LA	5.0	45.7	35.5	10.3	34.7	24.1	21.2	36.4	30.5	**4.8**	46.5	36.9	0.0	42.7	30.9	42.7	43.2	40.8
		TC	44.0	6.2	27.3	43.6	14.3	33.5	32.4	7.6	20.3	44.5	**4.8**	23.7	42.7	0.0	29.0	51.1	**4.5**	6.5
		TV	29.2	27.6	7.0	24.8	15.4	8.5	18.0	25.4	12.4	35.1	29.9	9.4	30.9	29.0	0.0	62.7	32.6	24.7
	S. a.	LA	47.3	57.2	65.4	52.6	55.6	60.0	53.8	48.0	55.8	39.2	55.8	64.1	42.7	51.1	62.7	0.0	47.8	54.0
		TC	44.9	10.3	31.2	45.1	18.0	36.5	34.3	8.9	23.4	44.5	8.2	27.7	43.2	**4.5**	32.6	47.8	0.0	10.2
		TV	41.5	5.7	22.0	40.5	9.4	29.2	27.8	6.2	15.1	43.0	7.2	18.3	40.8	6.5	24.7	54.0	10.2	0.0

In the case of ΔE_{ab} color difference results, where threshold analysis levels were available (see section 3.1.2.4), no colony combination featured a distance below the JND level (2.3). Meanwhile, several color differences lied below the relevant color difference threshold (5), these were differences between 16 h and 48 h TC *E. coli* colonies, and between their TV equivalents. Differences between *P. aeruginosa* 48 h LA values and *E. coli* LA values also appeared to be below the relevance threshold, as well as 48 h TC *P. aeruginosa* values when compared with 48 h TC and TV *E. coli* and *S. aureus* ones (see Table 4.3)

4.1.3.3. Color Measurements for Media Performance Comparison

Media performance was assessed through the use of Δ_{XYZ} and ΔE_{ab} metrics of colony color differences in the third crown of *E. coli* spiral plates. It was readily evident that considerably different conclusions could be taken depending on which of the two metrics was used. Data plots of the normalized values obtained using each metric were used to compare results (see Figure 4.17).

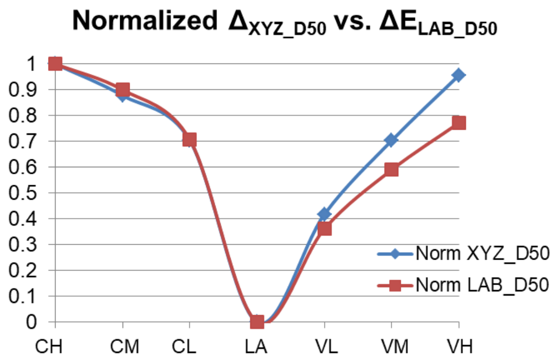

Figure 4.17. Plot of normalized Δ_{XYZ} and ΔE_{ab} values of images captured by CanoScan_1. D. CH, CM, CL, LA, VL, VM, VH, respectively stand for high medium and low TTC concentration media, Letheen agar, and low, medium and high TV concentration media.

When comparing the plots of TV and TTC media, performances of high concentration TV and TTC media formulations appeared to be very similar in the Δ_{XYZ} plot (see Figure 4.17). Meanwhile, ΔE_{ab} counterpart values differed greatly (see Table 4.4), The ΔE_{ab} plot indicated a superior performance of high TTC concentration media and close performances of low concentration TTC media and high concentration TV media (see Figure 4.17).

Use of the differences between normalized scales allowed to easily compare Δ_{XYZ} and ΔE_{ab} data. While values for TTC based media are very close, and display very low normalized differences, values for TV-based media have increasingly dissimilar relative values as the plot moves from low to high TV concentration media values, thus the numeric values in Table 4.4 confirm the increase in difference of relative Δ scale values as TV concentration in the chromogenic media increases.

Table 4.4. Values for ΔE_{ab} and Δ_{XYZ} values obtained when comparing tested media colonies to LA media *E. coli* third crown colonies. The table features values in their respective native scales, normalized, and differences between the normalized values.

Media	ΔE_{ab}	N. ΔE_{ab}	Δ_{XYZ}	N. ΔE_{XYZ}	N. Diff.
CH	22.86	1.000	0.0767	1.000	0.000
CM	20.65	0.900	0.0676	0.878	0.022
CL	16.37	0.706	0.0546	0.703	0.003
LA	0.76	0.000	0.0021	0.000	0.000
VI	8.77	0.362	0.0333	0.418	-0.056
VM	13.81	0.591	0.0546	0.704	-0.113
VH	17.82	0.772	0.0735	0.957	-0.185

4.1.3.4. Scanner Characterization, Gauge Reproducibility and Repeatability

4.1.3.4.1. Colorimetric Comparison of Scanner Reads

Colors captured by OpticSlim scanners differed radically from those of CanoScan and Perfection V39 models, registering very close values for all TTC media (see Table 4.5), this explains the flat shape of the first three points of the OpticSlim curve of normalized Δ_{XYZ} and ΔE_{ab} values (see Figure 4.18 A and B).Colony images in Figure 4.18 C evidence very close colors for all TTC media colonies imaged by the OpticSlim unit, regardless of their respective media TTC concentrations, and rather more apparent differences in TV media. OpticSlim ΔE_{ab} and Δ_{XYZ} values for TTC media appeared to be very close to each other, thus, only small fluctuations were detected between colonies of different TTC media, these results were statistically confirmed, as discussed in section 4.1.3.4.4. This flat trend in color change plots of TTC media scans differs radically from results obtained in the reads taken by other scanners (see Figure 4.18 A and B). In contrast, OpticSlim ΔE_{ab} and Δ_{XYZ} values for TV media followed a trend that was similar to that of Perfection V39 and CanoScan scans (see Figure 4.18 A and B), with a capacity to distinguish different color differences of colonies in each TV media.

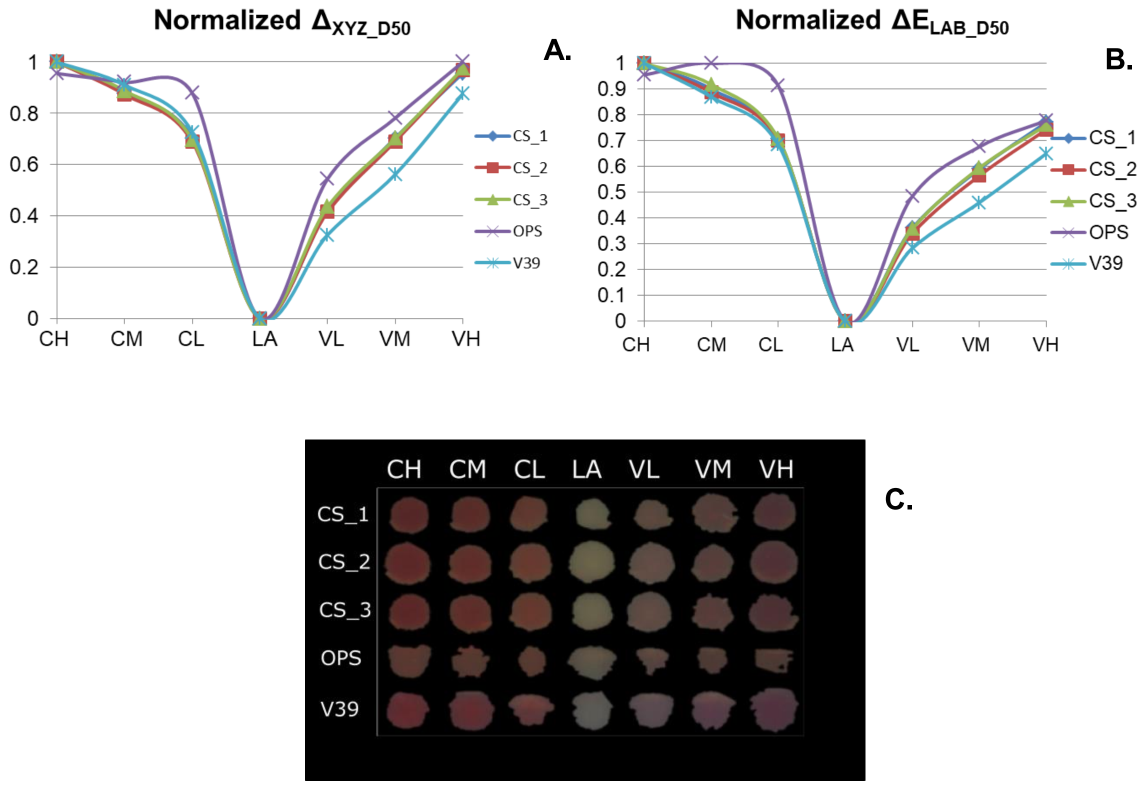

Figure 4.18. A and B. Value plot for the third crown of *E. coli* spiral plates of a given replicate. A. Δ_{XYZ} values plot. B. Δ E ab values. C. Image montage displaying images of colonies in the third spiral crown imaged by CanoScan scanners (m CS_1, CS_2, and CS_3), OpticSlim (OPS), and Perfection V39 (V39). CH, CM, CL, LA, VL, VM, VH, respectively stand for high medium and low TTC concentration media, Letheen agar, and low, medium and high TV concentration media.

Colony images taken by CanoScan and Perfection V39 displayed greater differences in color linked to different media formulations (see Figure 4.18 A and B). When comparing plot segments of ΔXYZ and ΔEab, CanoScan scanners all plot very close values while Perfection V39 values seem to follow very similar charting tendencies for TTC media while slight differences in TV media charting can be noted (see Figure 4.18 A and B).

Table 4.5. Δ_{XYZ} D50 and ΔE_{ab} regular and normalized values for third crown colony color differences of several media types in *E. coli* colonies. Norm. stands for normalized and Normalized diff. for the normalized difference between Δ_{XYZ} and ΔEab values Average values taken from two replicate plates for each media. CH, CM, CL, VL, VM, VH, respectively stand for high medium and low TTC concentration media, Letheen agar, and low, medium and high TV concentration media. Results obtained in each of the five scanners are displayed.

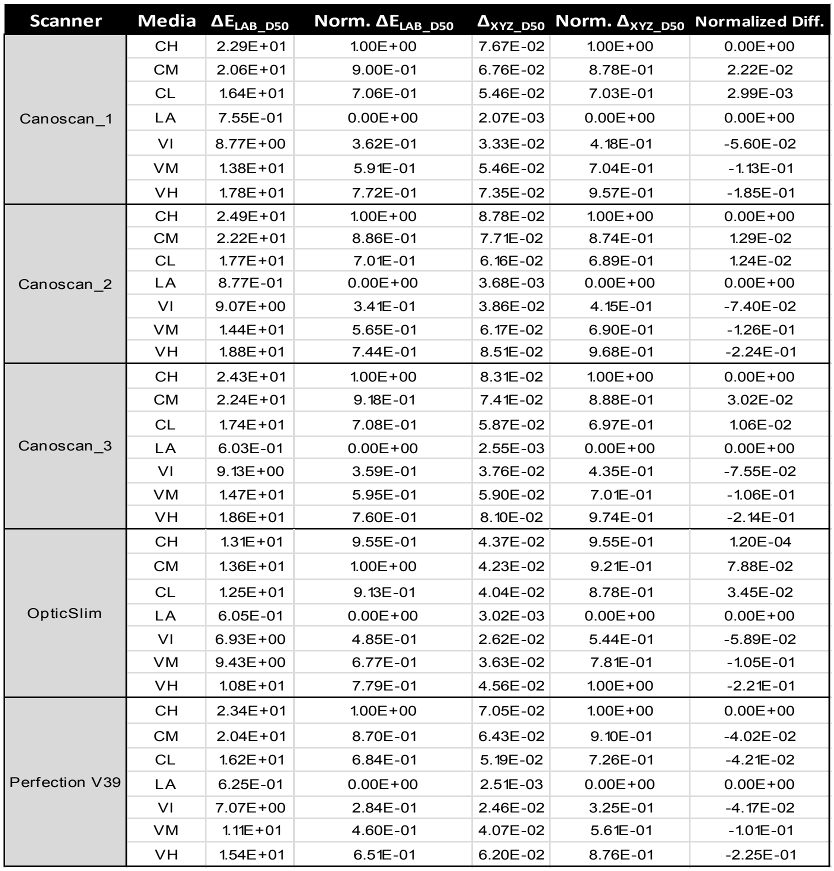

Scanner	Media	ΔE_{LAB_D50}	Norm. ΔE_{LAB_D50}	Δ_{XYZ_D50}	Norm. Δ_{XYZ_D50}	Normalized Diff.
Canoscan_1	CH	2.29E+01	1.00E+00	7.67E-02	1.00E+00	0.00E+00
	CM	2.06E+01	9.00E-01	6.76E-02	8.78E-01	2.22E-02
	CL	1.64E+01	7.06E-01	5.46E-02	7.03E-01	2.99E-03
	LA	7.55E-01	0.00E+00	2.07E-03	0.00E+00	0.00E+00
	VI	8.77E+00	3.62E-01	3.33E-02	4.18E-01	-5.60E-02
	VM	1.38E+01	5.91E-01	5.46E-02	7.04E-01	-1.13E-01
	VH	1.78E+01	7.72E-01	7.35E-02	9.57E-01	-1.85E-01
Canoscan_2	CH	2.49E+01	1.00E+00	8.78E-02	1.00E+00	0.00E+00
	CM	2.22E+01	8.86E-01	7.71E-02	8.74E-01	1.29E-02
	CL	1.77E+01	7.01E-01	6.16E-02	6.89E-01	1.24E-02
	LA	8.77E-01	0.00E+00	3.68E-03	0.00E+00	0.00E+00
	VI	9.07E+00	3.41E-01	3.86E-02	4.15E-01	-7.40E-02
	VM	1.44E+01	5.65E-01	6.17E-02	6.90E-01	-1.26E-01
	VH	1.88E+01	7.44E-01	8.51E-02	9.68E-01	-2.24E-01
Canoscan_3	CH	2.43E+01	1.00E+00	8.31E-02	1.00E+00	0.00E+00
	CM	2.24E+01	9.18E-01	7.41E-02	8.88E-01	3.02E-02
	CL	1.74E+01	7.08E-01	5.87E-02	6.97E-01	1.06E-02
	LA	6.03E-01	0.00E+00	2.55E-03	0.00E+00	0.00E+00
	VI	9.13E+00	3.59E-01	3.76E-02	4.35E-01	-7.55E-02
	VM	1.47E+01	5.95E-01	5.90E-02	7.01E-01	-1.06E-01
	VH	1.86E+01	7.60E-01	8.10E-02	9.74E-01	-2.14E-01
OpticSlim	CH	1.31E+01	9.55E-01	4.37E-02	9.55E-01	1.20E-04
	CM	1.36E+01	1.00E+00	4.23E-02	9.21E-01	7.88E-02
	CL	1.25E+01	9.13E-01	4.04E-02	8.78E-01	3.45E-02
	LA	6.05E-01	0.00E+00	3.02E-03	0.00E+00	0.00E+00
	VI	6.93E+00	4.85E-01	2.62E-02	5.44E-01	-5.89E-02
	VM	9.43E+00	6.77E-01	3.63E-02	7.81E-01	-1.05E-01
	VH	1.08E+01	7.79E-01	4.56E-02	1.00E+00	-2.21E-01
Perfection V39	CH	2.34E+01	1.00E+00	7.05E-02	1.00E+00	0.00E+00
	CM	2.04E+01	8.70E-01	6.43E-02	9.10E-01	-4.02E-02
	CL	1.62E+01	6.84E-01	5.19E-02	7.26E-01	-4.21E-02
	LA	6.25E-01	0.00E+00	2.51E-03	0.00E+00	0.00E+00
	VI	7.07E+00	2.84E-01	2.46E-02	3.25E-01	-4.17E-02
	VM	1.11E+01	4.60E-01	4.07E-02	5.61E-01	-1.01E-01
	VH	1.54E+01	6.51E-01	6.20E-02	8.76E-01	-2.25E-01

A review of Table 4.5 allows confirming a relative proximity of values for CanoScan scanners in general, with values of CanoScan 2 and 3 standing as closer to each other than to CanoScan 1 values. In fact, in all TTC media, regardless of the chromogen concentration, CanoScan1 reads appeared to be the closest to Perfection V39 scans. This changed radically for TV media reads.

In the case of OpticSlim reads, as expected, Table 4.5 displays TTC media values that diverge a lot from those in other scanners. Interestingly, normalized values obtained in the reads feature high concentration TV media as yielding the highest Δ_{XYZ} values, meanwhile TTC medium concentration media yield the largest ΔE_{ab}.

4.1.3.4.2. Gauge Reproducibility and Repeatability analysis

Different performance profiles were detected in the GRR in relation to the scanners and the grayscale and color metrics that were employed. Readers are referred to section 3.1.2.5.1 for a description of the criteria used to establish the validity of results. Several results held true, however, for all metrics. All interscanner GRR that featured the OpticSlim scanner yielded unacceptable Gauge R&R results. In particular, category discrimination levels were always very low, yielding values of 2, where five would be the minimum discrimination capacity for approval of the instrument's Gauge R&R analysis.

Use of OpticSlim in the performed interscanner GRRs was in fact motivated by the wish to assess the capability of the GRR ANOVA based methods to detect malfunctioning scanners. Thus, when discussing interscanner GRR results, results for the interscanner GRR that featured CanoScan, Perfection V39, and OpticSlim scanners will be referred to as "invalid", meanwhile the term "valid" will be used when referencing the second interscanner GRR set-up, which doesn't include OpticSlim scanners.

Indeed, the existence of such low category discrimination values implied incapability of separating the measurements of the different samples into distinct categories, this was mostly due to poor reproducibility standard deviation values, these will be discussed in the paragraphs to follow.

4.1.3.4.3. Grayscale Scanner Characterization, Gauge R&R

Interestingly all GRR ANOVAs yielded similar conclusions, indicating significant contributions to result variability by parts (these would correspond to different tested media) and instruments in the interscanner (same scanner model) GRR; and significant contributions by parts, instruments and interactions of these for all intrascanner GRRs (both in valid and invalid GRRs).

Interestingly, in all invalid intrascanner GRRs, repeatability values were good (below 10%), it was reproducibility values that accounted for most of the total GRR variability (see tables Table 4.6 through Table 4.9). This indicated that the scanner model (called instrument in the GRR scheme) and the instrument-part interaction were, in fact, responsible for most of the variability.

4.1.3.4.3.1. C_{Avg} GRR Results

Channel average grayscale conversion (C_{Avg}) was one of the two grayscales that yielded good results both in the interscanner and the valid interscanner GRR analysis.

In the intrascanner C_{Avg} GRR, the repeatability ratio was lower than the reproducibility ratio, the C_{Avg} GRR was the only intrascanner GRR where this was seen, furthermore, the total GRR uncertainty ratio was the largest of all the intrascanner GRRs. Since the respective ANOVAs for all intrascanner GRRs indicated a significant contribution of instruments to GRR reproducibilities and no instrument-part interactions, differences in performance of the instruments are to be held liable for the higher reproducibility uncertainty of C_{Avg}, the explanation for this might be an unequal reproducibility profile for the different RGB channels in the scanned images. More precisely, the increase in reproducibility-linked uncertainty appears to indicate that red and, especially, blue channels might have larger uncertainties associated to them than the green channel.

This would be deduced from the difference in weights of the rest of grayscale formulae when compared with the C_{Avg} conversion formula. Clarification of this was thought to be beyond the scope of this thesis, however. Nonetheless, variations in uncertainty related to the employed formula evidence need to address GRR specifically for every grayscale conversion.

The interscanner GRR featured optimal reproducibility and repeatability values, 1.93% and 0.91%, respectively, instrument induced variability values were also remarkably low, 1.76%, especially if compared with those obtained in the invalid interscanner assay that reached 8.36%. Furthermore, intrascanner assays pointed to a good discrimination capacity, 8 categories were distinguishable.

Both interscanner GRRs featured higher values of total GRR reproducibility, while values obtained for the invalid interscanner GRR were in the marginally acceptable range, with total standard deviation ratios of 19%, those for the valid interscanner assays were in the good range, reaching 6.47%. In both interscanner GRR, the highest uncertainty contributions were those linked to the instrument factor, however, a significant interaction factor between parts and instruments could also be detected (seeTable 4.6). Reaching 5 categories, the result obtained for the category discrimination confirmed the validity C_{Avg} to measure the existence of differences in colony color.

Table 4.6. Gage Reproducibility and Repeatability ANOVA results for channel average grayscale measurements (CAvg) of interscanner and intrascanner GRR tests. Abbreviations standing for the scanners used in each analysis are specified. Respectively, CS_1, CS_2, CS_3, OPS and V39 make reference to the three different CanoScan units, and to the OpticSlim, and Perfection V39 scanners.

Ch. Avg.	**GRR: CS_1, CS_2, CS_3**			**GRR: CS_1, OPS, V39**			**GRR: CS_1, V39**		
ANOVA α = 0.05	***F***	***p-val***	***sig.***	***F***	***p-val***	***Significant***	***F***	***p-val***	***sig.***
Part	3.89E+03	4.37E-292	Yes	1.50E+03	2.95E-228	Yes	2.45E+03	2.13E-191	Yes
Instrument	5.11E+01	5.88E-20	Yes	3.98E+02	6.29E-87	Yes	3.63E+02	1.26E-47	Yes
Instrument*Part	1.69E-01	9.99E-01	No	4.85E+01	2.80E-64	Yes	2.01E+01	1.50E-18	Yes
Variability	***Var.***	***%***	***Perf.***	***Var.***	***%***	***Performance***	***Var.***	***%***	***Perf.***
Tot Gage R&R	2.33E-05	2.84%	Good	1.29E+01	19.00%	Marginal	5.15E+00	6.47%	Good
Repeatability	7.47E-06	0.91%	Good	1.82E+00	2.68%	Good	9.80E-01	1.23%	Good
Reproducibility	1.58E-05	1.93%	Good	1.10E+01	16.32%	Marginal	4.17E+00	5.23%	Good
Instrument	1.44E-05	1.76%	Good	5.66E+00	8.36%	Good	3.00E+00	3.76%	Good
Inst*Part	-	-	-	5.39E+00	7.96%	Good	1.17E+00	1.47%	Good
Part-to-Part	7.98E-04	97.16%		5.48E+01	81.00%		7.44E+01	93.53%	
Tot Variation	8.21E-04	100.00%		6.77E+01	100.00%		7.96E+01	100.00%	
Categories	8		Good	2		Unacceptable	5		Good

4.1.3.4.3.2. L_{601} GRR Results

Good results were obtained in the intrascanner GRR tests for the L_{601} assay values, with very low total GRR standard deviation ratio of 1.4% and a powerful category discrimination of 11. As in the interscanner C_{Avg} GRRs, total GRR values for the invalid assay appeared to be marginally acceptable while those of the valid GRR were good (see Table 4.7). Meanwhile, interscanner assays featured category discrimination values below 5, rejecting the use of L_{601} for colony grayscale variation measurements linked to color differences (see Table 4.7).

Table 4.7. Gage Reproducibility and Repeatability ANOVA results for *Luma*$_{601}$ (*L*$_{601}$) of interscanner and intrascanner GRR tests. Abbreviations standing for the scanners used in each analysis are specified. Respectively, CS_1, CS_2, CS_3, OPS and V39 make reference to the three different CanoScan units, and to the OpticSlim, and Perfection V39 scanners.

Luma601	**GRR: CS_1, CS_2, CS_3**			**GRR: CS_1, OPS, V39**			**GRR: CS, V39**		
ANOVA α = 0.05	***F***	***p-val***	***sig.***	***F***	***p-val***	***Significant***	***F***	***p-val***	***sig.***
Part	4.90E+03	1.11E-307	Yes	1.78E+03	1.76E-239	Yes	2.79E+03	2.76E-197	Yes
Instrument	5.64E+01	1.13E-21	Yes	7.05E+02	5.17E-117	Yes	6.16E+02	2.40E-64	Yes
Instrument*Part	5.92E-02	1.00E+00	No	6.37E+01	8.66E-77	Yes	2.78E+01	2.63E-24	Yes
Variability	***Var.***	***%***	***Perf.***	***Var.***	***%***	***Performance***	***Var.***	***%***	***Perf.***
Tot Gage R&R	1.81E+00	1.41%	Good	2.11E+01	22.99%	Marginal	9.00E+00	8.39%	Good
Repeatability	1.19E+00	0.93%	Good	1.98E+00	2.16%	Good	1.14E+00	1.06%	Good
Reproducibility	6.13E-01	0.48%	Good	1.91E+01	20.83%	Marginal	7.86E+00	7.33%	Good
Instrument	6.13E-01	0.48%	Good	1.14E+01	12.36%	Marginal	5.96E+00	5.56%	Good
Inst*Part	0.00E+00	0.00%	Good	7.78E+00	8.47%	Good	1.90E+00	1.77%	Good
Part-to-Part	1.26E+02	98.59%		7.08E+01	77.01%		9.82E+01	91.61%	
Tot Variation	1.28E+02	100.00%		9.19E+01	100.00%		1.07E+02	100.00%	
Categories	11		Good	2		Unacceptable	4		Unacceptable

4.1.3.4.3.3. *L*$_{709}$ GRR Results

L$_{709}$ GRRs indicated good repeatability and reproducibility profiles in the intrascanner assay, with a high category discrimination (see Table 4.8). The valid interscanner GRR, displayed a good category discrimination of 5, with good repeatability and reproducibility values. As in other valid interscanner GRRs, repeatability ratio values were low, at 0.88%, while interscanner reproducibility was higher, with a higher contribution to variability coming from instruments than from the part-instrument interactions, which were both significant (see Table 4.8). Thus, results for the GRR indicated that *L*$_{709}$ readings could properly discriminate between colonies with different grayscale values.

Table 4.8. Gage Reproducibility and Repeatability ANOVA results for $Luma_{709}$ (L_{709}) of interscanner and intrascanner GRR tests. Abbreviations standing for the scanners used in each analysis are specified. Respectively, CS_1, CS_2, CS_3, OPS and V39 make reference to the three different CanoScan units, and to the OpticSlim, and Perfection V39 scanners.

Luma709	**GRR: CS_1, CS_2, CS_3**			**GRR: CS, OPS, V39**			**GRR: CS_1, V39**		
ANOVA α = 0.05	***F***	***p-val***	***sig.***	***F***	***p-val***	***Significant***	***F***	***p-val***	***sig.***
Part	6.07E+03	0.00E+00	Yes	2.30E+03	1.00E-256	Yes	3.40E+03	3.87E-206	Yes
Instrument	7.06E+01	4.67E-26	Yes	8.88E+02	3.27E-130	Yes	5.88E+02	8.52E-63	Yes
Instrument*Part	4.97E-01	9.16E-01	No	8.12E+01	8.63E-89	Yes	2.61E+01	4.49E-23	Yes
Variability	***Var.***	***%***	***Perf.***	***Var.***	***%***	***Performance***	***Var.***	***%***	***Perf.***
Tot Gage R&R	1.98E+00	1.25%	Good	2.56E+01	22.24%	Marginal	8.97E+00	6.71%	Good
Repeatability	1.22E+00	0.77%	Good	1.93E+00	1.68%	Good	1.18E+00	0.88%	Good
Reproducibility	7.69E-01	0.49%	Good	2.36E+01	20.56%	Marginal	7.78E+00	5.82%	Good
Instrument	7.69E-01	0.49%	Good	1.39E+01	12.12%	Marginal	5.93E+00	4.44%	Good
Inst*Part	0.00E+00	0.00%	Good	9.70E+00	8.43%	Good	1.85E+00	1.39%	Good
Part-to-Part	1.56E+02	98.75%		8.94E+01	77.76%		1.25E+02	93.29%	
Tot Variation	1.58E+02	100.00%		1.15E+02	100.00%		1.34E+02	100.00%	
Categories	12		Good	2		Unacceptable	5		Good

4.1.3.4.3.4. *L’* GRR Results

The *L’* intrascanner GRR indicated a good total uncertainty profile for same scanner device reads, with a high category discrimination, and very low reproducibility and repeatability uncertainty ratios (see Table 4.9). Meanwhile, despite having acceptable total GRR variability ratios, category discrimination appeared to be insufficient for both invalid and valid interscanner GRRs, these standing, holding, respectively, values of 2 and 4.

Table 4.9. Gage Reproducibility and Repeatability ANOVA results for luminance (*L'*) of interscanner and intrascanner GRR tests. Abbreviations standing for the scanners used in each analysis are specified. Respectively, CS_1, CS_2, CS_3, OPS and V39 make reference to the three different CanoScan units, and to the OpticSlim, and Perfection V39 scanners.

Luminance	**GRR: CS_1, CS_2, CS_3**			**GRR: CS_1, OPS, V39**			**GRR: CS_1, V39**		
ANOVA α = 0.05	***F***	***p-val***	***sig.***	***F***	***p-val***	***Significant***	***F***	***p-val***	***sig.***
Part	5.20E+03	0.00E+00	Yes	1.91E+03	1.69E-244	Yes	2.98E+03	3.12E-200	Yes
Instrument	5.12E+01	5.46E-20	Yes	7.95E+02	7.56E-124	Yes	7.20E+02	9.15E-70	Yes
Instrument*Part	6.29E-01	8.17E-01	No	6.45E+01	2.35E-77	Yes	3.20E+01	3.43E-27	Yes
Variability	***Var.***	***%***	***Perf.***	***Var.***	***%***	***Performance***	***Var.***	***%***	***Perf.***
Tot Gage R&R	1.72E+00	1.27%	Good	2.27E+01	22.97%	Marginal	1.02E+01	8.96%	Good
Repeatability	1.17E+00	0.86%	Good	1.97E+00	2.00%	Good	1.13E+00	0.99%	Good
Reproducibility	5.57E-01	0.41%	Good	2.07E+01	20.97%	Marginal	9.11E+00	7.97%	Good
Instrument	5.57E-01	0.41%	Good	1.29E+01	13.04%	Marginal	6.93E+00	6.06%	Good
Inst*Part	0.00E+00	0.00%	Good	7.82E+00	7.93%	Good	2.18E+00	1.91%	Good
Part-to-Part	1.35E+02	98.73%		7.60E+01	77.03%		1.04E+02	91.04%	
Tot Variation	1.36E+02	100.00%		9.86E+01	100.00%		1.14E+02	100.00%	
Categories	12		Good	2		Unacceptable	4		Unacceptable

4.1.3.4.4. Colorimetric Scanner Characterization: Δ_{XYZ} and ΔE_{ab} Gauge R&R

Instrument and instrument-part, that is instrument-media, interactions were deemed significant in all ANOVA GRR colorimetric analysis, with values far below the set significance level. Thus, instruments and their combinations with certain media influenced assay uncertainty (see Table 4.10 and Table 4.11).

Repeatability-linked variability remained low, below 1 % for all GRR analysis carried out with the exception of the invalid interscanner analysis, where it reached a value of 2.06% (see Table 4.10 and Table 4.11). These values indicate low values of standard deviation in same-sample reads taken by any given instrument, and point to reproducibility as the main source for variation.

The GRR ANOVA-based analysis of Δ_{XYZ} reads displayed optimal performance of interscan assays with low repeatability (0.91%) and reproducibility (1.93%) ratios of the total variance. Furthermore, the number of categories was above the threshold acceptance level of 5 (see Table 4.10). The invalid interscanner assays displayed remarkably high percentage ratios of reproducibility variance (20.7%), this indicated that measurements taken with the instruments could be considered marginally acceptable. Thus, the interscanner GRR analysis evidenced that instruments stood as a large source of variance when comparing all three instrument models that were evaluated.

Table 4.10. Gage Reproducibility and Repeatability ANOVA results for Δ_{XYZ} measurements of interscanner and intrascanner GRR tests. Abbreviations standing for the scanners used in each analysis are specified. Respectively, CS_1, CS_2, CS_3, OPS and V39 make reference to the three different CanoScan units, and to the OpticSlim, and Perfection V39 scanners.

Δ_{XYZ}	GRR: CS_1, CS_2, CS_3			GRR: CS, OPS, V39			GRR: CS, V39		
ANOVA α = 0.05	***F***	***p-value***	***sig.***	***F***	***p-value***	***sig.***	***F***	***p-value***	***sig.***
Part	5.13E+03	0.00E+00	yes	1.87E+03	8.46E-243	yes	3.24E+03	5.26E-204	yes
Instrument	2.20E+02	1.41E-60	yes	7.53E+02	9.97E-121	yes	3.86E+02	1.95E-49	yes
Instrument*Part	4.03E+00	7.70E-06	yes	6.36E+01	1.12E-76	yes	3.38E+01	1.99E-28	yes
Variability	***Variance***	***%***	***Performance***	***Variance***	***%***	***Performance***	***Variance***	***%***	***Performance***
Tot Gage R&R	2.33E-05	2.84%	Good	1.35E-04	22.76%	Marginal	3.91E-05	5.82%	Good
Repeatability	7.47E-06	0.91%	Good	1.22E-05	2.06%	Good	6.32E-06	0.94%	Good
Reproducibility	1.58E-05	1.93%	Good	1.23E-04	20.70%	Marginal	3.28E-05	4.88%	Good
Instrument	1.44E-05	1.76%	Good	7.51E-05	12.66%	Marginal	1.98E-05	2.95%	Good
Inst*Part	1.42E-06	0.17%	Good	4.77E-05	8.04%	Good	1.30E-05	1.93%	Good
Part-to-Part	7.98E-04	97.16%		4.58E-04	77.24%		6.34E-04	94.18%	
Tot Variation	8.21E-04	100.00%		5.93E-04	100.00%		6.73E-04	100.00%	
Categories	8		Good	2		Unacceptable	5		Good

Moreover, the number of categories detected in the invalid GRR was 2, well below the threshold acceptance value of 5. The latter implied the interscanner GRR analysis couldn't be considered acceptable due to the low number of groups distinguished in the data.

Removal of the OpticSlim results from the GRR interscanner analysis, produced a remarkable improvement in reproducibility variance ratios which decreased dramatically from roughly 20% (20.7% for Δ_{XYZ} and 19.67% for ΔE_{ab} measurements) to values of 4.88%, for Δ_{XYZ}, and 1.95%, for ΔE_{ab}, the number of detected categories rose beyond the acceptability threshold of 5 in both cases (see Table 4.10 and Table 4.11). Thus, discard of OpticSlim scans improved the precision of the measurements significantly, in particular through a decrease in reproducibility-linked variability.

Table 4.11. Gage Reproducibility and Repeatability ANOVA results for ΔE_{ab} measurements of interscanner and intrascanner GRR tests. Abbreviations standing for the scanners used in each analysis are specified. Respectively, CS_1, CS_2, CS_3, OPS and V39 make reference to the three different CanoScan units, and to the OpticSlim, and Perfection V39 scanners.

ΔE_{ab}	GRR: CS_1, CS_2, CS_3			GRR: CS, OPS, V39			GRR: CS, V39		
ANOVA α = 0.05	***F***	***p-value***	***sig.***	***F***	***p-value***	***sig.***	***F***	***p-value***	***sig.***
Part	1.05E+04	0.00E+00	yes	5.85E+03	0.00E+00	yes	4.98E+03	2.00E-223	yes
Instrument	1.12E+02	1.81E-37	yes	2.07E+03	4.93E-182	yes	1.48E+02	4.49E-26	yes
Instrument*Part	8.94E+00	9.15E-15	yes	1.98E+02	6.43E-139	yes	3.45E+01	7.86E-29	yes
Variability	***Variance***	***%***	***Performance***	***Variance***	***%***	***Performance***	***Variance***	***%***	***Performance***
Tot Gage R&R	7.04E-01	1.09%	Good	1.08E+01	20.34%	Marginal	1.55E+00	2.58%	Good
Repeatability	2.91E-01	0.45%	Good	3.58E-01	0.68%	Good	3.79E-01	0.63%	Good
Reproducibility	4.13E-01	0.64%	Good	1.04E+01	19.67%	Marginal	1.17E+00	1.95%	Good
Instrument	2.68E-01	0.42%	Good	5.99E+00	11.32%	Marginal	3.82E-01	0.64%	Good
Inst*Part	1.45E-01	0.22%	Good	4.42E+00	8.35%	Good	7.92E-01	1.32%	Good
Part-to-Part	6.38E+01	98.91%		4.22E+01	79.66%		5.86E+01	97.42%	
Tot Variation	6.45E+01	100.00%		5.29E+01	100.00%		6.01E+01	100.00%	
Categories	13		Good	2			8		Good

Despite yielding unacceptable GRR results, GRR ANOVAs carried out for Δ_{XYZ} and ΔE_{ab} indicated the presence of statistically significant differences in means (see Table 4.10 and Table 4.11, GRR for CS_1, OPS, and V39). Results for the Tukey *post-hoc* tests performed to assess adequate discrimination of different levels of color development in media with different concentrations of the same chromogen can be found in Table 4.12 and Table 4.13.

In reads taken with CanoScan and Perfection V39 models, all media formulated with different concentrations of a given chromogen displayed significant differences in the color distance metric (see Table 4.12 and Table 4.13), as revealed by *post-hoc* Tukey analysis. Arguably, this corroborated that these models were able to record how different concentrations of a given chromogen generated different levels of color development.

Table 4.12. Tukey ANOVA post-hoc test for the Δ_{XYZ} distance measurements of colonies in the third spiral crown. Q-stat values and p-values for combinations of color distance reads taken from media with different concentrations of the same chromogen. CH, CM, CL, LA, VL, VM, VH, respectively stand for high medium and low TTC concentration media, Letheen agar, and low, medium and high TV concentration media. Data are presented according to the values obtained for each scanner (CS_1, CS_2, and CS_3), OpticSlim (OPS), and Perfection V39 (V39). Results above significance level are shown in red.

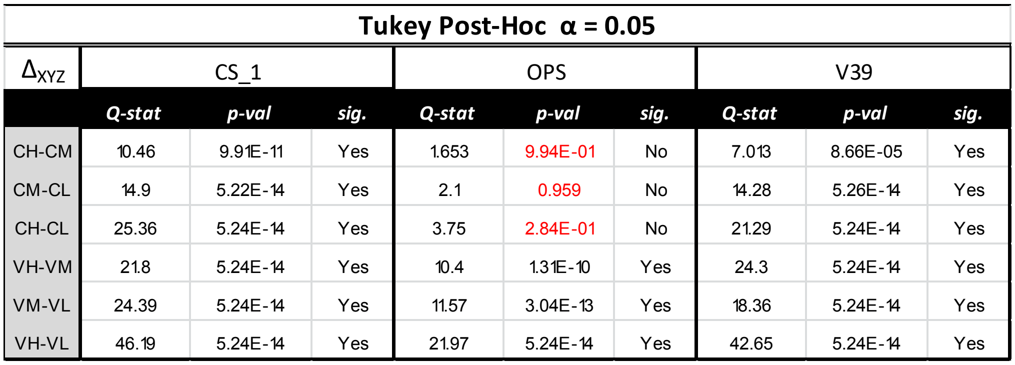

Tukey Post-Hoc α = 0.05									
Δ_{XYZ}	CS_1			OPS			V39		
	Q-stat	***p-val***	***sig.***	***Q-stat***	***p-val***	***sig.***	***Q-stat***	***p-val***	***sig.***
CH-CM	10.46	9.91E-11	Yes	1.653	9.94E-01	No	7.013	8.66E-05	Yes
CM-CL	14.9	5.22E-14	Yes	2.1	0.959	No	14.28	5.26E-14	Yes
CH-CL	25.36	5.24E-14	Yes	3.75	2.84E-01	No	21.29	5.24E-14	Yes
VH-VM	21.8	5.24E-14	Yes	10.4	1.31E-10	Yes	24.3	5.24E-14	Yes
VM-VL	24.39	5.24E-14	Yes	11.57	3.04E-13	Yes	18.36	5.24E-14	Yes
VH-VL	46.19	5.24E-14	Yes	21.97	5.24E-14	Yes	42.65	5.24E-14	Yes

OpticSlim Tukey HSD, instead, indicated the absence of color differences between several media with different TTC concentrations. Δ_{XYZ} TTC measurements didn't appear to display statistically significant discrepancies, regardless of having different chromogen concentrations (see Table 4.12). Likewise, OpticSlim ΔE_{ab} TTC measurements reflected significant differences between medium and low TTC concentration media but not between high and medium TTC concentration media or between high and low TTC concentration media (see Table 4.13). Hence, the crest that can be seen in Figure 4.18 B, in the OpticSlim ΔE_{ab} plot.

Table 4.13. Tukey ANOVA post-hoc test for the ΔE_{ab} distance measurements of colonies in the third spiral crown. Q-stat values and p-values for combinations of color distance reads taken from media with different concentrations of the same chromogen. CH, CM, CL, LA, VL, VM, VH, respectively stand for high medium and low TTC concentration media, Letheen agar, and low, medium and high TV concentration media. Data are presented according to the values obtained for each scanner (CS_1, CS_2, and CS_3), OpticSlim (OPS), and Perfection V39 (V39). Results above significance level are shown in red.

Tukey Post-Hoc α = 0.05									
ΔE_{ab}	CS_1			OPS			V39		
	Q-stat	***p-val***	***sig.***	***Q-stat***	***p-val***	***sig.***	***Q-stat***	***p-val***	***sig.***
CH-CM	14.8	5.22E-14	Yes	3.902	2.27E-01	No	19.8	5.24E-14	Yes
CM-CL	28.6	5.24E-14	Yes	7.608	1.11E-05	Yes	28.18	5.24E-14	Yes
CH-CL	43.4	5.24E-14	Yes	3.706	3.02E-01	No	47.99	5.24E-14	Yes
VH-VM	26.83	5.24E-14	Yes	8.916	1.58E-08	Yes	28.5	5.24E-14	Yes
VM-VL	33.72	5.24E-14	Yes	16.7	5.22E-14	Yes	26.86	5.24E-14	Yes
VH-VL	60.54	5.24E-14	Yes	25.61	5.24E-14	Yes	55.37	5.24E-14	Yes

4.1.4. Measures and Analysis of Colonies in Alternative Media

4.1.4.1. Qualitative Analysis of Alternative Media Images

Every tested alternative media featured a series of peculiarities, linked with its particular properties. Image background, that is image parts that did not belong to colonies, generated what could be considered noise. Noise was heavily conditioned by the texture of the growth pad regions of plates. Indeed, FilmPlate and Sanita-kun featured remarkably periodic noise profiles, strictly linked to their growth pad's texture, an additional source of noise was originated by the grid lines that were printed in the transparent covers of both consumables (see Figure 4.19).

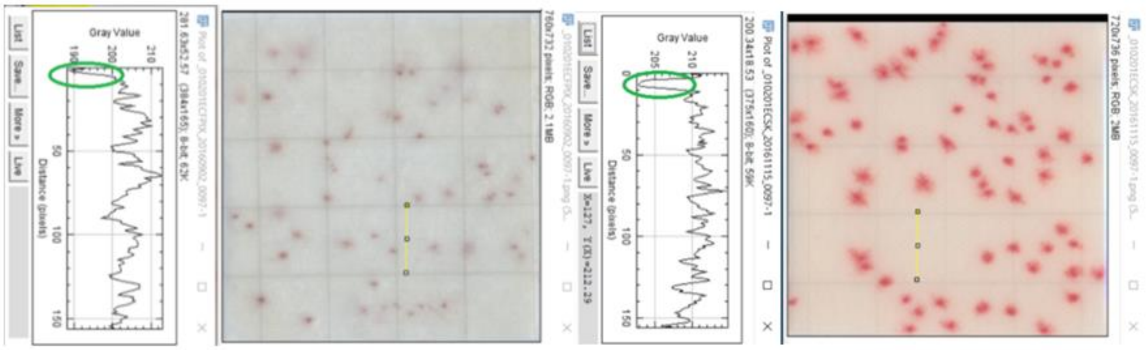

Figure 4.19. Montage built with Images of Filmplate and Sanita-kun plates with *E. coli* colonies, along with intensity plots of colony-free linear transects. Sampled linear transects are featured in yellow. Green ellipses surround sharp intensity variations due to the presence of grid lines.

4.1.4.2. Performance of ImageJ Denoising Scripts

Denoising scripts achieved very remarkable noise reduction in of the growth pads of Sanita-kun and FilmPlate consumables. Denoised images appeared to preserve colony shape and color characteristics while lacking background irregularities (see Figure 4.20). The FFT filtering approach performed by the Denz sub^2macro outperformed many other frequently used techniques such as median filtering, background compensation, and Gaussian blurring, unlike all of the former, FFT filtering caused minimal changes in colony size and shape.

It must be noted that, despite the clear difference that the intensity projections of colonies and non-woven textures display in Figure 4.20, denoising becomes critical when separating colonies from background noise in early phases of the incubation, where colonies are smaller and dimmer. Furthermore, in the case of Filmplate consumables, where often color development in colonies was poor, yielding low contrast with surrounding media, detexturization of plates was of the essence to detect certain colonies, regardless of the imaging time.

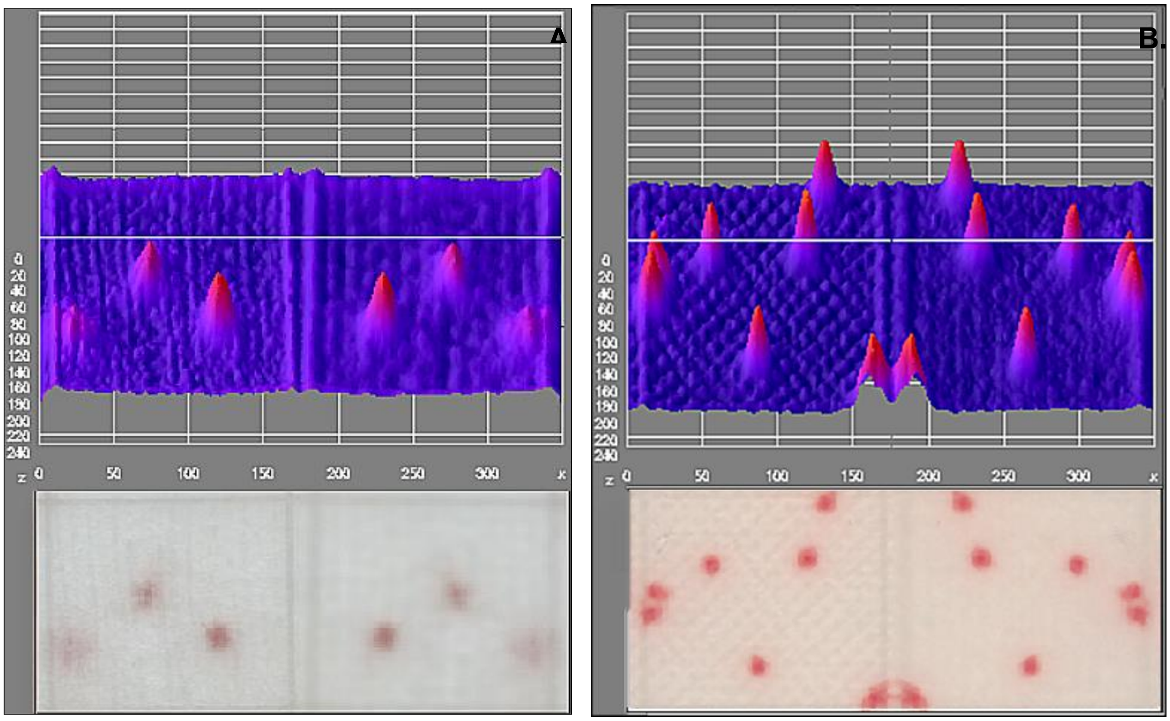

Figure 4.20. 3-D surface “Fire LUT” plots of specularly confronted unprocessed versus denoised images. A. FilmPlate scan detail of *E. coli* colonies. B. Sanita-kun scan detail of *E. coli* colonies.

4.2. Colony Analysis in Alternative Media

4.2.1. Growth Inhibition Assessment

The results obtained in the *E. coli* growth inhibition ANOVA indicated that Filmplate and Sanita-kun media produced different growth responses in *E. coli,* with a p-value of 2.52 E-5 in the media factor. Different growth recoveries also appeared to be statistically significant in relation to the matrix dilution (see Table 4.14).

Tukey test detection of interactions for the *E. coli* growth inhibition between 1:10 and 1:10^3, and 1:10 and 1:10^5 Filmplate dilutions, in combination with the descriptive statistics, seemed to indicate 1:10 dilution plates display lower inhibitions than 1:10^3 plates. Furthermore, colony recovery rates in 1:10^5 matrix dilution Filmplate plates were larger and positive, indicating they possibly outperformed the reference control media (see Table 4.14). The descriptive statistics indicated very large standard deviations in all the data with values that were close or even superior to the mean values for the data.

S. aureus growth inhibition ANOVA results indicated the existence of statistically significant differences between means of different media recoveries, for different matrix concentrations and interactions between both factors (see Table 4.15). Interaction disambiguation through post-hoc Tukey testing indicated interaction effects were always linked to Filmplate plates. 1:10 matrix dilution interaction existed between Filmplate and Sanita-kun plates. Meanwhile, 1:10 dilution in Filmplate media displayed differences in means with Filmplate data for 1:10^3 and 1:10^5 dilutions (see Table 4.15).

Table 4.14. ANOVA, descriptive statistics, and Tukey *post-hoc* analysis results for growth inhibition tests performed, respectively on Sanita-kun and Filmplate media inoculated with *E. coli*. Statistically significant tests are indicated by highlighting their p-values in red. E-1, E-3, and E-5, respectively, stand for 1:10, 1:103, and 1:105 dilutions. SK refers to Sanita-kun plates, while FP refers to Filmplate plates.

***E. coli* Growth Recovery ANOVA**			
ANOVA α = 0.05	***F***	***p-value***	***sig.***
Medium	1.70E+01	2.52E-05	Yes
Matrix Conc.	1.03E+01	3.73E-03	Yes
Interaction	8.16E+00	1.97E-03	Yes
Descriptive Statistics: Mean ± SD			
Dilution F.	Sanita-Kun	Filmplate	
E-1	2.30E+00±9.00E+00	-1.00E+00±1.18E+01	
E-3	-1.92E+01±1.54E+01	-1.15E+01±1.08E+01	
E-5	-1.10E+00±1.59E+01	4.50E+01±2.02E+01	
Tukey Post-Hoc Analysis			
Comparison α = 0.05	***Q-stat***	***p-val***	***sig.***
SK E-1 - E-3	3.35E+00	1.59E-01	No
SK E-1 - E-5	5.30E-01	9.96E-01	No
SK E-3 - E-5	-2.82E+00	2.99E-01	No
FP E-1 - E-3	1.64E+00	7.75E-01	No
FP E-1 - E-5	-7.17E+00	3.11E-04	Yes
FP E-3 - E-5	-8.80E+00	1.81E-05	Yes
E-1 SK - FP	5.14E-01	9.96E-01	No
E-3 SK - FP	-1.20E+00	9.13E-01	No
E-5 SK - FP	-7.18E+00	3.03E-04	Yes

Thus, globally, growth inhibition tests indicated significant interactions and mean differences for both factors in both tested microorganisms. Tukey tests coincided in pointing to differences between 1:10 matrix dilutions in Flimplate media and other dilutions and media types. The descriptive statistics of obtained results didn’t point to any common trends between both plate types, however.

Table 4.15. ANOVA, descriptive statistics, and Tukey *post-hoc* analysis results for growth inhibition tests performed, respectively on Sanita-kun and Filmplate media inoculated with *S. aureus*. Statistically significant tests are indicated by highlighting their p-values in red. E-1, E-3, and E-5, respectively, stand for 1:10, 1:10^3, and 1:10^5 dilutions. SK refers to Sanita-kun plates, while FP refers to Filmplate plates.

***S. aureus* Growth Recovery ANOVA**			
ANOVA α = 0.05	***F***	***p-value***	***sig.***
Medium	3.14E+01	1.98E-07	Yes
Matrix Conc.	3.13E+01	9.41E-06	Yes
Interaction	1.27E+01	1.70E-04	Yes
Descriptive Statistics: Mean ± SD			
Dilution F.	Sanita-Kun	Filmplate	
E1	-1.76E+01±1.54E+01	-1.07E+02±2.55E+01	
E3	-7.80E+00±2.53E+01	-2.04E+01±2.10E+01	
E5	1.15E+01±9.25E+00	-4.30E+00±1.27E+01	
Tukey Post-Hoc Analysis			
Comparison α = 0.05	***Q-stat***	***p-val***	***sig.***
SK E-1 - E-3	-1.14E+00	9.26E-01	No
SK E-1 - E-5	-3.39E+00	1.51E-01	No
SK E-3 - E-5	-2.25E+00	5.19E-01	No
FP E-1 - E-3	-1.01E+01	2.20E-06	Yes
FP E-1 - E-5	-1.19E+01	1.15E-07	Yes
FP E-3 - E-5	-1.87E+00	6.79E-01	No
E-1 SK - FP	1.04E+01	1.30E-06	Yes
E-3 SK - FP	1.47E+00	8.36E-01	No
E-5 SK - FP	1.84E+00	6.94E-01	No

4.2.2. Enumeration Limit Analysis

The automated enumeration limit analysis disclosed divergent performances between tested media. Filmplate media displayed growth of irregularly shaped colonies, which at times grew in string-like patterns following the texture of the paper in their growth-pad surface. Sanita-kun plates also featured growth linked to the trough areas of the growth pad's textured non-woven layer, however, this was less apparent.

In high count Filmplate plates, colonies were not discernible and, frequently, only some regions of the plates featured colonies with a fair color development (see Figure 4.21 A). Faint lawn-like color development regions were also seen in these plates. Meanwhile, Sanita-kun plate performance was remarkably better and yielded strong color development even when inoculated with high concentrations of bacteria (see Figure 4.21 B).

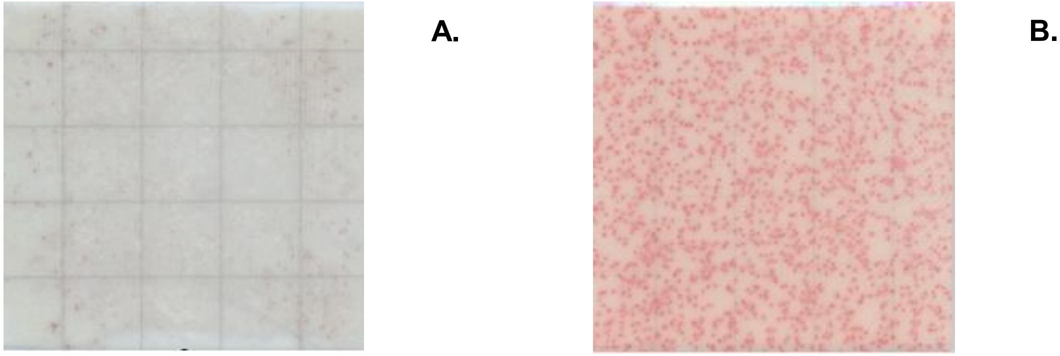

Figure 4.21. A. Scan detail of a Filmplate growth pad after 48 h of growth, after being spiked approximately with 1200 *E. coli* CFUs. B. Scan detail of a Filmplate growth pad after 48 h of growth, after being spiked approximately with 1500 *E. coli* CFUs.

Filmplate plates often featured irregularly distributed colonies, with higher concentrations of colonies in their central regions (see Figure 4.21 A). Sanita-kun plates had a balanced distribution of colonies throughout their surfaces, featuring strong homogenous color development throughout (see Figure 4.21 B).

According to the regression performance criteria specified in section 3.2.2.4. *E. coli* automated counts yielded poor linear regression results in Filmplate consumables (see Table 4.16), with slope values of 0.6187. An increase in deviations of actual counts from the Filmplate regression line could be detected around 10^3 CFU counts (see Figure 4.22 A). Sanita-kun counts appeared to display strong linearity, even in concentrations around 10^4 CFU (see Figure 4.22 A), overall regression performance for these classified as excellent (see Table 4.16).

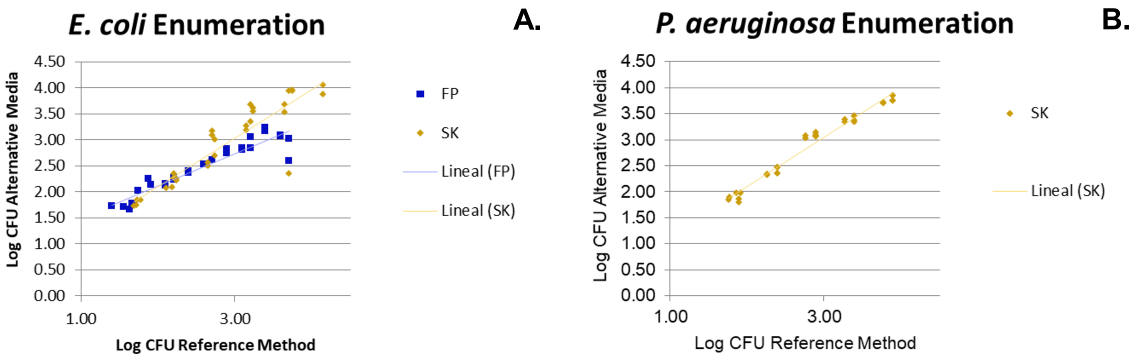

Figure 4.22. A. Plots of the *E. coli* counts obtained using FIlmplate and Sanita-kun plates confronted with expected counts established by standard methodology. Regression lines are plotted along with obtained counts. FP and SK, respectively, refer to Filmplate and Sanita-kun plates. B. Plots of the *P. aeruginosa* counts obtained using Sanita-kun plates confronted with expected counts established by standard methodology. Regression lines are plotted along with obtained counts. SK refers to Sanita-kun plate counts.

Sanita-kun linear regression of *P. aeruginosa* counts was the best of all tested microorganisms and media, classifying as excellent and featuring the best marks in all regression parameters (see Table 4.16 and Figure 4.22 B).

Table 4.16. Linear regression results obtained for alternative media (Filmplate and Sanita-kun) counts in all three evaluated model microorganisms (*E. coli*, *P. aeruginosa,* and *S. aureus*). Data for *P. aeruginosa* Filmplate regression is unavailable. Counts were compared with counts obtained in LA media according to standard surface plate count procedure.

Microorganism-Specific Linear Regression Analysis					
Microorganism	*E. coli*	*E. coli*	*P. aeruginosa*	*S. aureus*	*S. aureus*
Consumable	FilmPlate	Sanita-Kun	Sanita-Kun	FilmPlate	Sanita-Kun
m	0.6187	0.9337	0.9487	0.1379	0.8828
b	0.0395	0.0808	0.0296	0.0884	0.0316
r^2	0.8977	0.8266	0.9734	0.0799	0.9653

S. aureus Filmplate count regression featured a poor performance, with very low slope and determination coefficient values (see Table 4.16). Charted log CFU count values featured scattered points that didn't follow a linear tendency (see Figure 4.23 A). Sanita-kun regression of *S. aureus* counts exposed a good performance, according to employed performance criteria.

Table 4.17. Linear regression results obtained combining data for *E. coli*, *S. aureus*, and *P. aeruginosa* in Sanita-kun plates and for *E. coli* and *S. aureus* Filmplate plates. Counts were compared with counts obtained in LA media according to standard surface plate count procedure.

Global Linear Regression Analysis		
Microorganism	*E. coli* and S.aureus	*E. coli*, *P. aeruginosa*, and *S.aureus*
Consumable	FilmPlate	Sanita-Kun
m	0.3733	0.9150
b	0.0502	0.0341
r^2	0.4966	0.9058

Finally, a composite count linear regression analysis featuring all counts performed with Filmplate and Sanita-kun consumables pointed to a poor performance of Filmplate consumables which displayed a very erratic yet roughly linear plot (see Table 4.17 and

Figure 4.23 B). Opposed to this, Sanita-kun global regression featured excellent regression results and charted a clearly linear disposition of retrieved counts against reference values (see Table 4.17 and Figure 4.23 B).

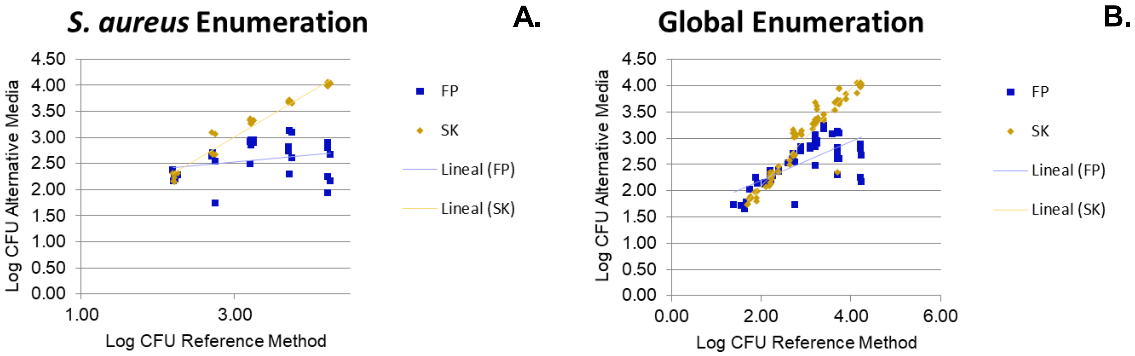

Figure 4.23. A. Plots of *S. aureus* counts obtained using Filmplate and Sanita-kun plates, confronted with expected counts established by standard methodology. Regression lines are plotted along with obtained counts. FP and SK, respectively, refer to Filmplate and Sanita-kun plates. B. Plots of all counts performed with Filmplate (*E. coli* and *S. aureus*) and Sanita-kun (*E. coli*, *S. aureus*, and *P. aeruginosa*) plates confronted with expected counts, established by standard methodology. Regression lines are plotted along with obtained counts. FP and SK, respectively, refer to Filmplate and Sanita-kun plates.

4.2.3. Time to Detection Assessment

Sanita-kun time to detection was assessed for *E. coli* and *S. aureus* colonies with divergent results. A quick overview of *E. coli* TTD histograms for all tested sample matrix concentrations and the matrix-free control, evidences a grouping of all histogram curves with varying degrees of overlap and subtle differences in modes (see Figure 4.24 A). The latter was confirmed by the recovered descriptive statistics. These establish equal mode values for low and medium matrix concentrations at 8.5 h, at 9 h for control plates, and at 10 h for high matrix concentrations (see Table 4.18).

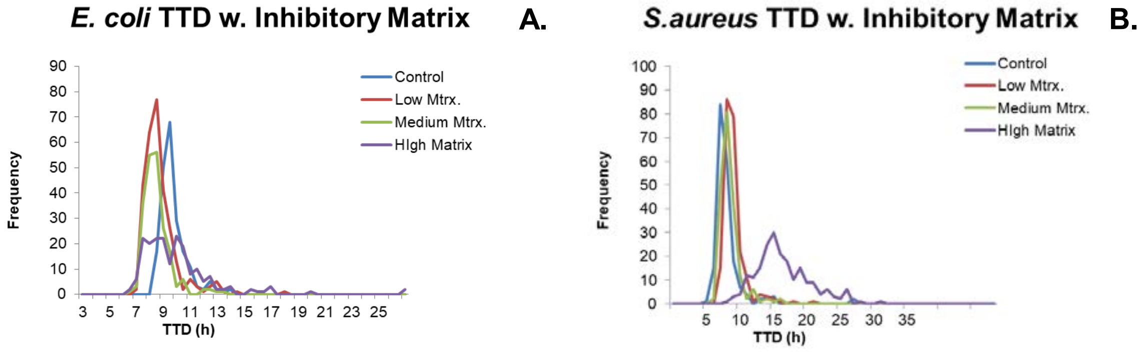

E. coli TTD w. Inhibitory Matrix A.

S.aureus TTD w. Inhibitory Matrix B.

Figure 4.24. A. Histogram plots for time to detection results obtained when monitoring plates with *E. coli* colonies. Respectively, control results correspond to matrix-free inocula while low, medium, and high matrix (Mtrx.) concentrations refer to the 1:10^5, 1:10^3, and 1:10 dilutions of cream lotion that were inoculated into plates. B. Histogram plots for time to detection results obtained when monitoring plates with *S. aureus* colonies. Respectively, control results correspond to matrix-free inocula while low, medium, and high matrix (Mtrx.) concentrations refer to the 1:10^5, 1:10^3, and 1:10 dilutions of cream lotion that were inoculated into plates.

Considering that the resolution of TTD values is of 0.5 h, mode differences appeared to be rather small in *E. coli* samples. General curve shape, however, differed markedly between curves. While high matrix concentration histogram curves appeared to resemble the shape of an irregular plateau, those belonging to the rest of samples featured marked peaks that concentrated high TTD frequencies around mode values. Statistically, this appreciation was seconded by larger standard deviations in the high concentration matrix samples when compared to the rest (see Table 4.18), this can be readily remarked in the box and whiskers chart of obtained values which, furthermore, points to the presence of very distanced outlier values in high matrix concentration plots (Figure 4.25 A).

S. aureus histograms, in turn, featured two histogram curve patterns. One such pattern belonged to high matrix concentration samples, positioned at the right-hand side of the histogram, indicating large TTD values, and a second cluster at the left side of the histogram where the rest of curves were plotted, with low TTD values. Differences in mean, mode and median between high matrix concentration plates and the rest were particularly conspicuous (see Table 4.18), while mean values for the rest of plates lied around the 8.5 to 10 h range, those for high concentration samples were close to 16 h. These differences were also very obvious when comparing respective box and whisker plots (see Figure 4.25 B). High concentration matrix TTD box and whisker plots, as in *E. coli*, featured larger standard deviations than the rest of samples (see Table 4.18).

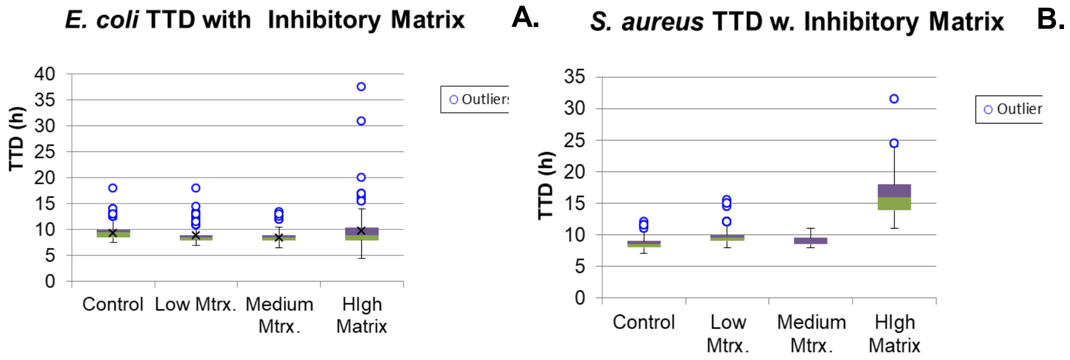

Figure 4.25. A. Box and whisker plot of time to detection results obtained when monitoring plates with *E. coli* colonies. Respectively, control results correspond to matrix-free inocula while low, medium, and high matrix (Mtrx.) concentrations refer to the 1:10^5, 1:10^3, and 1:10 dilutions of cream lotion that were inoculated into plates. B. Box and whisker plot of time to detection results obtained when monitoring plates with *S. aureus* colonies. Respectively, control results correspond to matrix-free inocula while low, medium, and high matrix (Mtrx.) concentrations refer to the 1:10^5, 1:10^3, and 1:10 dilutions of cream lotion that were inoculated into plates.

Table 4.18. Descriptive statistics for the time to detection (h).

Descriptive Statistics					
Microorganism	Parameter	Control	Low Mtrx.	Med. Mtrx.	HIgh Mtrx.
E. coli	Mean	9.14	8.67	8.29	9.57
	Median	9.50	8.50	8.50	9.00
	Mode	9.50	8.50	8.50	10.00
	SD	2.00	1.49	1.48	3.68
S. aureus	Mean	8.58	9.71	8.87	15.96
	Median	8.50	9.50	8.50	16.00
	Mode	8.00	9.50	8.50	18.00
	SD	1.23	1.45	0.72	4.79

4.3. Scope and Limitations of Published Images

Given the nature of this thesis, featured images are thought indispensable to adequately portray the topics covered in it. In particular, the results section features many images. Some of the topics covered, specifically color and more specifically device-independent colorimetry require interpretation of the images in this thesis with strong skepticism.

Readers are reminded that prints and even screen representations of the supplied images only intend to illustrate the concepts covered and the retrieved results and in no way can be considered fully representative of the original images.

The present thesis tries to narrow down the conclusions that can be taken from supplied images and points out the major image processing steps that images have undergone, however, it doesn’t mention color space conversions, image rescaling and other potentially distorting modifications that might have been carried out with published images.

5. DISCUSSION

5.1. Supplied Methods Adequately Assess Colorimetric Performance of Digital Scanners When Imaging Colonies

Although readily available and widely implemented in biological and chemical assays[94–99], consumer electronics imaging devices require being duly examined before their implementation as scientific measurement systems[22]. Usually, their output values must be processed for due analysis. The most common outputs of these devices are proprietary RGB spaces. Some authors suggest individual RGB channel calibration[22], while others go as far as manipulating output signals at the very sensor level [100]. Consulted bibliography, however, featured authors that were bold enough to supply full colorimetric or device proprietary RGB scale values without any kind of regard to imaging device calibration, most importantly, actionable data was obtained following these approaches [25,95].

Methods used in this thesis intended seamless retrieval of calibrated, device-independent, color values and pursued the establishment of a scheme that would allow reproducing experiments in different scanner devices. Device calibration, which consisted in the use of IT8 calibration cards for the establishment of ICC profiles for scanned images offered advantages over methods that suggest the adjustment of individual channel values[22]. Namely, the use of ICC profiles for the transformation of device proprietary RGB outputs into sRGB values allowed to use a very well established RGB color space[42,43], while resorting to standardized calibration practices that can be implemented with use of various software solutions such as José Pereira's Rough Profiler[101] or Andrew Stawowczyk's Color Camera Calibrator[102], both being freely available from the referenced web pages. A simple operation consisting in scanning

IT8/7.2 cards and adequately running CoCa software sufficed to establish a reproducible and universal procedure for the calibration of employed imaging devices.

Special attention was made to establish method reproducibility and repeatability in order to supply means to quantitatively screen for adequately performing scanning devices. The present work tackled a remarkably challenging scenario, with no known bibliographic precedents that covered colony colorimetry. Furthermore, no standards of colored colonies were available. Since no actual values of the scanned colony colors were known, accuracy couldn't be evaluated during the characterization of scanner colorimetric measurements.

Given the lack of reference standards, assessment of measurement precision, preferably termed uncertainty in industry guidelines[103], through experimentation, appeared as the sole sound way to characterize colony-related measurements. Thus, experimentally determined uncertainty, known as type A uncertainty, was used in the present work to characterize the proposed colorimetric measurement methods[54].

ANOVA GRR appeared as a good uncertainty measurement analysis given its well-established use in industrial scenarios and also the availability of clear cut-off values to assess measurement performance[91]. Calculation of GRR is rather simple, especially when compared to other uncertainty analysis[53,103]. Never-the-less, GRR allowed to easily attain sound and useful data regarding measurement validity. The particular instance of GRR that was used, featuring a variation of measurement instruments as the tested uncertainty source, allowed to first assess global uncertainty values for a set of scanners. In cases were unacceptable values were obtained, poor discrimination power of scanning units could be assessed by comparing reads of different media types in the same scanner through use of a post-hoc Tukey analysis. This proved particularly relevant in order to elucidate the device that was performing poorly and rendered the GRR ANOVA method as particularly useful. Indeed, OpticSlim's faulty performance was easily detected by the use of proposed GRR methodology in combination with *post-hoc* Tukey analysis.

Failure of GRR analysis to achieve passing values held true for all interscanner analysis that featured the OpticSlim model. *Post-hoc* Tukey analysis disambiguation, however, was only carried out with true colorimetric measurements, Δ_{XYZ} and ΔE_{ab}. Faulty performance of the OpticSlim model was confirmed through the results obtained in the follow-up Tukey HSD. The results of this test indicated similar color differences for media that had different concentrations of TTC. Thus, this supplied statistical backing to the apparent incapacity of discerning differences in color amongst TTC-based media (see Table 4.12 and Table 4.13). Both the qualitative and statistical analysis of OpticSlim scanner performance pointed out significant flaws in the unit's reads, OpticSlim scanners were therefore considered unfit for use.

In order to improve method performance, the faulty scanner model (OpticSlim) data was discarded from all the interscanner GRRs that were performed. Interscanner GRR calculations were repeated for CanoScan and Perfection V39 scanners only, yielding a remarkable improvement in interscanner repeatability and reproducibility in all metrics, and classifying the measurement system as good (see Table 4.10 and Table 4.11). The latter was due to the fact that the OpticSlim scanner constituted the main source of variability in the invalid interscanner GRRs (see Table 4.10 and Table 4.11), and was, in fact, responsible for the marginal acceptability of the reproducibility results. In the case of grayscale GRR, only C_{Avg} and L_{709} yielded good interscanner part discriminations, with values of 5. These results indicate the importance of performing such GRR tests for any chromogen-grayscale combination, in order to ensure adequate performance.

The use of GRR as presented in this work seems a rigorous approach to tackle measurement method characterization in absence of standards for performance comparison. Moreover, the use of GRR proved effective in pointing out dysfunctional reproducibilities and poor discrimination capacities when scanners with poor performance were tested. The use of an ANOVA contrast supplies interesting information regarding contributions to the variability of instruments and interactions with measured parts that contribute to variability. Thus, this test appears to be flexible, being applicable to any of the tested color difference metrics; simple, as it counts with clearly established cut-off values to define the validity of a measurement method[90] and refrains from the complex calculations of other uncertainty evaluation tests.

The IT-8/7.2 calibration target analysis pointed out an excellent performance of CanoScan scanners, acceptable performance in Perfection V39 and poor performance in the OpticSlim scanner, this was arguably an optimal result as the CanoScan stands out as a semi-professional quality unit, with a superior CCD core technology, while, respectively, Perfection V39 and the OpticSlim were the mid and low-quality exponents of less-performing CIS scanners[21].

In terms of color homogeneity, Perfection V39 performed poorly, with high luminance fluctuations. Meanwhile, CanoScan and OpticSlim luminance fluctuations were smaller. Patterns of areas with different colors were evident in OpticSlim scans. However, such faults were more marked in Perfection V39 scans.

HSB projection of obtained colors was remarkably easy to interpret and adequate for the purpose of detecting anomalies in the colors of scanned chips, in particular, the nature of this projection made it very useful when spotting low saturation and out of scale values. Indeed, HSB color plot representations of the examined color chips enabled to detect the presence of low saturation colors in OpticSlim scans as well as a lack of color resolution evidenced by the existence of discrete color points, instead of color cluster “clouds”. Thus, low resolution and poor hue color discrimination, given the closeness to the 0 saturation axis of most colors in OpticSlim images, both allowed discarding the OpticSlim scanner as an eligible colorimetric scanner.

Marked luminance fluctuations, color inhomogeneities, and saturated colors, characterized Perfection V39 image colors. Cloud-like color clusters that were plotted in the HSB plot featured a continuous array of colors, implying color resolution was adequate. Saturated values were particularly abundant in highly saturated color chips. Nevertheless, the scanner appeared as eligible for use as oversaturation was not expected to pose problems during colony imaging. The latter held true because colony colors were known to be less saturated than those producing saturated reads in the color chips. Beyond random luminance and color fluctuations, CanoScan performance was quite good throughout the calibration target analysis, suggesting a preference of choice for this device above the other two.

The presented approaches appeared as a valid set of practices to screen for scanners with adequate performance. This was confirmed when OpticSlim's faulty performance was detected through both statistical and qualitative methods.

5.2. Colony Colors, Grayscale Values, and Derived Metrics in Digital Images are Valid Measurements of Colony Phenotype

The use of Δ_{XYZ} and ΔE_{ab} color difference metrics proved useful in studying the development of color in colonies. Employing averaged LA control plate values as a reference, not only allowed establishing a reasonable frame of reference to assess differences in chromogen performance, it also allowed to employ an easy and objective measure of color development.

The present work resorted to 5.0 as the threshold ΔE_{ab} value for a relevant color difference between colonies arbitrarily. This value simply seemed to yield reasonable results and could somehow be compared to existing JND values. The establishment of a universal color JND value is still a controversial matter, while some authors point a single color difference unit (ΔE_{ab}=1) as the minimum discernible color difference[41], others suggest the use of values such as 2.3 [89] or 3 [22]. Despite offering an indicative reference frame to the perceptive relevance of a given color difference, JNDs of colony colors lie beyond the scope of the present work.

Readers are cautioned to note that in no way must the results hereby presented be interpreted as representative of the just noticeable color difference levels of colony colors for several reasons. Most importantly, as already mentioned, the cut-off "relevant color difference" value of 5 was established arbitrarily. Furthermore, the results presented compare average color values for colonies. Some colonies that were imaged featured regions with colors that were readily distinguishable from the rest of the colony, this holds particularly true for 48 h *S. aureus* colonies. Thus, the presented methods shall be better categorized as means to compare average colony colors with each other and to objectivate and quantify colony color development.

The most notable results that were observed during testing were very small changes ΔE_{ab} values for *E. coli* colonies between 16 h and 48 h reads, which matched results obtained using Δ_{Gray} metrics. The latter was interpreted as a lack of color development in *E. coli* colonies beyond 16 h reads. Conversely *S. aureus* and *P. aeruginosa* Δ_{Gray} values indicated active color development between 16 h and 48 h reads in all color and grayscale spaces that were used. Heat maps offered a very useful approach to compare obtained results. While *P. aeruginosa* and *S. aureus* TTC colonies appeared to display particularly close colors in 48 h reads, indicating converging tendencies between colonies growing with the same chromogen, TV values for *S. aureus* 48 h colonies appeared to be much closer to those obtained in any other TTC plate. Surprisingly, closeness to TTC colony colors was greater than to color of 16 h *S. aureus* TV colonies. Furthermore, *E. coli* and *P. aeruginosa* TTC and LA colors, respectively, display color differences below the established arbitrary threshold (see Table 4.3)

As depicted in Figure 4.8 B, normalization of all employed grayscales generated similar charts, this must be interpreted as a coincidental event, and not as an indication that all grayscales can supply equivalent information when their data is normalized. Both TV and TC dyes develop colony color by selectively reflecting lights of red and, in the case of TV, also blue wavelengths. TV also reflects, to a lesser degree, green light. Additionally, reference LA colonies mostly display colors with grayish green colors and, in the case of *S. aureus,* yellow ones (see Figure 4.13 C, Figure 4.14 C, and Figure 4.15 C).

Changes in sRGB channel values spotted when comparing LA colonies with chromogenic media colonies mostly lie in the green and blue channels, with very little red channel shifts. This can be remarked easily when reviewing Figure 4.10, which individually charts Δ_{Gray} values for sRGB Red, Green, and Blue channels along with L_{709}. Coincidence in shape of Δ_{Gray} of the Green channel and L_{709} is directly linked to the fact that green channel changes strongly contribute to Δ_{Gray} L_{709} values. Thus, the combination of very faint changes in the Red channel, high changes in the Green channel and intermediate changes in the blue channel produce plots that are heavily dependent on green values given the relative weights attributed to these in the respective L_{601}, L_{709} and luminance (L') equations (see section 3.1.2.3.4). Low red channel changes and blue channel tendencies that somewhat resemble those of the green channel all coalesce to produce an array of Δ_{Gray} values that can be easily transformed through normalization to produce very similar curves.

Capture of grayscale values from colonies is not a novel practice, the particular bottom-lit arrangement in combination with the use of calibrated images, however, does stand as a new approach. Other similar set-ups have used transmitted illumination[13,14,20]. Use of transmitted illumination was estimated to be incorrect for this work as the standard practice to read colony color is observing light reflected by colonies; typically this supplies a better contrast to detect color development. Thus, reflectance-based scans were thought of as being closer to standard manual plate reading practices.

The adopted imaging approach, however, does have several significant limitations when applied on conventional agar media. It can only capture images from the bottom of plates; this implies light must travel through the agar, allowing the agar to tamper with imaged light. Many chromogenic media formulations include contrasting agents that make the media opaque, evidently, such media wouldn't be eligible for imaging with the presented technique. Alternative reflective imaging approaches weren't studied due to issues related to condensation. Use of CIS flatbed scanners, as anticipated in the reviewed bibliography, produced field depth-related limitations that gave way to difficult segmentation of colonies.

A number of reviewed works refer to use of grayscales for quantitative purposes[24,36,37]. More specifically, colony grayscale metrics have been correlated with cell suspension absorbance values[14] and cell biomass measurements[13], demonstrating biological significance. To the knowledge of the author, recovery of colony colorimetric data using a flatbed scanner is indeed novel.

Use of digital imaging to analyze chromogenic plates is becoming a common practice, especially in clinical microbiology laboratories. Automated imaging systems commonly screen for the images that appear to feature targeted color colonies[28]. A number of works cite digital imaging devices and algorithms applied to discriminate color development in colonies. The aforementioned works don't employ calibrated color readers or device-independent color spaces to establish colony categories, thus, they don't rely on genuinely colorimetric algorithms. Instead, they employ simple HSV filters[29,31] or conventional classifier systems such as linear discriminant analysis[104]. Recent advances in this field use classifiers that apply CIELAB a* and b* channel data based on scalable vector machines and back-propagation neural networks[105].

Presented results indicate digital imaging can be used to assess the development of color by colonies through grayscale measurements, the combination of the measurements with statistical tests can supply statistically significant data regarding the existence of color development. Grayscale values such as those used in the present thesis, essentially assign different weights to input sRGB channels which are then added, with or without linearization and delinearization procedures. Thus, use of such grayscales doesn't supply precise color information. Two different colors, with their corresponding different primary RGB values, can be plotted to a single grayscale value.

An approach is suggested to optimize media formulations employing grayscale values. Use of Δ_{Gray} values to compare grayscale reads of colonies in a control media formulation with those of a tested formulation, in combination with a given Δ_{Gray} cut-off value, could allow assessing the existence of significant color development. This approach would require establishing reasonable cut-offs that would depend on the grayscale used and the particular color developed by colonies. Thus, this particular application would require assessment of the cut-off levels comparing Δ_{Gray} values with changes in perception or colorimetry of the color of colonies. Although this might seem a trivial matter, it certainly has great cost-related implications for media manufacturers. As evidenced by Figure 4.7, increasing concentrations of chromogen yield greater Δ_{Gray} values.

Chromogens are commonly amongst the most expensive ingredients in media formulations, thus, establishing which minimum chromogen concentrations yield good color development through quantitative means is of paramount relevance to media manufacturers and can be used for many media development and quality control applications. Particular care should be dedicated to assessing Δ_{Gray} values across a wide spectrum of color intensities of colonies for such applications. Assessing concrete applicability of this approach would require further testing. It must be highlighted that its use should be limited to a comparison of results obtained with a single chromogen.

While it is reasonable to deduce that a difference in grayscale value between two colonies indicates a difference in their color, it isn't reasonable to estimate that the particular magnitude of the difference is representative of what the difference in color actually is. Only when comparing colonies with different saturation degrees of the same hue can it be assumed that an increase in Δ_{Gray} denotes an increase in color difference. Hence, it is recommended to restrict the use of this approach to a single chromogen. Still, it is duly remarked that the very assumption that changes in colony color will occur within the same hue when using a given chromogen is in its own right a bold assumption.

Ideally, true colorimetric color spaces should be used to compare colony color. The present work assessed use of two of the most commonly employed color spaces, CIEXYZ and CIELAB. Advantages of the use of these in front of grayscale measurements are countless. Most importantly, when properly measured, colors in these color spaces can be said to correspond to a contrasted and widely adopted device-independent color space[47,106,107]. While CIEXYZ_{D50} measurements can be trusted to correspond to a physically sound colorimetric value, the use of CIELAB measurements, additionally, allows predicting the impact on the perception of a given color change. Thus, it appears evident that use of CIEXYZ_{D50}/CIELAB should be the approach followed when intending to accurately study color development from a phenotypic perspective.

As evidenced by the comparison of TV and TTC media, conclusions relating to color development performance vary largely depending on the reference color space used (see Figure 4.16). Thus, choice of adequate color space metrics should be related to the intended use of these. Δ_{XYZ} could be more suited for measurements that relate to color signal acquisition by digital imaging and uses thereof. Meanwhile, ΔE_{ab} values pose themselves as better candidates to characterize media performance for human assessment of colony color development.

Traditionally, published works that address color development in colonies rely on remarkably subjective color measurements. A wide array of qualitative evaluations of color development are used, encompassing, amongst others, color names[32], media comparison through choice-weighted scoring[34] or arbitrary unit ratings[35]. The methods supplied in the present work for colony color measurement, or, alternatively, objectivation of color development through grayscale changes, both appear as superior approaches to report color development results.

Chromogenic agar-based media are widely used in industrial and clinical scenarios[57,108]. No standardized color development measuring procedures have been found in reviewed bibliographic sources. Such procedures would assist media development through objective measurements of the performance of media formulations. Furthermore, such techniques would allow benchmarking and perhaps even quality control of commercial formulations. In the advent of the age of computer vision, it also seems obvious that truly established colorimetry in digital images of colonies is called for.

5.3. Kinetic Imaging Counts of Colonies in Alternative Media are a Powerful Alternative to Conventional Colony Counting

Colony counting is one of the oldest and most widely used techniques in microbiology, it has been used for an endless amount of applications and available literature on the topic is simply overwhelming, readers of this work are thus referred to general reference works and regulations [49,76,109]. Moreover, automated colony counting has given way to a large number of devices and solutions that have been developed and tested for many applications [17,110,111]. Exploration of the applications of automated colony counting[8,112] and further development of the processes underlying it[3,113,114] are both still active research fields. Use of kinetic imaging for the retrieval of colony enumeration data has been restricted to a select number of works, however, these feature colony detection through colony autofluorescence[115], development of specific microscopic sensors[116] and high-resolution scanning of colonies[9].

A number of regulations establish maximum enumeration limits[49,50,117]. Perhaps a key indication of past work on the topics is that, despite the existence of regulated clear-cut maximum enumeration limits, the nature of colonies and their remarkable variability can significantly affect acceptable colony enumeration limits and, thus, the performance of this technique. Certain authors highlight this variability and advocate for use of case-specific validations for any given microorganism when possible[118]. It must be noted, however, that this lies far from feasible for most applications, especially in quality control procedures where enumerated microorganisms are largely variable.

In the retrieved counts, Sanita-kun plates featured a remarkable logarithmic linear profile with a very good linear coefficient of determination (see Table 4.17), results in counts as high as these appear to be unprecedented. In the consulted bibliography, counts of up to 10^3 CFU, however, have been reported to count with an AOAC Performance Tested Method status[72]. Sanita-kun aerobic plate counts have been pointed to display excellent enumeration performance in several matrices and using a wide array of microorganisms[58]. Interestingly, the instruction leaflet supplied by Sanita-kun's manufacturer doesn't actually specify an enumeration limit, it only mentions the possibility of restricting counts to certain plate-grid areas and calculating whole plate concentrations in proportion to obtained counts[60].

It must be duly noted that Filmplate manufacturers don't establish well defined upper limits for counting[119]. Unfortunately, a very limited amount of literature is available regarding the use of Filmplate media. Consulted works encompassed a webpage section[119], a brief comparative study of aerobic plate counts[120], and a study of the efficacy of a disinfection method[121]. Good results using Filmplate alternative media for the enumeration of microorganisms in food were reported by Xia at al., with favorable linear correlations between microbial concentrations and performed counts, displaying r^2 lineal correlation coefficients of 0.93[120].

Results of counts in Filmplate media featured in the present work discourage use of this media in counts beyond concentrations specified by the Filmplate's manufacturer. Obtained linear regressions of automated counts display indeed particularly poor performance in this regard, especially in *S. aureus* colonies. Likewise discouraging, sample distribution throughout the growth pad wasn't satisfactory, colonies seemed to cluster around the point of inoculation indicating poor wicking. Poor wicking could be related to the composition of the sample pad, as this phenomenon wasn't remarked in Sanita-kun plates. Perhaps wicking in the cellulose-based paper matrix isn't as efficient as it is in the non-woven fibers of Sanita-kun plates. Moreover, color development in colonies was rather poor at times. When this happened, colonies that grew on plates were hardly discernible. At lower counts, performance in Filmplate consumables was better yet still rather erratic (data not shown). Thus, Filmplate consumables didn't display a good performance when counted automatically, even employing powerful denoising and time-series images.

The denoising approach that was used (see section 3.2.4.1) achieved successful noise reduction in both alternative media. As exemplified by Figure 4.20, the results of this denoising step were particularly remarkable and, in fact, quasi-indispensable to process the images of alternative media plates. No known academic works have been found of kinetic imaging using Filmplate and Sanita-kun growth media. This accounts for a lack of proper comparison possibilities for results that have been obtained. Despite the existence of colony counters that address automated colony counting of alternative media, no scientific bibliography has been found on the topic of endpoint imaging either. Thus, the remarkable performance of FT-based filtering to remove growth-pad texture-derived noise lacks any known bibliographic precedents for comparison. It can be remarked, however, that consulted works regarding agar-based media automated counts typically remove background-derived interferences through Gaussian smoothing of images[6] or median filtering[16], these are applied on smooth agar surface images, however. None-the-less, use of Fourier transforms to address texture-related phenomena in images hasn't been found to be unique to the present work. In fact, this very technique, implemented in a very similar fashion, is applied for digital enhancement of old analog photographs that feature textures or patterns[122,123].

5.4. Performances of Available Alternative Growth Media Differ When Inhibitory Matrices Are Present

Preservative systems that use a combination of phenoxyethanol and ethylhexylglycerin have been shown to display effective preservative efficacy in body lotions that were spiked with a broad spectrum of microorganisms, including *S. aureus* and *E. coli*[124]. The preservative mix of the tested matrix was neutralized according to consulted standard practices[125]. However, possible interactions between tested alternative media and trace amounts of preservatives might explain the existence of some of the effects that are discussed in the present section.

S. aureus growth inhibition results indicated statistically relevant differences in means related to the media and plate type factors (see Table 4.15). Interaction amongst these could also be detected. A general trend distinguishing Filmplate media plated with *S. aureus* and high matrix concentrations from other groups could be remarked. This appeared as an interesting pattern pointing to the possibility of inhibitory effects of high matrix concentrations that seemed to disappear as the matrix became more diluted, across test groups.

No differences were detected when comparing Sanita-kun *S. aureus* colony recoveries across different matrix concentrations (see Table 4.15). Furthermore, significant differences were detected between the colonies recovered by Sanita-kun media and those of Filmplate media in samples inoculated with high matrix concentrations. The latter would further support the absence of a growth recovery effect in Sanita-kun media.

Possible explanations for this might be differences in the composition of the Sanita-kun media which seemed to feature a better protection of bacteria against tetrazolium-induced toxicity. For example, the media could be supplemented with certain cations, as proposed by certain authors[67,68]. TTC toxicity is known to decrease when media formulations are supplemented with an iron source in *Listeria monocytogenes* cultures[68]. Junillon et al. linked addition of magnesium to *Salmonella spp.* cultures with an increase in apparent growth rate and signal enhancement when using tetrazolium violet (TV) as a growth indicator[67]. Addition of cations could be particularly useful to counteract the depletion of cations induced, if not fully neutralized, by tetrasodium glutamate diacetate, a chelant present in the tested matrix. Given the unavailability of the detailed formulation of both employed alternative media, only speculations are possible, in this regard.

A second explanation to diverging inhibitions would be a lower toxicity induced by differences in the interaction of tetrazolium salts of the Sanita-kun media formulation, which is known to contain TTC and at least two other tetrazolium salts[58].

Data from the growth recovery tests carried out in *E. coli* didn't appear to be as readily interpretable, despite the existence of statistically significant results. No patterns with biological relevance were spotted beyond larger colony recovery rates in Filmplate media with highly diluted matrix inocula. This was possibly due to lower matrix-media-linked inhibition, aligning with the existence of an interaction between matrix preservatives and the Filmplate tetrazolium dye, the interaction would possibly disappear once the preservative was further diluted.

Results in the time to detection assays carried out in Sanita-kun plates featured a strong increase in modes of time to detection of *S. aureus* colonies. This suggests that, despite having no significant impact on colony growth recovery, Sanita-kun tetrazolium salts do display a certain inhibitory effect on *S. aureus, at high matrix concentrations,* in the shape of an increase in the time to detection.

Authors that have worked with kinetic imaging of colonies point that the difference in time of apparition, a term that could be considered roughly similar to TTD, can be caused by a difference in lag phase span. Likewise, they also highlight that changes in growth rate also influence TTD[7,11].

Junillon and Flandrois studied TTC-induced toxicity on *Listeria monocytogenes* (*L. mono.*) broth cultures. Their work reported marked toxicity of TTC on *L. mono.*, in some cases, toxicity reached the point of total growth inhibition. When growth was detected, toxic effects of the TTC seemed to be limited to an increase in the lag phase[68]. Ernebjerg and Kishony suggest that time of appearance of colonies is mostly dictated by the lag phase, their work, however, is based on 1200 DPI resolution images of colonies with particularly long lag times[7], a scenario that diverges from that of presented results. Determining whether if changes in TTD are caused by changes in lag phase duration or growth rate would require performing calculations of lag-time beyond the scope of conducted experiments, thus, the present work will prudently refrain from drawing conclusions regarding lag phase extension.

Colony appearance times are widely used as indicators of colony phenotype[7,9,11,30]. Interestingly, similar shifts in TTD curve shape were detected in *E. coli* and *S. aureus* colonies that belonged to high matrix concentration samples. These featured lower heights and a wider breadth (see Figure 4.24), which produced an increase in standard deviations of TTD values (see Table 4.18). *S. aureus* colonies of high matrix concentration samples featured a marked increase in mode, as well, confirming a marked inhibitory effect (see Table 4.18). The decrease in TTD curve height that was detected in colonies of both *S. aureus* and *E. coli* colonies seems to match appearance time curves obtained by other authors. In particular, these resemble curves from colonies submitted to different starvation periods, where starvation is used to model microbial stress[30]. Thus, low height and wide breadth of the time to detection curve might be related to microbial stress. The fact that these results are consistent with bibliographic precedents and display similar profiles in markedly different microbial model microorganisms (*E. coli* and *S. aureus*), calls for further investigation of relations between height and breadth of TTD curves with microbial stress models.

In summary, while inhibitory patterns related to the presence of high matrix concentrations (in terms of growth recovery and TTD) aren’t as clearly apparent in *E. coli* cultures, these are marked and evident for *S. aureus*. Nonetheless, the results obtained with both model microorganisms indicate interactions between the tested matrix and alternative media, suggesting the necessity of proper assessment of such interactions before routine use of these media with any given matrix.

6. CONCLUSIONS

1. IT-8 target-based ICC profiling enables adequate calibration of scanner-retrieved images for the capture of truly colorimetric colony images.
2. Gauge Repeatability and Reproducibility ANOVA, in combination with post-hoc Tukey analysis poses a suitable methodology to characterize new colony color measurement devices and to discard devices with inadequate uncertainty profiles or poor discrimination capacities.
3. Establishment of reproducible and repeatable CIEXYZ_{D50} and CIELAB average colony colors is possible by means of a flatbed scanner, using a reflective illumination set-up.
4. Establishment of reproducible and repeatable average colony grayscale measurements by means of a flatbed scanner using a reflective illumination is possible employing L_{709} and C_{Avg} grayscales.
5. Grayscale values obtained in colonies are valid colony phenotypes that can be compared and used for the assessment of color development in colonies through measurement of differences in grayscale values (Δ_{Gray}).
6. CIEXYZ_{D50} and CIELAB color coordinates of average colony color can be used to calculate truly colorimetric color differences through Euclidean distance measurements (ΔE_{ab}, Δ_{XYZ}).
7. Application of the Fourier Transform to denoise textured growth pads in alternative media is efficient and highly recommendable when processing images of alternative growth media, in order to enhance detectability of colonies.
8. Kinetic imaging enumeration limits of Sanita-kun plates can reach counts of E3.5-E4 without compromising logarithmic linearity of *Escherichia coli*, *Pseudomonas aeruginosa* and *Staphylococcus aureus* counts.
9. *S. aureus* colony recovery is affected by use of Filmplate media in presence of high concentrations of neutralized hand lotion matrix, this doesn’t hold true for plating in Sanita-kun media.

10. *S. aureus* colonies grown in Sanita-kun plates display a marked increase in mode and standard deviation of time to detection values when neutralized hand lotion matrix is present in high concentrations.
11. *E. coli* colonies grown in Sanita-kun plates display an increase in standard deviation of time to detection values when neutralized hand lotion matrix is present in high concentrations.

REFERENCES

1. Mansberg, H. P. Automatic particle and bacterial colony counter. *Science.* **126,** 823–827 (1957).

2. Bray, M.-A., Vokes, M. S. & Carpenter, A. E. Using CellProfiler for automatic identification and measurement of biological objects in images. *Curr. Protoc. Mol. Biol.* **109,** 1–18 (2015).

3. Buzalewicz, I., Wysocka-Król, K. & Podbielska, H. Image processing guided analysis for estimation of bacteria colonies number by means of optical transforms. *Opt. Express* **18,** 12992–13005 (2010).

4. Chiang, P. J., Tseng, M. J., He, Z. S. & Li, C. H. Automated counting of bacterial colonies by image analysis. *J. Microbiol. Methods* **108,** 74–82 (2015).

5. Choudhry, P. High-throughput method for automated colony and cell counting by digital image analysis based on edge detection. *PLoS One* **11,** 1–23 (2016).

6. Clarke, M. L. *et al.* Low-cost, high-throughput, automated counting of bacterial colonies. *Cytometry* **77,** 790–797 (2010).

7. Ernebjerg, M. & Kishony, R. Distinct growth strategies of soil bacteria as revealed by large-scale colony tracking. *Appl. Environ. Microbiol.* **78,** 1345–1352 (2012).

8. Frost, H. R. *et al.* Validation of an automated colony counting system for group A Streptococcus. *BMC Res. Notes* **9,** article no. 72 (2016).

9. Ghodbane, R. *et al.* Rapid diagnosis of tuberculosis by real-time high-resolution imaging of Mycobacterium tuberculosis colonies. *J. Clin. Microbiol.* **53,** 2693–2696 (2015).

10. Lawless, C., Wilkinson, D. J., Young, A., Addinall, S. G. & Lydall, D. A. Colonyzer: automated quantification of micro-organism growth characteristics on solid agar. *BMC Bioinformatics* **11,** 287 (2010).

11. Levin-Reisman, I., Fridman, O. & Balaban, N. Q. ScanLag: high-throughput quantification of colony growth and lag time. *J. Vis. Exp.* 1–15 (2014).

12. Marotz, J., Lübbert, C. & Eisenbeiß, W. Effective object recognition for automated counting of colonies in Petri dishes (automated colony counting). *Comput. Methods Programs Biomed.* **66,** 183–198 (2001).

13. Shah, N. a, Laws, R. J., Wardman, B., Zhao, L. P. & Hartman, J. L. Accurate, precise modeling of cell proliferation kinetics from time-lapse imaging and automated image analysis of agar yeast culture arrays. *BMC Syst. Biol.* **1,** 3 (2007).

14. Takeuchi, R. *et al.* Colony-live a high-throughput method for measuring microbial colony growth kinetics- reveals diverse growth effects of gene knockouts in *Escherichia coli*. *BMC Microbiol.* **14,** 171 (2014).

15. Tong, A. H. Y. Systematic genetic analysis with ordered arrays of yeast deletion mutants. *Science.* **294,** 2364–2368 (2001).

16. Geissmann, Q. OpenCFU, a new free and open-source software to count cell colonies and other circular objects. *PLoS One* **8,** 1–10 (2013).

17. Mahapatra, A. K., Harris, D. L., Nguyen, C. N. & Kannan, G. Evaluation of an IUL Flash & Go automated colony counter. *Agric. Eng. Int.* **11,** 1–6 (2009).

18. Brugger, S. D. *et al.* Automated counting of bacterial colony forming units on agar plates. *PLoS One* **7,** e33695 (2012).

19. Cai, Z. *et al.* Optimized digital counting colonies of clonogenic assays using ImageJ software and customized macros: comparison with manual counting. *Int. J. Radiat. Biol.* **87,** 1135–1146 (2011).

20. Hartman, J. L. & Tippery, N. P. Systematic quantification of gene interactions by phenotypic array analysis. *Genome Biol.* **5,** R49 (2004).

21. Göröcs, Z. & Ozcan, A. Biomedical imaging and sensing using flatbed scanners. *Lab Chip* **14,** 3248–3257 (2014).

22. Kemp, D. B. Colorimetric characterisation of flatbed scanners for rock/sediment imaging. *Comput. Geosci.* **67,** 69–74 (2014).

23. Rahman, M., Kühn, I., Rahman, M., Olsson-Liljequist, B. & Möllby, R. Evaluation of a scanner-assisted colorimetric MIC method for susceptibility testing of Gram-negative fermentative bacteria. *Appl. Environ. Microbiol.* **70,** 2398–2403 (2004).

24. Martinez, A. W. *et al.* Simple telemedicine for developing regions: Camera phones and paper-based microfluidic devices for real-time, off-site diagnosis. *Anal. Chem.* **80,** 3699–3707 (2008).

25. Carey, J. R. J. *et al.* Rapid identification of bacteria with a disposable colorimetric sensing array. Supporting info. *J. Am. Chem. Soc.* **133,** 7571–6 (2011).

26. Sullivan, K. *et al.* High throughput virus plaque quantitation using a flatbed scanner. *J. Virol. Methods* **179,** 81–89 (2012).

27. Image Access GmbH. CCD or CIS : The Technology Decision. 1–6 (2018). Available at: https://www.imageaccess.de/?page=WhitePapersCCDOrCIS. (Accessed: 4th December 2018)

28. Kirn, T. J. Automatic digital plate reading for surveillance cultures. *J. Clin. Microbiol.* **54,** 2424–2426 (2016).

29. Faron, M. L. *et al.* Automatic digital analysis of chromogenic media for vancomycin-resistant-*Enterococcus* screens using Copan WASPLab. *J. Clin. Microbiol.* **54,** 2464–2469 (2016).

30. Levin-Reisman, I. *et al.* Automated imaging with ScanLag reveals previously undetectable bacterial growth phenotypes. *Nat. Methods* **7,** 737–739 (2010).

31. Faron, M. L. *et al.* Automated scoring of chromogenic media for detection of methicillin-resistant *Staphylococcus aureus* by use of WASPLab image analysis software. *J. Clin. Microbiol.* **54,** 620–624 (2016).

32. Samra, Z., Heifetz, M., Talmor, J., Bain, E. & Bahar, J. Evaluation of use of a new chromogenic agar in detection of urinary tract pathogens. *J. Clin. Microbiol.* **36,** 990–994 (1998).

33. Perry, J. D. *et al.* Development and evaluation of a chromogenic agar medium for methicillin-resistant *Staphylococcus aureus*. *J. Clin. Microbiol.* **42,** 4519–4523 (2004).

34. Malhotra-Kumar, S. *et al.* Evaluation of chromogenic media for detection of

methicillin-resistant *Staphylococcus aureus*. *J. Clin. Microbiol.* **48,** 1040–1046 (2010).

35. Browne, N. K., Huang, Z., Dockrell, M., Hashmi, P. & Price, R. G. Evaluation of new chromogenic substrates for the detection of coliforms. *J. Appl. Microbiol.* **108,** 1828–1838 (2010).

36. Li, Z. *et al.* A low-cost and high sensitive paper-based microfluidic device for rapid detection of glucose in fruit. *Food Anal. Methods* **10,** 666–674 (2017).

37. Zhu, X. *et al.* A dual enzyme–inorganic hybrid nanoflower incorporated microfluidic paper-based analytic device (μPAD) biosensor for sensitive visualized detection of glucose. *Nanoscale* **9,** 5658–5663 (2017).

38. Lindbloom, B. RGB Working Space Information. 10 (2014). Available at: http://www.brucelindbloom.com/WorkingSpaceInfo.html. (Accessed: 8th February 2018)

39. International Telecommunication Union. Studio encoding parameters of digital television for standard 4:3 and wide-screen 16:9 aspect ratios (ITU-R BT.601-7). *Recomm. ITU-R BT.601-7* **7,** 19 (2011).

40. Burger, W. & Burge, M. J. *Digital Image Processing An Algorithmic Introduction Using Java*. *Springer-Verlag* (Springer-Verlag, 2016).

41. Poynton, C. *Digital Video and HDTV Algorithms and Interfaces*. (Morgan Kauffman, 2003).

42. International Telecommunication Union. Parameter values for the HDTV standards for production and international programme exchange BT Series

Broadcasting service (ITU-R BT.709-6). *Recomm. ITU-R BT.709-6* **5,** 1–32 (2002).

43. ICC. Using the sRGB_ICC_v4_appearance.icc profile. (2014).

44. Ferreira, T. & Rasband, W. ImageJ User Guide. 187 (2003).

45. Burger, W. & Burge, M. J. *Principles of Digital Image Processing*. (2009).

46. ISO. ISO 11664-4:2008. **4,** 8 (2008).

47. ICC. Specification ICC.1:2004-10 Image Technology Colour Management - Architecture, Profile Format, and Data Structure. **1,** 98 (2004).

48. Bae, E., Kim, H., Rajwa, B., Thomas, J. G. & Robinson, J. P. Current status and future prospects of using advanced computer-based methods to study bacterial colonial morphology. *Expert Rev. Anti. Infect. Ther.* **14,** 207–218 (2016).

49. FDA. BAM Chapter 3 - Aerobic Plate Count. *Bacteriological Analytical Manual* 1–11 (2001). Available at: http://www.fda.gov/Food/FoodScienceResearch/LaboratoryMethods/ucm063346.htm#r10-Zipkes. (Accessed: 1st January 2017)

50. United States Pharmacopoeial Convention. Examination of nonsterile products : microbial enumeration tests. in *United States Pharmacopoeia* (ed. United States Pharmacopoeial Convention) 1–5 (United States Pharmacopoeial Convention, 2008).

51. JCGM. JCGM 200 : 2008 International vocabulary of metrology — Basic and general concepts and associated terms. 90 (2008).

52. Analytical Methods Committee. Terminology - the key to understanding analytical science. Part 1: Accuracy, precision and uncertainty. *AMC Tech. Br.* 1–2 (2003).

53. Taylor, B. N. & Kuyatt, C. E. Guidelines for evaluating and expressing the uncertainty of NIST measurement results. *NIST Tech. Note* **1297,** 20 (1994).

54. Analytical Methods Committee. Terminology – the key to understanding analytical science. Part 2: Sampling and sample preparation. *AMC Tech. Br.* 1–2 (2005).

55. Merck. *Merck Microbiology Manual*. (Merck, 2005).

56. Laboratorios Conda. Media for Industrial Microbiology (Catalogue). 25

57. Perry, J. D. A Decade of development of chromogenic culture media for clinical microbiology in an era of molecular diagnostics. *Clin. Microbiol. Rev.* **30,** 449–479 (2017).

58. Teramura, H., Iwasaki, M., Ushiyama, M. & Ogihara, H. Evaluation of a novel dry sheet culture method for rapid enumeration of total aerobic count in foods. *J. Food Prot.* **78,** 1885–1890 (2015).

59. Guangdong Dayuan Oasis Food Safety Technology. Filmplate *Stacphylococcus aureus* count plate (BT206). 2

60. JNC Corporation. Instruction Manual of Sanita-kun. 1–2 (2016).

61. Teramura, H., Ushiyama, M. & Ogihara, H. Evaluation of a novel dry sheet culture method (Sanita-kun R) for rapid enumeration of yeasts and molds in foods. *J. Microbiol. Methods* **109,** 16–19 (2015).

62. Chisso Corporation. Sanita-Kun: User friendly microbial detection (Presentation). 18 (2016).

63. Berridge, M., Herst, P. & Tan, A. Tetrazolium dyes as tools in cell biology: New insights into their cellular reduction. *Biotechnol. Anu. Rev.* **11,** 127–152 (2005).

64. Tachon, S. *et al.* Experimental conditions affect the site of tetrazolium violet reduction in the electron transport chain of *Lactococcus lactis*. *Microbiology* **155,** 2941–2948 (2009).

65. Beloti, V. *et al.* Frequency of 2,3,5-Triphenyltetrazolium chloride (TTC) non-reducing bacteria in pasteurized milk. *Rev. Microbiol.* **30,** 137–140 (1999).

66. Merck. Lactose TTC Agar with Tergitol 7 (Brochure). *Merck* 1–4

67. Junillon, T., Morand, L. & Flandrois, J. P. Enhanced tetrazolium violet reduction of *Salmonella spp.* by magnesium addition to the culture media. *Food Microbiol.* **42,** 132–135 (2014).

68. Junillon, T. & Flandrois, J. P. Diminution of 2,3,5-triphenyltetrazolium chloride toxicity on *Listeria monocytogenes* growth by iron source addition to the culture medium. *Food Microbiol.* **38,** 1–5 (2014).

69. Wragg, P., Randall, L. & Whatmore, A. M. Comparison of Biolog GEN III MicroStation semi-automated bacterial identification system with matrix-assisted laser desorption ionization-time of flight mass spectrometry and 16S ribosomal RNA gene sequencing for the identification of bacteria of veterina. *J. Microbiol. Methods* **105,** 16–21 (2014).

70. Minesota Mining and Manufacturing Company. AC Aerobic Count Product Instructions. 1–4 (2017).

71. Minesota Mining and Manufacturing Company. EB *Enterobacteriaceae* Count Plate. 1–8

72. Morita H, Ushiyama M, Aoyama S, I. M. Sensitivity and specificity of the Sanita-kun aerobic count: internal validation and independent laboratory study. *J. AOAC Int.* **86,** 355–366 (2003).

73. Park, J. & Kim, M. Comparison of dry medium culture plates for mesophilic aerobic bacteria in milk , ice cream , ham , and codfish fillet products. *Prev. Nutr. Food Sci.* **18,** 269–272 (2013).

74. Kim, K. H., Yu, J. & Nahm, M. H. Efficiency of a Pneumococcal opsonophagocytic killing assay improved by multiplexing and by coloring colonies. *Clin. Diagn. Lab. Immunol.* **10,** 616–621 (2003).

75. Putman, M., Burton, R. & Nahm, M. H. Simplified method to automatically count bacterial colony forming unit. *J. Immunol. Methods* **302,** 99–102 (2005).

76. Geis, P. A. *Cosmetic Microbiology : A Practical Approach*. (Taylor & Francis Group, 2006).

77. Weber, K., Goroncy-, P., Langsrud, S., Steinhauer, K. & Lu, S. Ethylhexylglycerin impairs membrane integrity and enhances the lethal effect of phenoxyethanol. *PLoS One* 1–16 (2016). doi:10.1371/journal.pone.0165228

78. Orús, P. & Leranoz, S. Estrategias de conservación. 1–37 (2015).

79. Detmer, A., Jorgensen, C. & Nylén, D. *A guidance document on microbiological control of cosmetic products*. (2010).

80. Orús, P. & Leranoz, S. Ensayos de eficacia conservante. 1–38 (2015).

81. Schindelin, J., Rueden, C. T., Hiner, M. C. & Eliceiri, K. W. The ImageJ ecosystem: An open platform for biomedical image analysis. *Mol. Reprod. Dev.* **82,** 518–529 (2015).

82. Schindelin, J. *et al.* Fiji: An open-source platform for biological-image analysis. *Nat. Methods* **9,** 676–682 (2012).

83. Mutterer, J. & Rasband, W. ImageJ Macro Language Programmer's Reference Guide v1.46d. 45

84. Miura, K. Macro Programming in ImageJ. 134 (2013).

85. Girdhar, A. & Singh, M. J. Review of transforms used in image enhancement. *Int. J. Comput. Math. Sci.* **6,** 50–62 (2017).

86. Barthel, K. 3D-Data Representation with ImageJ. *ImageJ Conf.* **11,** 274 (2006).

87. IUL. Eddy Jet 2 User's Guide. 60 (2014).

88. Lindbloom, B. RGB/XYZ Matrices. *Revised Fri, 07 Apr 2017 20:00:12 GMT* 1–3 (2017). Available at: http://www.brucelindbloom.com/index.html?Eqn_RGB_XYZ_Matrix.html. (Accessed: 3rd May 2018)

89. Sharma, G. *Digital Color Imaging Handbook.* (CRC Press, 2002).

90. Immel, S. M. *Applications of gauge reproducibility and repeatability (GR&R) in final finish tire testing*. (2010).

91. Wheeler, D. J. An Honest Gauge R&R Study. in *ASQ/ASA Fall Technical Conference* 1–19 (2006).

92. AutoHotkey. Using the Program. (2018). Available at: https://www.autohotkey.com/docs/Program.htm. (Accessed: 15th May 2018)

93. Ferrati, A. R., Tavolaro, P., Destro, M. T., Landgraf, M. & Franco, B. A comparison of ready-to-use systems for evaluating the microbiological quality of acidic fruit juices using non-pasteurized orange juice as an experimental model. *Int. Microbiol.* **8,** 49–53 (2005).

94. Guzmán, C., Bagga, M., Kaur, A., Westermarck, J. & Abankwa, D. ColonyArea: An ImageJ plugin to automatically quantify colony formation in clonogenic assays. *PLoS One* **9,** 14–17 (2014).

95. Baş, D. Sensitive and reliable paper-based glucose sensing mechanisms with smartphone readout using the L * a * b * color space. *Anal. Methods* **9,** 6698–6704 (2017).

96. Cantrell, K., Erenas, M. M., De Orbe-Payá, I. & Capitán-Vallvey, L. F. Use of the hue parameter of the hue, saturation, value color space as a quantitative analytical parameter for bitonal optical sensors. *Anal. Chem.* **82,** 531–542 (2010).

97. Funes-Huacca, M. *et al.* Portable self-contained cultures for phage and bacteria made of paper and tape. *Lab Chip* **12,** 4269–78 (2012).

98. Grasel, F. dos S., Marcelo, M. C. A. & Ferrão, M. F. Development of inexpensive,

practical and non-destructive methodology based on digital images of scanner to classification of the commercial tanning from *Acacia mearnsii*. *Anal. Methods* **9,** 3977–3982 (2017).

99. Gupta, S., Kamboj, P. & Kaushik, S. A Novel Methodology for Automatic Bacterial Colony Counter. *Adv. Intell. Soft Comput.* **166 AISC,** 559–565 (2012).

100. Göröcs, Z. *et al.* Giga-pixel fluorescent imaging over an ultra-large field-of-view using a flatbed scanner. *Lab Chip* **13,** 4460 (2013).

101. Pereira, J. Rough Profiler 2 (Windows) Version : alpha. 1 (2018). Available at: http://www.jpereira.net/descargar-rough-profiler-windows. (Accessed: 15th May 2018)

102. Stawowczyk, A. ICC Color Camera Calibrator. 1–7 (2016). Available at: http://www.muscallidus.com/coca/. (Accessed: 15th May 2018)

103. JCGM. Evaluation of measurement data — Guide to the expression of uncertainty in measurement. *1st Eddition* (2008).

104. Croxatto, A., Dijkstra, K., Prod'Hom, G. & Greub, G. Comparison of inoculation with the InoqulA and WASP automated systems with manual inoculation. *J. Clin. Microbiol.* **53,** 2298–2307 (2015).

105. Neves-Silva, R., Jain, L. C. & Howlett, R. J. Automatic image classification for the urinoculture screening. *Smart Innov. Syst. Technol.* **39,** 31–42 (2015).

106. Sharma, A. Understanding color management. *IPA Bull.* **94,** 16–21 (2005).

107. Stone, E. Completely Painless Programmer Guide to XYZ , RGB ,C IC , xyY , and

TRCs. 1–32 (2017). Available at: https://ninedegreesbelow.com/photography/xyz-rgb.html. (Accessed: 7th September 2017)

108. Tavakoli, H., Bayat, M., Kousha, A. & Panahi, P. The application of chromogenic culture media for rapid detection of food and water borne pathogen. *Am. J. Agric. Environ. Sci.* **4,** 693–698 (2008).

109. FDA. Pharmaceutical Microbiology Manual. 3–30 (2015).

110. Wilson, I. G. Use of IUL countermat automatic colony counter for spiral plated total viable counts. *Appl. Environ. Microbiol.* **61,** 3158–3160 (1995).

111. Garry, E., Quatarra, G., Williams, P. & Pesta, M. Enumerating chromogenic agar plates using the color QCount automated colony counter. *J. Rapid Methods Autom. Microbiol.* **17,** 46–54 (2009).

112. Hallas, G. & Monis, P. Evaluation of heterotrophic plate and chromogenic agar colony counting in water quality laboratories. *MethodsX* **2,** 415–422 (2015).

113. Ferrari, A., Lombardi, S. & ... Bacterial colony counting by convolutional neural networks. in *Engineering in Medicine* ... (ed. Engineering in Medicine and Biology Society (EMBC), 2015 37th Annual International Conference of the IEEE) 1–3 (IEEE, 2015).

114. Vera, S. *et al.* Automated annotation removal in agar plates. in *Proceedings of the Annual International Conference of the IEEE Engineering in Medicine and Biology Society* (ed. IEEE EMBS) 3016–3019 (IEEE, 2013).

115. London, R. *et al.* An automated system for rapid non-destructive enumeration of growing microbes. *PLoS One* **5,** (2010).

116. Jung, J. H. & Lee, J. E. Real-time bacterial microcolony counting using on-chip microscopy. *Sci. Rep.* **6,** 1–8 (2016).

117. AOAC International. AOAC Official Methods 966.23 Microbiological Methods. *AOAC International* 17–18 (2000).

118. Sutton, S. Accuracy of plate counts. *J. Valid. Technol.* **17,** 42–46 (2011).

119. Guangdong Dayuan Oasis Food Safety Technology, n. d. . Bacteria colony count plate. 3 (2018). Available at: http://www.chinafst.cn/en/showp.php?id=1348&parent_id=106&classid=118. (Accessed: 20th May 2018)

120. Xia, S. U. N., Lian, J. & Xin, L. U. Comparison of three test methods for aerobic plate count in foods. *Chinese J. Jealth Lab Technol.* **24,** 1250–1254 (2014).

121. Yi, Y. *et al.* A pilot study on using chlorine dioxide gas for disinfection of gastrointestinal endoscopes. *J Zhejiang Univ Sci B* **17,** 526–536 (2016).

122. Luijk, G. Eliminación de tramas mediante FFT. N/A (2008). Available at: http://www.guillermoluijk.com/tutorial/fft/index.htm. (Accessed: 21st May 2018)

123. Jung, H. & Burger, W. A spectral retouching tool for removing repetitive image noise. *2009 Int. Symp. ELMAR* 28–30 (2009).

124. Siegert, W. ISO 11930 - A comparison to other methods to evaluate the efficacy of antimicrobial cosmetics. *SOFW-Journal* **7,** 44–53 (2012).

125. Orús, P. & Leranoz, S. Control microbiológico del producto acabado. 1–51 (2015).

126. Poynton, C. Color FAQ - Frequently Asked Questions Color. *Colour FAQ -*

Frequently Asked Questions Colour 1 (2006). Available at: http://www.poynton.com/notes/colour_and_gamma/ColorFAQ.html. (Accessed: 19th December 2017)

Appendix I: List of Abbreviations

BIPM	Bureau Internationale des Poids et Mesures
C_{Avg}	Channel average value
CCD	Charge-coupled device
CIE	Comission Internationale de l'Écleraige
CIELAB	Comission Internationale de l'Écleraige's 1976 L*a*b* color space
CIEXYZ	Comission Internationale de l'Écleraige's 1931 XYZ color space
$CIEXYZ_{D50}$	Comission Internationale de l'Écleraige's 1931 XYZ color space under illuminant D50
CIS	Contact image sensor
D50	Illuminant D50
EDCCA	End-point digital colony counting and analysis
FT	Fourier transform
GRIN	Gradient index (lens array)
GRR	Gauge repeatability and reproducibility analysis
GUI	Graphical user interface
HSB	Hue Saturation Brightness color space
HSD	Honest significant distance test
ICC	International Color Consortium
IJM	ImageJ macro language
ITU	International Telecommunications Union
JND	Just noticeable difference
KinCAn	Kinetic count and analysis macro
L601	International Telecommunication Union's Luma as reflected in BT 601
L709	International Telecommunication Union's Luma as reflected in BT 709
LA	Letheen agar
NIST	National Institute of Standards and Technology
PBM	Paper-based Microfluidics
PC	Personal computer

PCB	Parc Científic de Barcelona
RGB	Red/ green/ blue primaries, and color spaces constructed with these
TTC	2,3,5-triphenyltetrazolium chloride
TTD	Time to detection
TV	Tetrazolium violet

Appendix II: VBA Functions and Annotations

Gamma-Based Linearization Function

```
Function gamma2Lin(Value)


       If Value <= 0.04045 Then

              gamma2Lin = Value / 12.92

              Else: gamma2Lin = ((Value + 0.055) / 1.055) ^ 2.4

       End If


End Function
```

Notes

Calculation according to [40] p. 353 Equation 14.35

Linear to Gamma Delinearization Function

```
Function lin2Gamma(Value)


       If Value <= 0.0031308 Then

              lin2Gamma = 12.92 * Value

              Else: lin2Gamma = (1.055 * ((Value) ^ (1 / 2.4))) - 0.055

       End If


End Function
```

Notes

Calculation according to [40] p.352 Equation 14.33.

sRGB to Luminance Conversion Function

```
Function sRGB2Lmnc(R, G, B)


        'Array with values for each channel

        Dim ch_array(3)

        ch_array(0) = R / 255

        ch_array(1) = G / 255

        ch_array(2) = B / 255


        'Array with Values for Each Coefficient

        Dim ch_coef(3)

        ch_coef(0) = 0.2126

        ch_coef(1) = 0.7152

        ch_coef(2) = 0.0722


        ch_sum = 0 ' Carries value of summing all array value products


        'Loop to calculate weighed channel sum

        For i = 0 To 2

                ch_array(i) = ch_coef(i) * gamma2Lin(ch_array(i))

                chSum = chSum + ch_array(i)

        Next


        sRGB2Lmnc = lin2Gamma(chSum) * 255


End Function
```

Notes

sRGB to Luminance (*L'*) function according to [40] , <chSum> variable in the present function corresponds to 1931 CIEXYZ Y channel. This "1931CIE Y" channel is a linear (non-gamma compressed value). Summed values are delinearized in order to obtain the grayscale luminance. This is why <lin2Gamma(chSum) * 255> is used.

sRGB to Luma$_{601}$ Conversion Function

```
Function sRGB2LumaRec601(R, G, B)


       sRGB2LumaRec601 = (0.299 * R) + (0.587 * G) + (0.114 * B)


End Function
```

Notes

The Luma$_{601}$ (L_{601}) conversion function is also known as “luminance function”. It was initially meant for implementation with RGB primaries other than those of sRGB. Values obtained with this function are referred to as simply luma and confusions wirth Luma$_{709}$ are profuse. <R, G, B> correspond to R', G', B' that is non-delinearized value (see [126]). Coded according to according to ITU-R BT.601-7[39].

sRGB to Luma$_{709}$ Conversion Function

```
Function sRGB2LumaRec709(R, G, B)


       sRGB2LumaRec709 = (0.2126 * R) + (0.7152 * G) + (0.0722 * B)


End Function
```

Notes

The Luma$_{709}$ (L_{709}) conversion function is also known as “luminance function”. It uses sRGB primaries. Values obtained with this function are referred to as simply luma and confusions with

Luma_{601} are profuse. <R, G, B> correspond to R', G', B' that is non-delinearized values (see [126]). Coded according to according to ITU-R BT.709-6[42].

Average Channel Grayscale Conversion

```
Function sRGB2AvgCh(R, G, B)


       sRGB2AvgCh = (R + G + B) / 3


End Function
```

Notes

Common approach, as featured in [40] p. 353 Equation 12.7. Subtle differences might be found when comparing values with certain software and calculators as a fraction is used in the formula to maximize precision.

Delinearization Function for CIELAB

```
Function ch_prime(channel)


        rho = 0.008856

        kappa = 7.8787


        If channel > rho Then

           channel = channel ^ (1 / 3)

        Else

           channel = (16 / 116) + kappa * channel

        End If


           ch_prime = channel

End Function
```

Notes

General Conversion Formula from [40]p. 347, comes from equations 14.8 to 14.10.

Conversion of sRGB (D65) to CIEXYZ (E)

```
Function sRGB2XYZ(R, G, B)


       ch_array = Array(R / 255, G / 255, B / 255)

       Dim XYZ_vec(0 To 2) As Single



       conv_col = Array(0.438495829, 0.222853759, 0.017320809, _

                        0.392140205, 0.708672719, 0.11046009, _

                        0.16936401, 0.068473651, 0.872219101)


       Dim new_comp(0 To 2, 0 To 2) As Single


       For i = 0 To 2

              ch_array(i) = gamma2Lin(ch_array(i)) 'ch_array gets linearized

              counter = 0

              For j = i * 3 To (i * 3) + 2

                     new_comp(counter, i) = ch_array(i) * conv_col(j)

                     counter = counter + 1

              Next

       Next


       XYZ_vec(0) = new_comp(0, 0) + new_comp(0, 1) + new_comp(0, 2)

       XYZ_vec(1) = new_comp(1, 0) + new_comp(1, 1) + new_comp(1, 2)

       XYZ_vec(2) = new_comp(2, 0) + new_comp(2, 1) + new_comp(2, 2)
```

```
        sRGB2XYZ = XYZ_vec

End Function
```

Notes

This sRGB to CIEXYZ conversion function is based on a conversion matrix that accounts for chromatic adaptation from sRGB's illuminant D65 to CIEXYZ Standard illuminant E and a color space conversion (from sRGB to CIEXYZ). The full conversion matrix was obtained from [88] and it requires linearization of input RGB values. This conversion follows the model feature in equation 14.48, p. 359 in [40].

Conversion of CIEXYZ (E) to CIELAB D50

```
Function XYZ_D502CIELAB_D50(X, Y, Z)


        ch_array = Array(X, Y, Z)


        For i = 0 To 2

                ch_array(i) = ch_prime(ch_array(i))

        Next


        L_ast = (116 * ch_array(1)) - 16

        a_ast = 500 * (ch_array(0) - ch_array(1))

        b_ast = 200 * (ch_array(1) - ch_array(2))

        XYZ_D502CIELAB_D50 = Array(L_ast, a_ast, b_ast)


End Function
```

Notes

General Conversion Formula as per ISO 13655, formula originated from [40] p. 347. This function and subfunctions stem from equations 14.4 to 14.10. The formula includes a chromatic addaptation from illuminant E to D50.

sRGB (D65) to CIELAB D50

```
Function sRGB2LAB_D50(R, G, B)


       XYZ_50 = sRGB2XYZ(R, G, B)

       ch_LAB = XYZ2CIELAB(XYZ_50(0), XYZ_50(1), XYZ_50(2))

       sRGB2LAB_D50 = ch_LAB


End Function
```

Notes

General conversion formula which simply resorts to the consecutive conversions of sRGB2XYZ, which produces XYZ coordinates under illuminant E and XYZ2CIELAB_D50, which generates CIELAB coordinates under illuminant D50. It must be acknowledged that expected input is D65 sRGB while output is CIELAB$_{D50}$.

sRGB (D65) to CIEXYZ D50 Conversion

```
Function sRGB2XYZ_D50(R, G, B)


       ch_array = Array(R / 255, G / 255, B / 255)

       Dim XYZ_vec(0 To 2) As Single


       conv_col = Array(0.436075, 0.222505, 0.013932, _

                                 0.385065, 0.716879, 0.097104, _
```

```
                        0.14308, 0.060617, 0.714173)


        Dim new_comp(0 To 2, 0 To 2) As Single


        For i = 0 To 2
                ch_array(i) = gamma2Lin(ch_array(i)) 'ch_array gets linearized
                counter = 0


                For j = i * 3 To (i * 3) + 2
                        new_comp(counter, i) = ch_array(i) * conv_col(j)
                        counter = counter + 1
                Next
        Next


        XYZ_vec(0) = new_comp(0, 0) + new_comp(0, 1) + new_comp(0, 2)
        XYZ_vec(1) = new_comp(1, 0) + new_comp(1, 1) + new_comp(1, 2)
        XYZ_vec(2) = new_comp(2, 0) + new_comp(2, 1) + new_comp(2, 2)
        sRGB2XYZ_D50 = Array(XYZ_vec(0), XYZ_vec(1), XYZ_vec(2))

End Function
```

Notes

Full conversion matrix (from sRGB D65 to CIEXYZ$_{D50}$) is implemented in array <conv_col>, original matrix is converted into an array in order to simplify coding of the matrix multiplication. Original full conversion matrix can be found in [88]. R, G, B inputs must be linearized in order to be multiplied with the conversion matrix. This chomatic addaptation and color space conversion follows the model featured in equation 14.48, p. 359 of [40].

Color Difference Calculation

```
Function DeltaE(L1, a1, b1, L2, a2, b2)

       DeltaE = (((L2 - L1) ^ 2) + ((a2 - a1) ^ 2) + ((b2 - b1) ^ 2)) ^ (1 / 2)

End Function
```

Notes

Since this formula simply consists in the calculation of Euclidean distance in a tridimensional space, its range of applications is particularly extense. It can be used to calculate ΔE_{ab} and Δ_{XYZ} color differences as featured in Equation 3.13 and Equation 3.14, respectively. The ΔE_{ab} calculation formula, as featured was proposed in 1976 by CIE and is implemented according to [40] p. 350, equation 14.26.

Appendix III: IJM Scripts and Annotations

KinCAn

```
//Defining origExt to locate the macro-containing folder
        origExt = "Kinetic\\KAL_03\\";

//Opening Higher Order Folders through which Sequencer can run
        directory = getDirectory("");
        targetAr = folderScan1(directory, "/");
        n = targetAr.length;

//Running <Sequencer> sub^1macro
        for (i=0; i<n; i++){
                tarDir = directory + targetAr[i];
                runMacArg("Sequencer", tarDir);
        }


//Functions

                function runMacArg(mac, arg){
                        if(arg !=""){mac = mac + ">" + arg;  }
                        IJD = getDirectory("ImageJ");
                        runMacro(IJD+"ZZXXYY\\LatestVersion\\LtVr_00.ijm","ZZXXYY\\"+origExt+mac);
                        print("************\n<" + mac +"> has been run");
                }


                function folderScan1(directory, endMotif){
                        directory_list = getFileList(directory);
                        targetAr = newArray();

                        for (i=0; i < directory_list.length; i++){
                                if(endsWith(directory_list[i], endMotif)){
                                        targetAr = Array.concat(targetAr, directory_list[i]);
                                }
                        }
                        return targetAr;
                }
```

Notes

Kinetic Count and Colony analysis Macro, (KinCAn) is an upper hierarchy macro for count and analysis of colonies in alternative growth media. It duly makes use of Sequencer, a submacro and the sub^2macros that are executed from Sequencer. This macro loops through folders located in a given path in search of subfolders that will be duly analyzed by Sequencer in search of image series, in order to perform kinetic counts of these.

Functions

function runMacArg(mac, arg):

- Function that calls a subMacro's latest version and passes arguments on to it.
- N.B. Will require containing script to include <origExt> path that points to folders where submacros are located.

function folderScan1(directory, endMotif):

- Returns array with all the image files & opens ROI zip file folder that should contain ROIs for all the growth pads in the imaged consumables.

Sequencer

```
n=10; //Number of plates in scanned images


//Defining origExt to locate the macro-containing folder

        origExt = "Kinetic\\KAL_03\\";
        numAr =newArray(3, 11, 23, 35, 47, 59, 71, 83, 95); // Array that establishes the
#images that must be processed, note 2
closer("Stack");
closer("ROI Manager");

//Locate Source Directory and Get Image File List

        directory = getArgument(); // UHM kinCAn establishes target directory
        directory_list = getFileList(directory);
        image_list = folderScan(directory_list); // Gets list of image files available
        fp=0;// Variable that trigers counting procedure for FP plates
        pltType = pltStr(image_list[0]); // Retrieves consumable type
        pltType0=pltType; // variable specifically created for resCountTbl function
        expType = substring(image_list[0], 1,7); //Retrieves experiment series

//Loop1: Open Files + ROI.zip & Create Stack

        for (i=0; i < numAr.length; i++){
                number = numAr[i];
                open(directory + image_list[number]);
        }

        run("Images to Stack", "name=Stack title=[] use");
        selectWindow("Stack");

        if(roiManager("count")!=10){exit("Wrong # of ROIs available");}

//Loops through ROIs creating partial stacks (names partial stacks with numbers)

        for(i=0; i<n; i++){
                selectWindow("Stack");
                roiManager("select", i);
```

```
                run("Duplicate...", "title=-" + i + " duplicate");
        }


//Loop 3: denoises every individual image selecting it from a list
        countAr = newArray(); // Array that will be used to save count values
        for(i=0; i<n; i++){
                selectWindow("-"+i);
                run("Stack to Images");
                denz(i);
                run("Images to Stack", "name=Prc_" + i + " title=Prc_ use");
                run("Images to Stack", "name=" + i + " title=[] use");
                selectWindow("Prc_" + i);
                countAr = consuCount(pltType, countAr);
        }

        resCountTbl(countAr, expType, pltType0); // Retrieves and records count values

        closerIm();


//Functions


                function closer(winName){
                                if(isOpen(winName)){
                                        selectWindow(winName);
                                        run("Close");
                                }
                }


                function closerIm(){
                        arOpen = getList("image.titles"); // Array with all open titles
                        for(i=0; i<arOpen.length; i++){close(arOpen[i]);}
                }


                function runMacArg(mac, arg){
                        if(arg !=""){mac = mac + ">" + arg;}
                        IJD = getDirectory("ImageJ");
                        ltDir = "ZZXXYY\\LatestVersion\\LtVr_00.ijm";
                        header = "************\n<";
                        print("activating macro: " + IJD + ltDir);
                        print(header + "ZZXXYY\\"+ origExt + mac +"> will be run");
                        runMacro(IJD + ltDir, "ZZXXYY\\"+ origExt + mac);
                        print(header + mac +"> has been run");
                }


                function folderScan(file_list) {
                        imageArray = newArray();

                        for (i=0; i < file_list.length; i++){

                                st1 = endsWith(file_list[i], ".jpeg");
                                st2 =  endsWith(file_list[i], ".jpg");
                                st3 = endsWith(file_list[i], ".tif");
                                if(st1 || st2  ||st3){
                                        Dialog.create("Warning");
                                        Dialog.addMessage("Invalid file extensions");
```

```
                        Dialog.show();
                }

                if(endsWith(file_list[i], ".png")){
                        imageArray = Array.concat(imageArray, file_list[i]);
                }

                if(endsWith(file_list[i], ".zip")){
                                        open(directory + file_list[i]);
                }
        }
        return imageArray;
}


function pltStr(str){
        outStr = substring(str, 7, 9);
        statement = (outStr!="FP"&&outStr!="SK");

        if (statement){       //Loop for legacy image file codes
                outStr = substring(str, 9 , 11);
        }

        statement = ( outStr!="FP"&&outStr!="SK");
        if(statement){exit("Coding doesn't allow locating consumable type.");}
        print("Plate type: " + outStr);
        return outStr;
}


function denz(i){
        for (j=0; j < numAr.length; j++){
        img = image_list[numAr[j]];
        selectWindow(substring(img, 0, indexOf(img,".png")));

        runMacArg("Denz", pltType);
        }
}


function consuCount(pltType, countAr){
        if(pltType =="SK"){runMacArg("sKCount","");}
        if(pltType =="FP"){runMacArg("fPCount","");}
        maxThr = getResult("Threshold", nResults-1);
        upClose();
        selectWindow("CountI");
        run("Find Maxima...", "noise=" + maxThr + " output=List light");
        selectWindow("CountI");
        saveAs("png", directory +  i + "_count.png");
        selectWindow("Results");
        saveAs("Results", directory +  i + ".xls");
        close();
        countAr = Array.concat(countAr, d2s(nResults,0));
        upClose();
        return countAr;
}


function upClose(){
        updateResults();
        if (isOpen ("Results")){
```

```
                selectWindow("Results");
                run("Close");
        }
}


function resIdent(str){
        plt1 = str;
        expType = substring(str, 1,7);
        mo = substring(str,7,9);
        cons =  substring(str,9,11);
        expConc =""; // stays empty for 010201
        if (expType == "010103"){expConc = substring(str,12,14);}
        place1 = lengthOf(str)-17;
        place2=lengthOf(str)-9;
        print(place1, place2);
        date = substring(str, place1, place2);
        expId = expType + mo + cons + expConc + date;
        resIdAr = newArray(expId,  mo, cons, expType, date, plt1);
        tagResIdAr = newArray("Full Identification", "MO", "Cons.", "Experiment", "Date", "1st Plate");

        for (i=0; i<resIdAr.length; i++){
                setResult(tagResIdAr[i], 0, resIdAr[i]);
        }

        return plt1;
}


function resCountTbl(countAr, expType, pltType0){
        pltType = pltType0;
        upClose();

        if(expType == "010201"){ tagAr = newArray("T_E0.0_1","T_E0.0_2","T_E0.5_1","T_E0.5_2","T_E1.0_1","T_E1.0_2","T_E1.5_1","T_E1.5_2","T_E2.0_1","T_E2.0_2");}
        if(expType == "010103"){tagAr = newArray(pltType+"1.1",      pltType+"1.2",pltType+"2.1",          pltType + "2.2",pltType+"3.1",pltType + "3.2",      pltType+"4.1",              pltType + "4.2",pltType+"5.1",pltType + "5.2");}

        plt1 = resIdent(image_list[0]);

        for (i=0; i < countAr.length; i++){
                        setResult(tagAr[i], 0, countAr[i]);
        }
        updateResults();
        selectWindow("Results");
        print("plt1 is : " + plt1);
        resNm = substring (plt1, 0,indexOf(plt1, "_000"));
        saveAs("Results", directory +  resNm + ".xls");
        upClose();
}
```

Notes

Sequencer macro stacks images, separates individual consumable ROIs within the stack and denoises these by activating the Denz macro, in order to denoise stacks. Next, resulting stacks are processed by a second macro. While the <Denz> macro features procedures that are applied to each plate that is processed, the second macro that is run by Sequencer is specific to the plate type.

Functions

function closer(winName):

- Closes windows with a given name, used as safety measure to prevent interferences.

function closerIm():

- Closes all open images, used to wrap up loop script execution.

function runMacArg(mac, arg):

- Function that calls a subMacro's latest version and passes arguments on to it.

N.B. Will require containing script to include <origExt> path that points to folders where submacros are located.

function folderScan(file_list):

- Returns array with all the image files.
- Ensures correct images are processed by interrupting script if files have an incorrect file extension.
- Opens ROI zip file for folder.

function pltStr(str):

- Processes image name code to retrieve the plate type being processed.

function denz(i):

- Runs the Denz sub^2macro to denoise the consumable image stacks.

function consuCount(pltType, countAr):

- Counts the colonies in individual consumables and records results in countAr for further retrieval.

function upClose():

- Updates and closes the results table in order to prevent result-table related bugs.

function resIdent(str):

- Retrieves identification information for experiment replicate and records it in the results table.

function resCountTbl(countAr, expType, pltType0):

- Saves all results in a new table inside the input images directory.

Special Notice

This code was modified to omit confidential data, this should not, however, interfere with accurate reproduction of all the tests performed based on the original script. Unforeseen bugs might be encountered, however, when running the script.

Denz

```
       a=getTitle;

//Capture Input Plate Type

       pltType = getArgument ();
       coef=0.1;
       thresh=120;
       selectWindow (a);
       run ("Duplicate...", "title=Dup_");
       selectWindow ("Dup_");

//Denoising of images according to media  type that is used

       if (pltType !="FP" ){nonFPProc ("Dup_");}
       if (pltType=="FP"){FPProc ("Dup_");}
       rename ("Prc_" + a);

//Functions



              function nonFPProc (imageNm){
                     run ("FFT");
                     run ("Duplicate...", " title=filFFT");
                     close ("Dup_");
                     selectWindow ("filFFT");
                     run ("Median...", "radius=1");
                     setThreshold (105, 255);
                     run ("Convert to Mask");
                     selectWindow ("filFFT");
                     run ("Options...", "iterations=2 count=1 do=Dilate");
                     run ("Gaussian Blur...", "sigma=2");
                     setThreshold (123, 255);
                     run ("Convert to Mask");
                     selectWindow ("filFFT");
                     run ("RGB Color");
                     selectWindow ("filFFT");

                     //Selection of Power Spectrum Screened Area
```

```
        makeOval (0.43359375*getHeight,0.43359375*getHeight, 0.1328125*getHeight,0.1328125*getHeight);
        setOption ("BlackBackground", false);
        run ("Fill");
        run ("Select All");
        run ("Invert");
        imageCalculator ("Subtract", "FFT of Dup_", "filFFT");
        close ("filFFT");
        selectWindow ("FFT of Dup_");
        run ("Inverse FFT");
        close ("FFT of Dup_");
        selectWindow ("Inverse FFT of Dup_");
}



function FPProc (imageNm){
        diam = coef*getHeight;
        selectWindow (imageNm);

        //Conduct first FFT

        run ("FFT");
        close (imageNm);

        //Conduct masking and reverse FT

        selectWindow ("FFT of " + imageNm);
        run ("Duplicate...", "title=Dup2_");
        selectWindow ("Dup2_");
        run ("Sharpen");
        run ("Median...", "radius=1");
        setThreshold (thresh, 255);
        run ("Convert to Mask");
        selectWindow ("Dup2_");
        run ("Options...", "iterations=3 count=1 do=Dilate");
        selectWindow ("Dup2_");
        frame = (getHeight*0.5)- (diam/2); // Defines reference corner
        makeOval (frame, frame, diam, diam);
        setOption ("BlackBackground", false);
        run ("Fill", "slice");
        imageCalculator ("Subtract", "FFT of Dup_", "Dup2_");
        close ("Dup2_");
        selectWindow ("FFT of Dup_");
        run ("Inverse FFT");
        close ("FFT of Dup_");
        selectWindow ("Inverse FFT of Dup_");
        run ("Enhance Contrast...", "saturated=0");

        //Channel-based denoising

        selectWindow ("Inverse FFT of Dup_");
        rename ("ChannelSplit");
        run ("RGB Stack");
        selectWindow ("ChannelSplit");
        run ("Stack to Images");
        close ("Blue");
        selectWindow ("Red");
        run ("Invert");
        imageCalculator ("Add", "Green", "Red");
        close ("Red");
```

```
                selectWindow ("Green");
                run ("Enhance Contrast...", "saturated=0");
        }
```

Notes

Denz macro removes periodic noise present in images of alternative media images due to the texture of their growth pads. Two denoising paths are implemented, one for Sanita-kun media and one for Filmplate media plates. Denoising is based on the use of filters that are selectively applied to certain frequencies of the power spectrum (see section 3.2.4 for a more extended explanation on the matter).

Functions

function FPProc (imageNm):

- Triggers FFT-filter based denoising for Filmplate (FP) plates.

function nonFPProc (imageNm):

- Triggers FFT-filter based denoising for non Filmplate (nonFP) plate processing.

fPCount

```
//Variables

fPCount (getTitle ());
rename ("CountI");


        function fPCount (imageNm){
                selectWindow (imageNm);
                setSlice (1);
                run ("Duplicate...", "title=Sub");
                selectWindow ("Sub");
                setAutoThreshold ("Intermodes");
                setOption ("BlackBackground", false);
                run ("Convert to Mask");
                selectWindow ("Sub");
                run ("Options...", "iterations=2 count=1 do=Dilate");
                run ("Invert");
                selectWindow (imageNm);
                run ("Duplicate...", "title=PrcStack duplicate range=2-9");
                selectWindow ("PrcStack");
                run ("RGB Color");
                selectWindow ("Sub");
                run ("RGB Color");
                imageCalculator ("Add stack", "PrcStack","Sub");
```

```
                close ("Sub");
                selectWindow ("PrcStack");
                run ("Z Project...", "projection=[Average Intensity]");
                close ("PrcStack");
                selectWindow ("AVG_PrcStack");
                run ("8-bit");
                selectWindow ("AVG_PrcStack");
                run ("Median...", "radius=2");
                if (isOpen ("Results")){setResult ("Threshold", nResults-1, 10);}
                else{setResult ("Threshold",  0, 10);}
        }
```

Notes

Filmplate counting macro (fPCount) is a macro devised for the processing of denoised stacks, it generates an STD z-projection of the stack in order to highlight colonies which indeed induce high image SD values in image regions where they grow given their initial absence. Before generating the projection, the first image in the stack is thresholded, inverted, and added to the rest.

sKCount

```
a=getTitle;
origExt = "Kinetic\\KAL_03\\";
cFUCount =  lowCount (a);

if (cFUCount > 500) { //Process for high counts
        close ("AVG_PrcStack");
        highCount (a);
}

rename ("CountI");


//Functions


function   lowCount (imageNm){
        selectWindow (imageNm);
        run ("Duplicate...", "title=PrcStack duplicate Stack");
        selectWindow ("PrcStack");
        setSlice (1);
        run ("Duplicate...", "title=Subtracting");
        selectWindow ("Subtracting");
        run ("Invert");
        imageCalculator ("Add stack", "PrcStack","Subtracting");
        close ("Subtracting");
        selectWindow ("PrcStack");
        run ("8-bit");
```

```
        selectWindow ("PrcStack");
        setSlice (nSlices);
        run ("Convert to Mask", "method=Otsu background=Light list");
        selectWindow ("PrcStack");
        run ("RGB Color");
        run ("Z Project...", "projection=[Average Intensity]");
        close ("PrcStack");
        selectWindow ("AVG_PrcStack");
        run ("8-bit");
        selectWindow ("AVG_PrcStack");
        setThreshold (0, 225);
        run ("Create Mask");
        selectWindow ("mask");
        run ("RGB Color");
        selectWindow ("AVG_PrcStack");
        run ("RGB Color");
        imageCalculator ("Add stack","AVG_PrcStack", "mask");
        close ("mask");
        selectWindow ("AVG_PrcStack");
        run ("Median...", "radius=2");
        run ("Find Maxima...", "noise=10 output=Count light");
        setResult ("Threshold", nResults-1, 10);
        return getResult ("Count", nResults-1);
}


function highCount (imageNm){

        selectWindow (imageNm);

        //STD
        run ("Duplicate...", "title=StackProc duplicate");
        selectWindow ("StackProc");
        run ("Z Project...", "projection=[Standard Deviation]");
        selectWindow ("STD_StackProc");
        run ("Invert");
        runMacArg ("Denz","");
        run ("RGB Stack");
        run ("Stack to Images");
        close ("Blue");
        close ("Inverse FFT of Dup_");
        selectWindow ("Red");
        run ("Invert");
        imageCalculator ("Add", "Green", "Red");
        close ("Red");
        selectWindow ("Green");
        run ("Enhance Contrast...", "saturated=0");
        rename ("Proc8bt");
        runMacArg ("Denz","");
        close ("STD_StackProc");
        setAutoThreshold ("Otsu");
        run ("Create Mask");
        selectWindow ("mask");
        run ("Options...", "iterations=2 count=1 do=Dilate");
        run ("Gaussian Blur...", "sigma=2");
        setAutoThreshold ("Otsu");
        setOption ("BlackBackground", false);
        selectWindow ("mask");
        run ("Convert to Mask");
        selectWindow ("mask");
        run ("RGB Color");
```

```
        selectWindow ("Proc8bt");
        run ("RGB Color");
        imageCalculator ("Subtract", "Proc8bt","mask");
        selectWindow ("mask");
        run ("Invert");
        imageCalculator ("Subtract", "Prc_Proc8bt","mask");
        close ("mask");
        imageCalculator ("Add", "Prc_Proc8bt","Proc8bt");
        close ("Proc8bt");
        close ("StackProc");
        if (isOpen ("Results")){setResult ("Threshold",nResults-1, 6);}
        else{setResult ("Threshold",0, 6);}
        selectWindow ("Prc_Proc8bt");
        resetThreshold ();
}


function runMacArg (mac, arg){
        if (arg !=""){mac = mac + ">" + arg;}
        IJD = getDirectory ("ImageJ");
        print ("activating macro: " + IJD + "ZZXXYY\\LatestVersion\\LtVr_00.ijm");
        print ("************\n<" + "ZZXXYY\\"+ origExt + mac +"> will be run");
        runMacro (IJD + "ZZXXYY\\LatestVersion\\LtVr_00.ijm", "ZZXXYY\\"+ origExt + mac);
        //Obviously, paths can be changed
        print ("************\n<" + mac +"> has been run");
}
```

Notes

Sanita-kun counting macro (sKCount) is a macro devised for the processing of denoised stacks. It relies on two alternative algorithms that depend on the total count value, the first being applied to counts below 501 (lowCount) CFU and the second for counts above 500 CFU (highCount). In order to determine whether if the > 500 CFU algorithm must be activated, the lowCount algorithm is run first.

Functions

function lowCount (imageNm):

- Special denoising function for high count plates.

function highCount (imageNm):

- Special denoising function for high count plates.

function runMacArg (mac, arg):

- Function that calls a subMacro's latest version and passes arguments on to it.

N.B. Will require containing script to include <origExt> path that points to folders where submacros are located.